The role of Natural Killer T cells in atherosclerosis



Suzanne E. Engelen, MD

The Queen's College

University of Oxford

A thesis submitted for the degree of *Doctor of Philosophy* in Molecular and Cellular Medicine

Michaelmas, 2022

Abstract

Atherosclerosis is a multifactorial, chronic inflammatory disease of the arterial wall starting in childhood. It is characterised by the gradual formation of lipid-, connective tissue- and immune cell containing plaques. The interplay between lipids and the immune system has proven key in its development. Natural Killer T (NKT) cells are at the interface between lipid metabolism and immunity, due to their restriction to lipid antigen-mediated activation by antigen presenting cells (APC). Although considered pro-atherogenic in mouse, the mechanisms involved in NKT cell activation in humans remain elusive and their role in human cardiovascular disease requires further study.

In this thesis, I identify lipoproteins very-low-density- (VLDL) and low-density (LDL) as vehicles for lipid antigen delivery and subsequent activation of invariant NKT cells. In the circulation, model lipid antigens bind to VLDL and LDL. Subsequent uptake by APCs is LDL-receptor (LDLR)-mediated, demonstrated *in vitro* and *in vivo* in mouse models. As a consequence, LDLR-mutant APCs of patients with familial hypercholesterolemia are impaired in their ability to activate invariant NKT cells, validating this mechanism in a human context. Moreover, the relation of NKT cell plaque-abundance with clinical outcome, patient- and plaque characteristics was studied in a human cohort. NKT cell abundance in plaques is inversely associated with plaque vulnerability, suggesting a protective role for NKT cells in stabilisation of the human plaque. Evidence of APC-NKT cell interaction in human atherosclerosis is currently lacking. To this end, I applied Hyperion Imaging Mass Cytometry (IMC) to human atherosclerotic plaques to study the NKT cell niche, revealing spatial evidence in situ of close cellular interactions of macrophages and NKT cells.

In conclusion, this thesis defines the mechanism of lipid antigen delivery to APCs by circulating lipoproteins, and its fundamental role in invariant NKT cell activation. It proposes innovative imaging modalities to study the APC-iNKT axis in the human plaque, and associates NKT plaque-abundance with clinical parameters for the first time. These novel insights further our understanding of the interplay of lipids and the immune system, underlying atherosclerosis.

Acknowledgements

First and foremost, thank you to my supervisors. Claudia Monaco, I have learnt so much from you over the past three years. I especially enjoyed the stimulating conversations we had whilst writing the literature review. Thank you for passing on your knowledge. I thank Christopher Buckley for showing what is possible as a clinician scientist, your work is truly inspiring. To Henk Schipper, I am incredibly grateful for your guidance during my DPhil. Thank you for teaching me a wide variety of laboratory techniques during the time you were working in the laboratory, which allowed me to work more independently in later stages of my DPhil. Above all, thank you for making working in the laboratory so much fun.

I am very grateful to the Kennedy Trust for awarding me a studentship to pursue my DPhil at the Kennedy Institute of Rheumatology.

I would like to thank the current and former members of the Monaco group, for their advice, the laughs, friendship and support. My time in this team has had a huge impact on my personal and professional development. Thank you for being such an important part of that. I learnt a lot from each of you.

A huge thank you to my friends and extended family in the UK, as well as The Netherlands. The dinners, coffees, laughter, and B&Bing made this experience unforgettable.

I thank my grandparents for their love and support, every video call with you was a joy. You mean a lot to me.

Finally, thank you:

To my sisters Maartje, Eveline and Ruth and their partners (Wouter and Marco) for being amazing people. I am so proud to have you as my sisters. Big hugs to the little sunshines: Tuur, Saar, Thijs, Hidde and Nienke.

To my parents, whose unconditional love and support have provided the basis to make all this possible. I realise how lucky I am to have grown up in the loving home you provided. Therefore I dedicate this thesis to you.

To Max, the love of my life, thank you for everything. You make my day, everyday. I am really grateful we were able to go on this amazing adventure together and I look forward to the next chapters of our lives.

Table of contents

Abstract ... *2*
Acknowledgements ... *3*
Table of contents ... *4*
Table of contents ... *4*
List of Figures ... *8*
List of Tables ... *10*
List of abbreviations ... *11*
1 Introduction ... *12*
1.1 Introduction to atherosclerosis ... **12**
1.2 The immune system in atherosclerosis ... **15**
1.2.1 Lipids and the innate immune response ... 16
1.2.2 The adaptive immune response ... 16
1.3 Lipid antigen presentation by antigen presenting cells ... **20**
1.3.1 CD1 molecules ... 20
1.3.2 CD1d expression ... 21
1.3.3 CD1d loading and presentation ... 21
1.4 Natural Killer T cells ... **22**
1.4.1 Defining Natural Killer T cells ... 22
1.4.2 Natural Killer T cell activation ... 23
1.4.3 Lipid antigens activating NKT cells ... 26
1.4.4 Natural Killer T cells in healthy and diseased settings ... 27
1.4.5 Natural Killer T cells in atherogenesis ... 29
1.5 Lipoproteins ... **33**
1.5.1 Lipoprotein composition ... 33
1.5.2 The contribution of lipoproteins to atherogenesis ... 34
1.5.3 Systemic lipoprotein metabolism: exogenous and endogenous pathways ... 34
1.5.4 Cellular cholesterol metabolism: uptake, synthesis and efflux ... 37
1.6 Hypothesis and Aims ... **41**
2 Lipid antigen delivery to antigen presenting cells ... *42*
2.1 Introduction ... **42**
2.2 VLDL and LDL form stable complexes with the model iNKT cell ligand *α*GalCer ... **44**
2.3 LDL-αGalCer complexes are stable after 1 week ... **49**
2.4 Alternative lipid antigens form complexes with human LDL ... **50**
2.5 Uptake of LDL-αGalCer-complexes is LDLR mediated ... **51**

2.6 LDLR-mediated activation of iNKT cells by (V)LDL-αGalCer complexes in vitro 52

2.7 The role of ApoE in complex uptake and activation 55

2.8 VLDL-*α*GalCer complexes activate iNKT cells in vivo in a LDLR-dependent fashion 57

2.9 Human LDLR mutations are associated with impaired iNKT cell activation and proliferation 62

2.10 Discussion 67

3 NKT cells in human atherosclerosis 71

3.1 Introduction 71

3.2 Study population 73

3.3 Natural Killer T cell staining on human atherosclerotic plaque 74

3.4 Natural Killer T cell counts in the human atherosclerotic plaque 75

3.5 The location of NKT cells in the human atherosclerotic plaque 76

3.6 The relationship between patient characteristics and the number of NKT cells in the human plaque 77

3.7 The relationship between clinical outcome and NKT cell numbers in the human plaque 80

3.8 The relationship between plaque histomorphology and NKT cell numbers 81

3.9 Discussion 85

4 Spatial mapping of the APC-INKT axis in the human atherosclerotic plaque 89

4.1 Introduction 89

4.2 Development of an antibody panel to characterize the human atherosclerotic plaque microenvironment 91

4.2.1 Validation of antibody affinity and specificity on human tonsil tissue 91

4.2.2 Validation of antibody affinity and specificity on human atherosclerotic plaque tissue 94

4.2.3 Establishment of tetramer based selective staining for iNKT cells 94

4.3 Image analysis identified distinct immune cell subsets in human atherosclerotic plaque tissue 100

4.3.1 Extraction of single-cell data 100

4.3.2 Cell type clustering of immune cell subsets in human atherosclerotic plaque 102

4.3.3 Macrophages are the APC subset residing in the closest proximity to iNKT cells in the human atherosclerotic plaque 104

4.4 Discussion 106

4.4.1 Validation of Hyperion Imaging Mass Cytometry on human atherosclerotic plaque tissue 106

4.4.2 Identification of the APC-iNKT axis in the human atherosclerotic plaque 108

5 Final discussion ... 110

5.1 Summary ... 110

5.1.1 Lipoproteins act as vehicles for lipid antigen delivery to APCs and iNKT cell activation ... 110

5.1.2 NKT cells in human atherosclerotic plaques are associated with plaque stability ... 111

5.1.3 Spatial mapping of the APC-iNKT axis in the human atherosclerotic plaque 112

5.2 Future perspective ... 113

5.3 Concluding remarks ... 113

6 Material and Methods ... 115

6.1 List of antibodies and buffers ... 115

6.2 Study approval ... 115

6.3 Patient samples ... 115

6.3.1 Peripheral blood mononuclear cells ... 115

6.3.2 Atherosclerotic plaque tissue ... 116

6.3.3 Tonsil tissue ... 116

6.4 Animal work ... 116

6.4.1 Mouse maintenance ... 116

6.4.2 Genotyping ... 116

6.4.3 Polymerase Chain Reaction (PCR) ... 117

6.4.4 Generation of bone marrow chimeras ... 117

6.4.5 Immunization with VLDL-αGalCer complexes ... 117

6.4.6 Isolation of mouse leukocytes and flow cytometry ... 118

6.5 Cell culture ... 119

6.5.1 Cell culture mouse bone marrow ... 119

6.5.2 Cell culture of DN32.D3 mouse NKT hybridoma ... 119

6.5.3 Generation of human primary iNKT cell line ... 120

6.6 Serum or lipid related assays ... 121

6.6.1 Serum cholesterol assay ... 121

6.6.2 Lipoprotein isolation ... 121

6.6.3 Fluorescent labeling of lipoproteins ... 122

6.6.4 Synthesis of AF488-labeled αGalCer ... 123

6.6.5 Fluorescent labeling of iGb3, OCH and GSL-1 ... 124

6.6.6 Lipoprotein-lipid antigen complex formation ... 124

6.7 2-Color Fluorescence Cross-Correlation Spectroscopy (2c-FCCS) . 124

6.8 Uptake of lipoprotein-αGalCer complexes by THP1 cells ... 125

6.9 Cocultures of antigen presenting cells and NKT cells ... 126

6.9.1 THP1 macrophage like cells in coculture with human primary iNKT cells 126

6.9.2 Mouse BMDM in coculture with iNKT hybridoma ... 126

6.9.3 Human iNKT cell activation and proliferation assay 127
6.10 Athero-Express Cohort Study 127
6.10.1 Study design 127
6.10.2 Patients 128
6.10.3 Sample procurement 128
6.10.4 Plaque phenotyping 129
6.10.5 Immunohistochemical staining of Natural Killer T cells 129
6.10.6 Image processing, counting and reproducibility 130
6.10.7 Study endpoints 131
6.11 Hyperion Imaging Mass Cytometry 132
6.11.1 Antibody panel 132
6.11.2 Metal-conjugation of antibodies 132
6.11.3 Haematoxylin and Eosin (H&E) staining and selection of region of interest 132
6.11.4 Hyperion tissue staining and antibody validation 133
6.11.5 Imaging Mass Cytometry data acquisition 133
6.11.6 Cell segmentation 134
6.11.7 Data transformation and visualisation 134
6.11.8 Cell clustering and spatial analysis 134
6.12 Statistics 135
7 Bibliography 142
8 Appendix 1. Supplemental data 170
8.1 Gating strategy iNKT cells 170
8.2 Gating strategy antigen presenting cells 171
8.3 THP1 cells overexpressing CD1d and LDLR 172
8.4 Bone marrow chimeras reconstitution 173
9 Appendix 2. Publications, presentations and awards 174
9.1 Publications 174
9.2 Presentations at scientific conferences 174
9.3 Awards 174

List of Figures

Figure 1.1 | History of research into the role of inflammation in atherosclerosis. 13
Figure 1.2 | Inflammation in atherosclerosis. 19
Figure 1.3 | Schematic overview of the interaction between APC and iNKT cell. 25
Figure 1.4 | Schematic overview of lipoprotein composition. 33
Figure 1.6 | Schematic overview of cellular cholesterol metabolism. 39
Figure 2.1 | The principle of 2-color fluorescence cross-correlation spectroscopy. 44
Figure 2.2 | Lipoproteins LDL and VLDL form stable complexes with the prototypic iNKT cell ligand αGalCer. 46
Figure 2.3 | Mouse and human lipoproteins LDL and VLDL form complexes with model lipid antigen αGalCer independent of ApoE. 48
Figure 2.4 | Stability of LDL-αGalCer complexes after 1 week. 49
Figure 2.5 | Human LDL forms complexes with alternative lipid antigens iGb3 and OCH. 51
Figure 2.6 | LDLR-mediated uptake of LDL-αGalCer complexes. 52
Figure 2.7 | LDLR-mediated uptake of (V)LDL-αGalCer complexes in vitro. 54
Figure 2.8 | The role of scavenger receptor A in the uptake of VLDL-αGalCer complexes. 55
Figure 2.9 | The role of ApoE in uptake of lipoprotein-αGalCer complexes and subsequent iNKT cell activation. 56
Figure 2.10 | Experimental set-up injection lipoprotein-αGalCer complexes. 57
Figure 2.11 | Baseline characteristics of bone marrow chimeras before administration of VLDL-αGalCer complexes. 58
Figure 2.12 | LDLR-proficient antigen presenting cells promote iNKT cell activation by VLDL-αGalCer complexes in hypercholesterolemic mice. 59
Figure 2.13 | Tetramer staining invariant Natural Killer T cells. 60
Figure 2.14 | iNKT cell number and phenotype of bone marrow chimeras 2 weeks post-administration of VLDL-αGalCer complexes. 61
Figure 2.15 | Principle of the human iNKT cell activation and proliferation assay. 62
Figure 2.16 | Phenotyping of PBMCs of patients with LDLR mutations and controls. 63
Figure 2.17 | Cytokine production in supernatant PBMCs cocultured with lipoprotein-αGalCer complexes. 64
Figure 2.18 | Human LDLR mutations are associated with impaired iNKT cell activation. 65
Figure 2.19 | APC specific human LDLR mutations are associated with impaired iNKT cell activation. 66
Figure 3.1 | Natural Killer T cell staining in human atherosclerotic plaque. 74

Figure 3.2 | (NK)T cell counts by two independent observers. *75*

Figure 3.4 | Univariate linear regression between NKT cell counts per mm2 and patient characteristics. *79*

Figure 3.6 | Relation between plaque characteristics and NKT cell counts. *82*

Figure 3.7 | Relation between Plaque Vulnerability Index and NKT cells per mm^2. ... *84*

Figure 4.1 | Schematic overview of the workflow used for Hyperion Imaging Mass Cytometry. *92*

Figure 4.2 | Hyperion IMC panel to characterize the human tonsil microenvironment. *93*

Figure 4.3 | Antibody titration on human atherosclerotic plaque tissue. *96*

Figure 4.4 | Hyperion IMC panel to characterize the human atherosclerotic plaque. *97*

Figure 4.5 | Multiplex imaging of human atherosclerotic plaque tissue to identify immune cell subsets in human atherosclerotic plaque tissue using Hyperion IMC. *99*

Figure 4.6 | Establishing an image analysis pipeline to characterize the human atherosclerotic plaque microenvironment. *101*

Figure 4.7 | High dimensional cellular profiling via clustering analysis. *103*

Figure 4.8 | Spatial representation of cell clusters in human atherosclerotic plaque tissue. *104*

Figure 4.9 | Macrophages reside in close proximity to iNKT cells in the human atherosclerotic plaque. *105*

Figure 6.1 | Lipoprotein isolation from human serum. *122*

Figure 6.2 | Human atherosclerotic plaques from the Athero-Express cohort. *129*

Supplemental Fig. 2.1 | Representative flow cytometry imaging of gating strategy in spleen. *170*

Supplemental Fig. 2.2 | Gating strategy antigen presenting cells. *171*

Supplemental Fig. 2.3 | Overexpression of CD1d and LDLR in THP1 cells upon lentiviral transduction *172*

Supplemental Fig. 2.4 | Reconstitution bone marrow chimeras. *173*

List of Tables

Table 1.1 | NKT cells in murine models of atherosclerosis. *32*

Table 1.2 | Lipoprotein classes and characteristics in human plasma. *34*

Table 3.1 | Baseline characteristics of patients of Athero-Express Biobank study *73*

Table 3.2 | Inter-rater reliability of (NK)T cells counts in human atherosclerotic plaque. *76*

Table 3.3 | Univariate linear regression analysis of baseline characteristics with NKT cell counts. *78*

Table 3.4| Definition of clinical endpoint *80*

Figure 3.5 | Relation between Composite Cardiovascular Endpoint and NKT cell counts. *81*

Table 3.5 | Univariate linear regression analysis of plaque histomorphology and clinical outcome with NKT cell counts. *84*

Table 6.1 | Antibodies for staining of Natural Killer T cells *130*

Table 6.2 | Plaque vulnerability index *131*

Table 6.3 | Fluorochrome-conjugated antibodies used for Flow Cytometry on mouse leukocytes. *136*

Table 6.4 | Fluorochrome-conjugated antibodies used for Flow Cytometry on human PBMCs. *137*

Table 6.5 | Metal-conjugated antibodies validated for Imaging Mass Cytometry on human atherosclerotic plaque tissue. *138*

Table 6.6 | Other metal-conjugated antibodies tested for Imaging Mass Cytometry on human atherosclerotic plaque tissue. *139*

Table 6.7 | Buffers, media and solutions made in-house. *139*

Table 6.8 | Mouse strains used in experiments. *141*

Table 6.9 | Sequences of primers used for genotyping. *141*

Supplemental Table 2.1 | Lipid antigens and their chemical structure. *173*

List of abbreviations

Abbreviation	Term
APC	Antigen presenting cell
ApoE	Apolipoprotein E
CVD	Cardiovascular disease
CyTOF	Cytometry Time Of-Flight
DC	Dendritic cell
ER	Endoplasmic Reticulum
DNA	Deoxyribonucleic Acid
GSL-1	Glycosphinolipid-1
HDL	High Density Lipoprotein
iGb3	Isoglobotrihexosylceramide
IMC	Imaging Mass Cytometry
iNKT	Invariant Natural Killer T cells
LDL	Low Density Lipoprotein
LDLR	Low Density Lipoprotein Receptor
PBMC	Peripheral blood mononuclear cell
RPM	Revolutions per minute
RT	Room temperature
TCR	T cell receptor
VLDL	Very Low Density Lipoprotein
WT	Wild type
αGalCer	α-Galactosylceramide

1 Introduction

1.1 Introduction to atherosclerosis

Atherosclerosis, a chronic inflammatory disease of the vessel wall, is characterised by the gradual formation of lipid-, connective tissue and immune-cell containing plaques in the intima of large and medium sized arteries (Berenson et al., 1998; Libby, 2012). Atherogenesis starts in childhood with the formation of fatty streaks first in the aorta, followed by the carotid arteries. In autopsy studies 19% of children between 2-15 years old had lesions in the aorta and 8% in the coronary arteries (Berenson et al., 1998). Atherogenesis can gradually result in narrowing and stiffening of the vessel wall, leading to coronary artery disease, cerebrovascular disease, thromboembolism and peripheral vascular disease. Over time, this can cause cardiovascular events including myocardial infarction or stroke. The primary goal of treatment is to prevent cardiovascular events by targeting modifiable risk factors, such as hypertension, hyperlipidemia, obesity, diabetes mellitus, physical inactivity, smoking and alcohol intake, through lifestyle changes and drug treatment. A second pillar of treatment is surgical re-establishment of arterial blood flow (Neumann et al., 2020; Timmis et al., 2020). Although immense progress has been achieved in prevention and management of CVD due to therapeutic targeting of these risk factors, it remains a leading cause of death throughout the world, representing 32% of all global deaths (WHO, 2019).

Inflammation has been identified as the major contributor to this residual cardiovascular risk (Aday & Ridker, 2019; Hansson, 2005b; Libby et al., 2002; Lieb et al., 2018; Ross, 1999). In 1858 Rudolf Virchow already recognized the inflammatory nature of atherosclerotic plaques (Virchow, 1858). Over the last 35

years evidence for the role of inflammation in atherosclerosis has accumulated (Fig. 1.1), and in 2017 the first proof of the benefits of targeting inflammation in CVD arrived with the CANTOS trial, showing improved clinical outcome in patients that received treatment with antibodies against IL-1β (Ridker et al., 2017a). This was followed by evidence that the anti-inflammatory effects of colchicine could reduce the cardiovascular risk of patients with acute and chronic coronary disease (Nidorf et al., 2020a; Tardif et al., 2019). These studies underscore immunotherapeutics as the next step in cardiovascular disease management, which requires a fundamental understanding of the cellular and molecular drivers of athero-inflammation (Engelen et al., 2022).

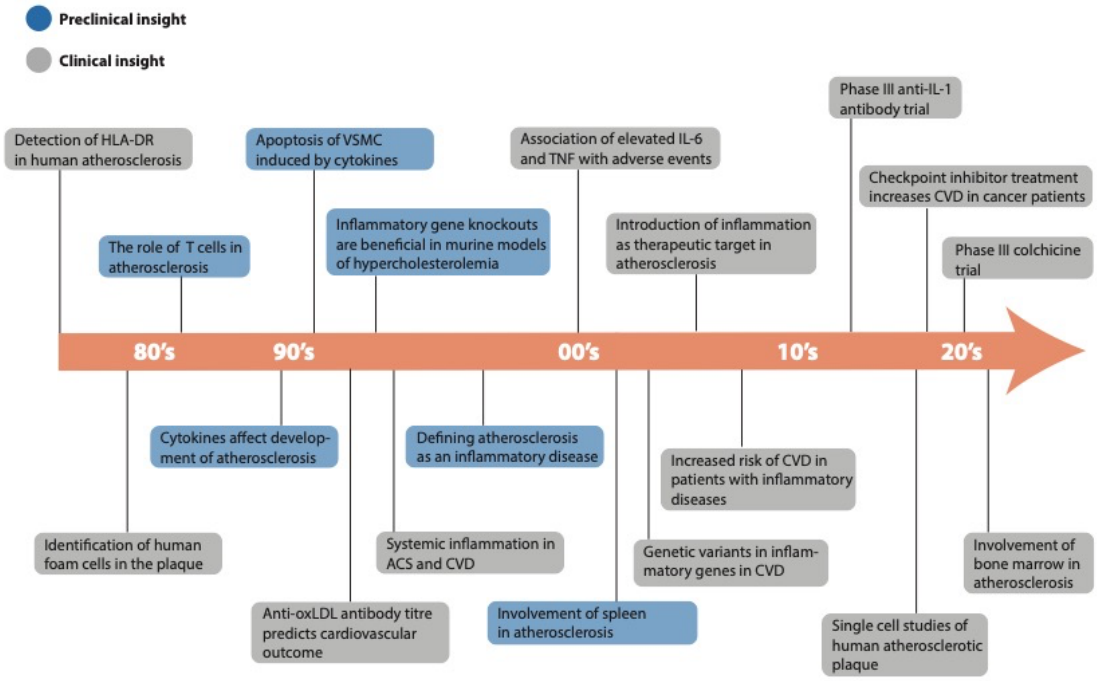

Figure 1.1 | History of research into the role of inflammation in atherosclerosis. The timeline summarizes the main milestones since the 80s in the field of inflammation in atherosclerosis.

80's: Immunohistochemical techniques were developed for atherosclerotic plaques tissue. This led to identification of human leukocyte antigen-DR (HLA-DR) expression in human atherosclerotic plaques, monocytes, macrophages and T cells

in the plaque (Aqel et al., 1985; Emeson & Robertson, 1988; Hansson et al., 1986, 1989; Jonasson et al., 1985, 1986; Robbins et al., 2012; Swirski et al., 2007; Vedeler et al., 1984).

90's: Pro-inflammatory cytokines, such as tumour necrosis factor (TNF), were detected for the first time in human atherosclerotic plaque tissue (Amento et al., 1991; De Villiers et al., 1998; Geng et al., 1996; Warner et al., 1987; Warner & Libby, 1989). The association of CRP and increased risk of acute coronary syndrome was discovered (Berk et al., 1990; Liuzzo et al., 1994), and hypercholesterolemia mouse models with inflammatory gene knockout were developed (De Villiers et al., 1998; Rajavashisth et al., 1998; Smith et al., 1995). It was shown that anti-oxidized LDL (oxLDL) antibody titres in the serum predict cardiovascular disease outcomes (Salonen et al., 1992).

00's: Associations between increased levels of inflammatory markers and increased risk of cardiovascular events were discovered (Burton et al., 2007; NJ et al., 2007). Studies showed that patients with inflammatory disease have an increased risk of CVD (Aviña-Zubieta et al., 2008; Ha et al., 2009; Roman et al., 2003). It was found that elevated levels of C-reactive protein (CRP), IL-6 and TNF in the plasma were associated with inferior clinical outcome in patients with coronary heart disease (Ridker et al., 1998; Ridker, Rifai, Pfeffer, et al., 2000; Ridker, Rifai, Stampfer, et al., 2000; Ross, 1999), leading to the introduction of inflammation as a therapeutic target in CVD (Hansson, 2005a).

10's: Checkpoint inhibitor treatment targeting negative regulators of atherosclerosis such as PD-1 and CTLA-4, is associated with increased risk of CVD in cancer patients (Bar et al., 2019; Tomita et al., 2017). Clinical trials were conducted showing beneficial effects of targeting inflammation in cardiovascular disease (Nidorf et al., 2020b; Ridker et al., 2017b; Tardif et al., 2019). Studies described the involvement of the bone marrow in atherosclerosis (Fuster et al., 2020; Jaiswal & Libby, 2020; Wang, Sano, et al., 2020), and single cell sequencing analysis of the human atherosclerotic plaque was performed (Depuydt et al., 2020a; Fernandez et al., 2019).

Blue boxes: Preclinical insights, Grey boxes: Clinical insights. Abbreviations: ACS = acute coronary syndrome; MI = myocardial infarction; TNF = Tumor Necrosis

Factor; VSMC = vascular smooth muscle cell. *This figure is adapted from Engelen et al., 2022.*

1.2 The immune system in atherosclerosis

The arterial wall is populated by a variety of immune cells, both in health and disease (Galkina et al., 2006; Roy et al., 2021). Human and mouse single-cell studies showed high heterogeneity of vascular leukocytes, which underscores the complexity of athero-inflammation (Cochain et al., 2018; Cole et al., 2018; Depuydt et al., 2020a; Fernandez et al., 2019; Gu et al., 2019; Kim et al., 2018; Lin et al., 2019; McArdle et al., 2019; Winkels et al., 2018; Zernecke et al., 2020). In a nutshell, athero-inflammation is orchestrated by the innate and adaptive immune system (Roy et al., 2021; Tabas & Lichtman, 2017) (Fig. 2). The innate immune system is the immediate defence against invading pathogens and is generally initiated by pattern recognition receptors, including Toll-like receptors (TLRs) that recognize pathogen-associated molecular patters (PAMPS) (Akira et al., 2006; O'Neill et al., 2013). The innate immune response leads to activation of antigen presenting cells (APCs) such as dendritic cells and macrophages enabling antigen presentation, co-stimulation and cytokine production by APCs. This is followed by engagement of the immune synapse to start the adaptive immune response. B and T cells are the key players in the adaptive immune response, which is slower but more specific and long-lasting than the innate immune response (Fig 2). Altogether, the continuous presence of inflammatory stimuli and failure of resolution mechanisms of inflammation lead to chronic inflammation in the vessel wall (Moore & Tabas, 2011).

1.2.1 Lipids and the innate immune response

A distinctive characteristic of athero-inflammation compared to other types of chronic inflammation is the key role for lipid particles in the immune response. Lipid particles enter the subendothelial space, mainly at sites of low shear stress due to haemodynamics, and undergo modification. Modified lipoproteins, namely oxidized LDL (oxLDL), provoke the immune response in the subendothelial space by acting as adjuvant molecular patterns activating the innate immune response (Binder et al., 2016; Stewart et al., 2010), and by acting as antigens activating the adaptive immune response (Roy et al., 2021; Stemme et al., 1995). The danger signals activate TLR signalling and the inflammasome in innate immune cells, evoking responses that drive inflammation, including cytokine secretion, release of neutrophil extracellular traps (NETs), upregulation of co-stimulatory molecules and stimulation of monocyte recruitment to the plaque (Hansson and Hermansson, 2011). Monocytes are recruited to atherosclerotic plaques where they differentiate into DCs and macrophages that show high functional and phenotypic heterogeneity (Tacke et al., 2007). In the plaque, macrophages take up lipoproteins and become lipid-laden foam cells, a hallmark of atherosclerosis. Foam cells in the plaque can be derived from transdifferentiation of vascular smooth muscle cells (VSMCs) as well (Fig.1.2). Foam cells drive necrotic core formation through increased endoplasmic reticulum (ER) stress and cell death, and lay the foundation for the plaque necrotic core (Zhao & Mallat, 2019).

1.2.2 The adaptive immune response

At the immune synapse, APCs such as macrophages, dendritic cells and B cells, present (lipid) antigens to invariant natural killer T (iNKT) cells and T cells,

engaging the adaptive component of the immune response (Roy, Orecchioni and Ley, 2021) which plays a key role in atherogenesis (Ketelhuth & Hansson, 2016; Saigusa et al., 2020). Activated T cells directly perform effector functions within the arterial wall or provide help to B cells to produce antibodies. $CD4^+$ T cells can promote atherogenesis or protect against it subject to the sublineage involved. The T_H1 subset has a pro-atherogenic role, while T_{regs} protect against atherosclerosis through secretion of anti-inflammatory cytokines such as IL-10 and TGFβ. Studies on the subsets T_H2 and T_H17 show that these hold more conflicting functions (Saigusa et al., 2020). $CD8^+$ T cells in the plaque also report dual functions, promoting atherogenesis through IFNγ production and macrophage activation, and protective effects via B cell modulation (Saigusa et al., 2020). $CD8^+$ T cells promote plaque inflammation and apoptosis driving instable plaque phenotypes and plaque erosion (Kyaw et al., 2013; van Duijn et al., 2018). In advanced atherosclerotic plaques $CD8^+$ T cells outnumber $CD4^+$ T cells and an increase of the number of $CD8^+$ cells has been found within the carotid plaque of symptomatic patients (Fernandez et al., 2019; Rossmann et al., 2008).

B cells are usually located within the adventitia or in tertiary lymphoid organs surrounding the artery in chronic inflammation, but are not always present (Ketelhuth & Hansson, 2016). Depending on the subset they either promote atherogenesis or protect against it. B_1 cells, derived from the foetal liver, play an athero-protective role via production of IgM antibodies that prevent the uptake of oxLDL by macrophages within lesions (Binder et al., 2016; Kyaw et al., 2011). B_2 cells, originating from the bone marrow, are considered pro-atherogenic mediated

by the production of high affinity antibodies that further drive adaptive immunity (Sage et al., 2015).

Altogether, these processes contribute to sustained endothelial dysfunction leading to continued monocyte recruitment, increased uptake of lipoproteins contributing to the plaque lipid core, VSMC activation and proliferation, and fibroblast migration contributing to fibrous cap formation. In advanced atherosclerosis, the culmination of complex chronic inflammatory processes results in formation of an atherosclerotic plaque with a large necrotic core covered by a thin fibrous cap, or other plaque morphologies associated with clinical vulnerability to rupture (Fig. 1.2).

Considering the central role of lipids in the development of atherosclerosis, Natural Killer T (NKT) cells are compelling, due to their restriction to lipid antigens presented on CD1d by antigen presenting cells (APC). Therefore, my thesis focuses on the role of NKT cells in atherosclerosis.

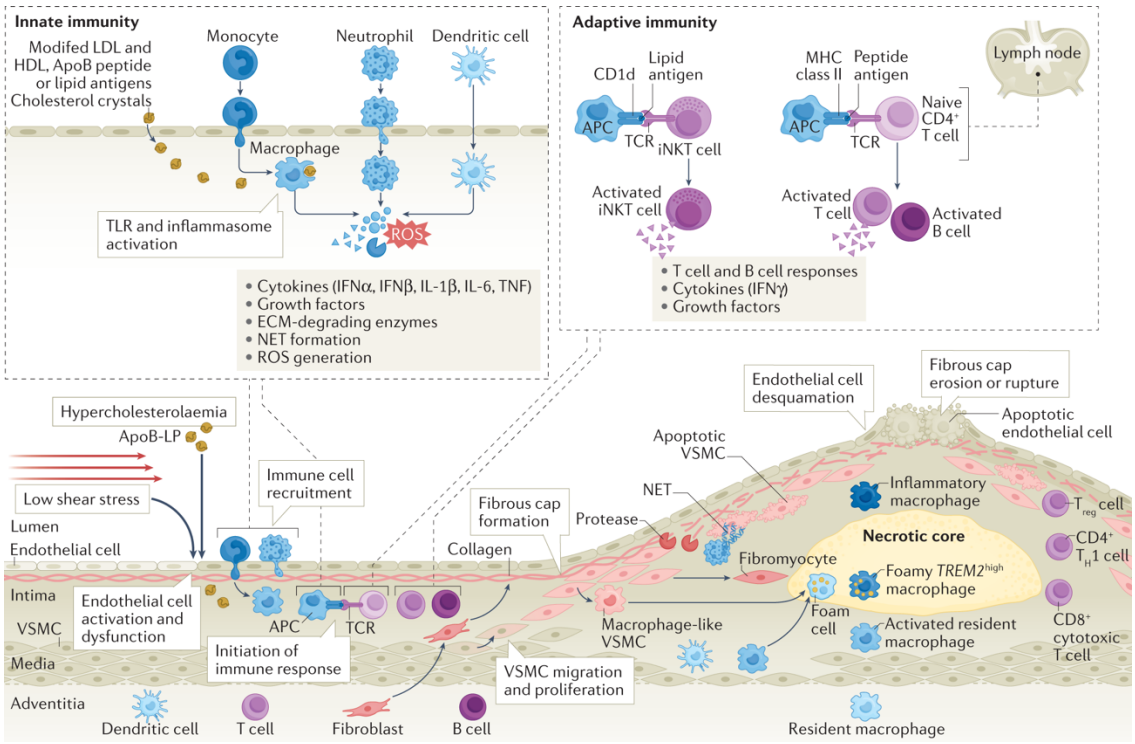

Figure 1.2 | Inflammation in atherosclerosis.

Haemodynamic forces within medium-large arteries create areas of low shear stress that determine the location of atherosclerotic plaque formation. In the early stages of atherogenesis circulating lipoproteins and ApoB peptides enter the sub-intimal space where they can undergo modification and can be recognised by immune cells as danger signals. This is followed by activation of TLRs and the inflammasome, evoking the innate response. The innate response drives inflammation through the production and secretion of cytokines, NETs and upregulation of co-stimulatory molecules. Macrophages ingest plaque lipoproteins and become lipid laden foam cells which are the basis of necrotic core formation. At the immune synapse in the atherosclerotic plaque, APCs such as dendritic cells, B cells an macrophages present (lipid) antigens to (iNK)T cells, eliciting the adaptive immune response including B and T cell responses. Antigen presentation occurs in secondary lymphoid organs, such as the lymph node as well. Here, APCs present to naïve T cells that differentiate into Treg or Teff cells. While Treg cells have atheroprotective functions, Teff cells engage the B cell response to produce circulating antibodies, promoting inflammation and immune cell recruitment to the plaque. Altogether this contributes to endothelial dysfunction leading to further aggravation of inflammation through monocyte recruitment, increased uptake of

lipoproteins adding to the lipid burden and smooth muscle cell activation and proliferation contributing to fibrous cap formation. In advanced atherosclerosis, the plaque becomes vulnerable to rupture or erosion due to thinning of the fibrous cap and increase of necrotic core size. Eventually this can lead to ischaemic events such as myocardial infarction or stroke. Abbreviations: APC = Antigen Presenting Cell; DC = Dendritic Cell; HDL = High Density Lipoprotein; IFN = Interferon; IL = Interleukin; iNKT = invariant Natural Killer T cell; LDL = Low Density Lipoprotein; NETs = Neutrophil Extracellular Traps; TNF = Tumor Necrosis Factor; ROS = Reactive Oxygen Species. This figure is adapted from Engelen et al., 2022.

1.3 Lipid antigen presentation by antigen presenting cells

1.3.1 CD1 molecules

CD1d is an MHC-like transmembrane protein that is part of the CD1 molecule family, which is involved in the presentation of rather lipid antigens than peptides antigens to non-MHC restricted T cells (Brigl et al., 2003). In humans, the CD1 family includes five isoforms which are divided in three groups. CD1a, CD1b and CD1c are part of group 1 and play a role in antigen presentation to polyclonal T cells. CD1d is part of group 2 and is restricted to presentation of lipid antigens to invariant Natural Killer T cells. CD1e, which is not expressed on the cell surface, is part of group III and is involved in intracellular lipid handling (Facciotti et al., 2011). In mice, only the Cd1d isoform is expressed which is encoded for by two separate genes, Cd1d1 and Cd1d2, which display similar structural characteristics to human CD1d (Zimmer et al., 2009).

The antigen-presentation site of CD1d consists of two α-helices (α1 and α2), below which two deep hydrophobic channels are located, the A' and F' channels. This structure facilitates the capture of the hydrophobic tails of lipid antigens, with the

hydrophilic group pointing outwards, allowing for TCR interaction (D. C. Barral & Brenner, 2007).

1.3.2 CD1d expression

CD1d is expressed on professional APCs such as dendritic cells, B cells and macrophages (Sugita et al., 2007). The majority of studies on iNKT cell biology are conducted in this context. However, several non-immune cell subsets express CD1d as well, including adipocytes, hepatocytes, Kupffer cells, Paneth cells and tumour cells (Dougan et al., 2007; Lacasse & Martin, 1992; W.-Y. Lee et al., 2010; Liu et al., 2013). In the adipose tissue, iNKT cell function is modulated by adipocytes, acting as lipid antigen-presenting cells in a CD1d-mediated fashion (Schipper et al., 2012). In the liver, CD1d expression on hepatocytes plays a role in homing of NKT cells in the liver, where NKT cells are enriched (Geissmann et al., 2005). CD1d-positive tumour cells in medulloblastoma cross-presented glycolipid antigens to activate iNKT cell cytotoxicity (Liu et al., 2013). In this thesis, I focus on CD1d expressed on professional APCs.

1.3.3 CD1d loading and presentation

Loading of lipid antigens onto CD1d occurs through two general routes, the secretory pathway and the endolysosomal pathway. The secretory pathway, which is similar in mouse and human, starts in the ER, where the newly synthesized CD1d binds to β_2-microglobulin (B2M). Subsequently, the CD1d-B2M transitions to the Golgi, where it binds endogenous chaperone glycolipids. Microsomal triglyceride transfer proteins (MTPs) mediate the binding of glycolipids to CD1d in the Golgi. The lipid-loaded CD1d is then transported from the Golgi to the plasma membrane

for potential recognition by the TCR on iNKT cells. In the endolysosomal pathway, CD1d from the cell membrane is endocytosed to the endolysosomes, where glycolipids can be loaded onto the CD1d molecule. In addition to MTPs, additional lipid transfer proteins, such as saposins and Niemann–Pick C 1 and 2, mediate the loading of lipids onto CD1d in the endolysosomes. When properly loaded with an antigen, the CD1d complex transitions to the cell membrane, where it engages the invariant TCR on the iNKT cell. The TCR recognizes the surface-exposed polar moieties of the presented lipids and induces a subsequent rapid response by the iNKT cells (D. C. Barral & Brenner, 2007; Sugita et al., 2007).

1.4 Natural Killer T cells

1.4.1 Defining Natural Killer T cells

NKT cells are so called because they express both characteristics of adaptive immunity such as a T cell receptor (TCR), and surface receptors for NK cells (NK1.1/CD161, Ly49), which are part of the innate immune response. This co-expression illustrates the hybrid nature of these cells bridging innate and adaptive immunity (van Puijvelde & Kuiper, 2017). There are two major types of NKT cells: Type 1 NKT cells, also known as invariant NKT (iNKT) cells, express a semi-invariant TCR that in mice is composed of the TCRα chain Vα14–Jα18 coupled with a limited set of TCRβ chains (Vβ8.2, Vβ7, and Vβ2) and in humans of Vα24–Jα18 TCRα chain paired with the TCRβ chain Vβ11. Type II NKT cells express a more variable repertoire of TCRs. Type I and type II NKT cells are also distinct in terms of lipid antigen recognition. Type I NKT cells are potently activated by α-galactosylceramide (αGalCer), while the nature of the lipids that activate type II NKT cells is not well established (Bendelac et al., 2007). iNKT cells are further divided into four

sublineages based on their expression of transcription factors and cytokine production. Tbet$^+$ NKT1 cells, the most predominant iNKT cells, produce IFNγ and IL-4. GATA3$^+$ NKT2 cells produce mainly IL-4, FOXP3$^+$ NKT10 cells produce IL-10 and RORγt$^+$ NKT17 cells produce IL-17A, IL-21, and IL-22 (Y. J. Lee et al., 2013; Monteiro et al., 2010).

iNKT cells develop in the thymus, and go through a similar trajectory as αβ T cells up to the point of becoming CD4$^+$CD8$^+$ or double positive (DP) thymocytes in the thymic cortex. Next, thymic education drives iNKT cell differentiation through TCR interactions with CD1d molecules bound with self-glycolipid on other double positive (DP) thymocytes in the thymic cortex (Bendelac, 1995; Griewank et al., 2007).

1.4.2 Natural Killer T cell activation

To date, two distinct modes of NKT cell activation have been described, which are both involved in atherogenesis (Fig. 1.3). First, APCs activate NKT cells by presenting lipid antigens bound to the CD1d molecule on their cell surface. The lipid antigens are loaded onto CD1d molecules in the endosomal/lysosomal compartments and can be either endogenous self-lipids or exogenous lipids. Via interaction with the invariant TCRs expressed on the surface of NKT cells, lipid antigens presented on CD1d can activate NKT cells (Freigang et al., 2012; Getz & Reardon, 2017; Ververs et al., 2018). Co-stimulatory and co-inhibitory interactions between iNKT and APCs can modulate CD1d-mediated activation iNKT cell activation. Examples of co-stimulatory interaction pairs include inducing co-stimulators CD28/B7, ICOS/ICOSL (ICOS ligand), CD28/B7, CD40L/CD40, and

inhibitory pathways such as PD1/PDL1 (Shissler et al., 2017). Second, NKT cells express receptors for various cytokines which play a role in NKT cell activation, including IL-12, IL-18, IL-23, and IL-25 (L. Chen & Flies, 2013). APCs can initiate production of these cytokines by binding of components of oxidized LDL to TLR4 on APCs (Zajonc & Girardi, 2015). Cytokine stimulation is typically less strong and an additional TCR signal is required for robust NKT cell activation.

Upon activation, iNKT cells employ their immunomodulatory potential through secretion of cytokines, promotion of cytolytic effects, and modulation of the activity of bystander immune cells. They can rapidly secrete a variety of pro-inflammatory Th1 cytokines (IFNγ, IL-2 and IL-12), anti-inflammatory Th2 cytokines (IL-4 and IL-10), and regulatory Th17 cytokines (IL-17) (Bendelac et al., 2007). Furthermore, NKT cells obtain cytolytic activity by production of granzyme B, perforin and Fas Ligand (FasL) (van Puijvelde & Kuiper, 2017). Finally, iNKT cells can activate other immune cells (e.g. macrophages, DCs, NK cells, conventional T cells, and B cells), and other immune cells on their turn modulate the activity of iNKT cells (Eberl et al., 2000; Fujii et al., 2003; Hegde et al., 2009; Kitamura et al., 2000; Nishimura et al., 2000; Villanueva et al., 2015). For example, IFNγ secretion from iNKT cells induces transactivation of NK cells (Smyth et al., 2001) and iNKT cells provide CD1d-restricted help to B cells inducing B cell proliferation and antibody production (Galli et al., 2003).

Repeated stimulation of iNKT cells, particularly with a strong agonist such as αGalCer, induces unresponsiveness to a subsequent stimulus or anergy (Sullivan & Kronenberg, 2005). The unresponsiveness lasts for over a month and can be

reversed by addition of exogenous IL-2 (Parekh et al., 2005). The exact mechanism behind iNKT cell anergy remains elusive. However, blockade of PD1 can partly prevent the induction of iNKT cell anergy suggesting a role for PD1/PDL1 costimulatory pathway in induction of iNKT cell anergy (Parekh et al., 2009).

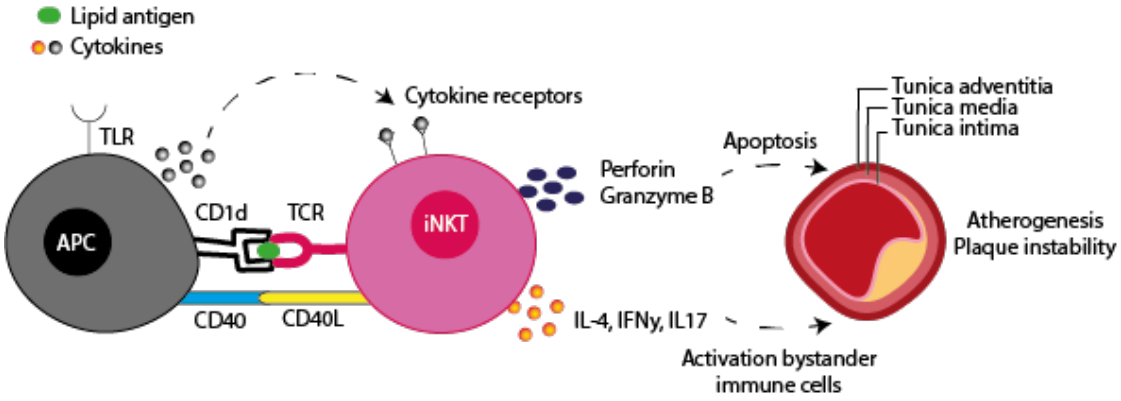

Figure 1.3 | Schematic overview of the interaction between APC and iNKT cell. iNKT cells can be activated via two distinct pathways. 1) CD1d-TCR mediated activation: APCs present lipid antigens on CD1d and activation occurs through interaction with the invariant TCRs expressed on the surface of iNKT cells. Co-stimulatory and co-inhibitory interactions between iNKT and APCs regulate CD1d mediated iNKT cell activation. 2) Cytokine mediated activation: APCs produce cytokines including IL-12, IL-18, IL-23, and IL-25 which can directly activate iNKT cells through cytokine receptors. Cytokine stimulation is typically required together with a TCR signal for robust iNKT cell activation. Upon activation iNKT cells rapidly secrete pro- and anti-inflammatory cytokines, cytotoxins (perforin and granzyme B), and modulate the activation of bystander immune cells. This leads to apoptosis which induces necrotic core formation and drives atherogenesis and plaque instability. Abbreviations: APC = Antigen Presenting Cell; IL = Interleukin; IFN = Interferon; iNKT = invariant Natural Killer T cell; TCR = T cell receptor; TLR = Toll Like Receptor.

1.4.3 Lipid antigens activating NKT cells

The model lipid antigen used in the NKT field is *α*-GalactosylCeramide (αGalCer), because of its high potency *in vivo* and *in vitro*. αGalCer is a glycosphingolipid (GSL) originally derived from Sphingmonas bacteria which are present in the marine sponge *Agelas mauritianus*. Nowadays, αGalCer is chemically synthesized and this compound is known as KRN7000. The *α* indicates the orientation of the linkage between the hydrophilic carbohydrate head group and the hydrophobic lipid tails (Brennan et al., 2013). Other exogenous lipid antigens include mainly bacteria derived lipids such as α-galactosyldiacylglycerol derived from *Borrelia burghdorferi* and *Streptococcus pneumoniae* (Kinjo et al., 2006), glycosphingolipid-1 (GSL-1) which is found in *Sphingomonas* (Long et al., 2007), and cholesteryl α-glucoside from *Helicobacter Pylori* (Chang et al., 2011).

Lipid antigens are required for iNKT cell development in the thymus and iNKT cells can be activated by APCs through stimulation with TLR agonists in absence of infection, and thus in absence of pathogen-associated lipid antigens (Paget et al., 2007; Salio et al., 2007). Various mammalian GSL, such as isoglobotryhexosylceramide (iGb3) and *β*-glucosylceramide (*β*GlcCer), have been identified as endogenous lipid antigens (Brennan et al., 2013). However, the relevance of these lipid antigens is questionable given that iGb3-synthase deficient mice showed normal iNKT cell development and phenotype and the ability of iGb3 to activate iNKT cells in humans is limited (Porubsky et al., 2007). Furthermore, humans lack the iGb3 synthase making it unlikely that active iGb3 is naturally expressed in humans (Christiansen et al., 2008). Studies on *β*GlcCer showed conflicting results as well, with some studies indicating iNKT reactivity to *β*GlcCer

in humans and mice (Brennan et al., 2011), whereas others showed absence of iNKT cell responses upon CD1d βGlcCer presentation (Stanic et al., 2003). These contradicting results could be explained by two studies showing that there was a small fraction of α-linked glycosylceramides present in βGlcCer preparations (Brennan et al., 2014; Kain et al., 2014). Lysophosphaditylcholine, β-lactosylceramide, (plasmalogen lyso-) phosphatidylethanolamine and phosphatidylinositol are also possible candidates for endogenous lipid antigens due to their role in NKT cell development and ability to potently activate iNKT cells in mice (Facciotti et al., 2012). It remains unknown which lipid antigens drive iNKT cells function in atherogenesis and how they are transported through the circulation.

1.4.4 Natural Killer T cells in healthy and diseased settings

iNKT cells are distributed through a variety of tissues. In mice, iNKT cell numbers are the highest in the liver (12-30% of lymphocytes), and are present in lower frequencies in the spleen, lungs, thymus, bone marrow and blood ranging from 0.05-1%. The overall tissue distribution of iNKT cells in humans and mice is similar, but their frequency is around ten times lower in humans compared to mice (Slauenwhite & Johnston, 2015).

NKT cells have been implicated in the pathophysiology of various diseases. In microbial infection, NKT cells play a protective role owing to their rapid cytokine response and their ability to activate bystander immune cells (Brigl et al., 2003). Administration of the lipid antigen αGalCer provides protection against several bacterial and viral microbial infections including *M. Tuberculosis, Pseudomonas*

aeruginosa, respiratory syncytial virus and encephalomyocarditis virus (Chackerian et al., 2002; Exley et al., 2001; Johnson et al., 2002; Nieuwenhuis et al., 2002).

In Non Obese Diabetic (NOD) mice, a model for type I diabetes, iNKT cells are defective and treatment of these mice with αGalCer has anti-diabetogenic effects (Fletcher et al., 2008). Cytokine release by iNKT cells is probably important for this protection, but the mechanisms by which endogenous iNKT cells provide protection *in vivo* are not understood. In human identical twins of which one developed type 1 diabetes, lower frequencies of iNKT cells were found in the diabetic sibling compared to the healthy sibling. iNKT cells isolated form the diabetic sibling produced IFNγ upon stimulation, while the healthy sibling produced both IL-4 and IFNγ indicating anti-inflammatory properties in the latter (Wilson et al., 1998).

In the adipose tissue, iNKT cells exhibit anti-inflammatory properties by secretion of IL-4. They help maintain adipose tissue homeostasis and protect against insulin resistance and inflammation. In obesity, iNKT cells lose the ability to produce IL-4 leading to tissue inflammation, insulin resistance and subsequent development of type 2 diabetes (Lynch et al., 2014; Schipper et al., 2012).

In murine cancer models, administration of αGalCer has shown impressive results on anti-tumour immunity, mainly through activation of bystander immune cells in the tumour environment (Berzins & Ritchie, 2014). Furthermore, mouse studies on a T cell lymphoma model showed that iNKTs can directly kill tumour cells expressing CD1d via perforin and granzyme B secretion (Gorini et al., 2017). In

human trials predominantly focussing on lung cancer or head and neck squamous cell carcinoma, the anti-tumour effect has been limited due to iNKT cell anergy upon repetitive stimulation with αGalCer (Waldowska et al., 2017). However, the first results of an ongoing study in patients with neuroblastoma using CAR-NKT cells has shown promising results on tumour regression (Heczey et al., 2020).

Unlike the above, iNKT cells seem to induce disease in asthma (Umetsu & DeKruyff, 2010). iNKT cells have been found to be essential is mouse models of allergic asthma (Akbari et al., 2003; Lisbonne et al., 2003), and bronchoalveolar lavage fluid samples from patients with asthma were shown to have very high numbers of iNKT cells (more than 50% of the total CD4+ T cells) (Akbari et al., 2006).

Altogether, NKT cells play a protective role in several diseases such as microbial infection, type 1 diabetes, obesity and cancer. However, they are promoting disease in asthma and atherosclerosis (described below). The exact mechanism of skewing of iNKT cells toward an anti- or pro-inflammatory mechanism remains unknown.

1.4.5 Natural Killer T cells in atherogenesis

In 2002, the role of NKT cells in atherosclerosis was implied for the first time in a study showing correlation between increased plaque size and increased number of IL-4 producing T cells in *ApoE*$^{-/-}$ mice treated with lipopolysaccharide (Ostos et al., 2002). This is followed-up by numerous murine studies showing that NKT cells can promote atherogenesis (Table 1). In these studies, several models of NKT cell deficiency and atherosclerosis were used. *Jα18*$^{-/-}$ mice lack the invariant TCRα chain and are deficient in iNKT cells. *Cd1d*$^{-/-}$ mice lack CD1d and therefore there is no

development of iNKT and type II iNKT cells in the thymus (Y. H. Chen et al., 1997; Cui et al., 1997). These models have been combined with classic murine models of hypercholesterolemia driving atherosclerosis including the *ApoE*$^{-/-}$ strain, which leads to spontaneous development of atherosclerosis, and the *Ldlr* $^{-/-}$ strain, which requires a high cholesterol diet to develop atherosclerosis (Daugherty, 2002; Nakashima et al., 1994).

Studies investigating murine models of deficiency of NKT cells have consistently shown reduced atherosclerotic lesion formation (Aslanian et al., 2005; Major et al., 2004; Nakai et al., 2004; Rogers et al., 2008; Tupin et al., 2004). For example, *Jα18*$^{-/-}$ *Ldlr* $^{-/-}$ mice showed reduced lesion size and reduced expression of IFNγ in the plaque compared to *Ldlr* $^{-/-}$ mice (Rogers et al., 2008). Furthermore, lesion size was significantly reduced in *CD1d*$^{-/-}$ *Apoe*$^{-/-}$ mice compared with *Apoe*$^{-/-}$ mice (Table 1.1) (Major et al., 2004).

Activation of iNKT cells with αGalCer *ApoE*$^{-/-}$ mice resulted in a 1.5-2.0 fold increase in aortic root atherosclerosis compared with untreated *ApoE*$^{-/-}$ mice and increased mRNA levels of IFNγ, IL4 and IL-10 in the aorta upon treatment (Major et al., 2004; Nakai et al., 2004; Tupin et al., 2004). In one single study αGalCer has shown atheroprotective effects. This study investigated carotid perivascular collar induced atherosclerosis in *ApoE*$^{-/-}$ and *Ldlr* $^{-/-}$ mice fed a western type diet for nine weeks. This resulted in a strong reduction of atherosclerosis in *Ldlr* $^{-/-}$ mice and had no effect in *ApoE*$^{-/-}$ mice (Van Puijvelde et al., 2009). Here, the use of a different model of atherosclerosis complicates interpretation of the results in comparison to other studies mentioned above (Table 1.1).

Adoptive transfer experiments further corroborated the proatherogenic activity of iNKT cells. Lymphocyte deficient *Rag2*$^{-/-}$ crossed with *ApoE*$^{-/-}$ mice underwent adoptive transfer with CD4^{+} NKT cells which led to an increase in atherosclerotic plaque size (Y. Li et al., 2015). To unravel whether cytokines or cytotoxic proteins were the main driver of the proatherogenic effect of NKT cells, hyperlipidemic mice lacking iNKT cells (*Jα18*$^{-/-}$ *ApoE*$^{-/-}$) were adoptively transferred with CD4^{+} NKT cells derived from mice lacking IFNγ, IL-14 or IL-21, or granzyme B or perforin. These studies showed that granzyme B and perforin were the main drivers of the proatherogenic effects of NKT cells (Table 1.1) (Li et al., 2015).

More recently, treatment of *ApoE*$^{-/-}$ mice with 1,2-dipalmitoyl-sn-glycero-3-phosphoethanolamine-N[methoxy (polyethyleneglycol)−350 (DPPE-PEG_{350}) showed reduced inflammation and necrotic core size. DPPE-PEG_{350} is a CD1d dependent lipid antagonist that prevents presentation of lipid antigens on CD1d. Although these results propose DPPE-PEG_{350} as a promising therapeutic to target iNKT cells, no follow-up studies have been published (Li et al., 2016).

Table 1.1 | NKT cells in murine models of atherosclerosis.

Alteration NKT cells	Mouse strain	Diet	Manipulation	Effect on plaque
Increased activation or number	*Apoe*$^{-/-}$	Chow WTD	αGalCer	⬆ Aortic root (Major et al., 2004; Nakai et al., 2004; Tupin et al., 2004) = Carotid (perivascular collar) (Van Puijvelde et al., 2009)
	Ldlr$^{-/-}$	WTD	αGalCer	⬇ Carotid (perivascular collar) (Van Puijvelde et al., 2009)
Adoptive transfer	*Rag1*$^{-/-}$ *Ldlr*$^{-/-}$	WTD	Adoptive transfer splenocytes iNKT cells	⬆ Aortic root (VanderLaan et al., 2009)
	Rag2$^{-/-}$ *ApoE*$^{-/-}$	WTD	Adoptive transfer of purified NKT cells	⬆ Aortic root (Y. Li et al., 2015)
	Rag1$^{-/-}$ *Ldlr*$^{-/-}$	WTD	Adoptive transfer of *Cd1d*$^{-/-}$ splenocytes	= Aortic root, = Aorta (VanderLaan et al., 2007)
Deficiency	*Cd1d*$^{-/-}$	WTD	NKT cell-deficient	⬇ Aortic root (Nakai et al., 2004)
	Ldlr$^{-/-}$	WTD	Transplanted with *Cd1d*$^{-/-}$ bone marrow	⬇ Aortic root (Nakai et al., 2004)
	CD1d$^{-/-}$ *Apoe*$^{-/-}$	Chow	NKT deficient, αGalCer	⬇ Aortic root (Major et al., 2004; Tupin et al., 2004)
	CD1d$^{-/-}$ *Ldlr*$^{-/-}$	WTD	NKT cell deficient	⬇ Aortic root (Aslanian et al., 2005)
	Jα18$^{-/-}$ *Ldlr*$^{-/-}$	WTD	iNKT cell deficient	⬇ Aortic root (Rogers et al., 2008)
CD1d antagonist	*Apoe*$^{-/-}$	WTD	DPPE-PEG$_{350}$	⬇ Aortic root (Y. Li et al., 2016)

Abbreviations: αGalCer = alpha-galactosylceramide; iNKT = invariant Natural Killer T cell; WTD = western type diet. *Table adapted from Getz et al., 2017.*

1.5 Lipoproteins

1.5.1 Lipoprotein composition

Lipids, such as cholesterol and triglycerides, are hydrophobic and are therefore carried in lipoproteins that transport the lipids to various tissues to contribute to energy metabolism, synthesis of hormones and bile acid formation. Lipoproteins consist of a hydrophobic core containing cholesterol esters and triglycerides surrounded by a shell containing free cholesterol, phospholipids, and apolipoproteins. Plasma lipoproteins are divided into seven classes (chylomicrons, chylomicron remnants, VLDL, IDL, LDL, HDL, and Lp (a)) based on size, lipid content and apolipoproteins (Table 1.2) (Mahley et al., 1984). Apolipoproteins have four major functions including providing structure, lipoprotein assembly, acting as ligands for lipoprotein receptors, and activation or inhibition of enzymes involved in lipoprotein metabolism (Mahley et al., 1984).

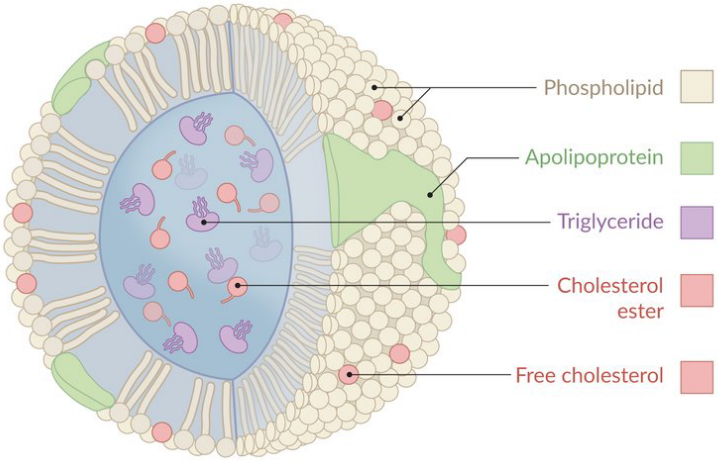

Figure 1.4 | Schematic overview of lipoprotein composition. Lipoproteins consist of a hydrophobic core containing cholesterol esters and triglycerides surrounded by a shell containing free cholesterol, phospholipids, and apolipoproteins. Figure adapted from Amboss Medical Encyclopaedia.

Table 1.2 | Lipoprotein classes and characteristics in human plasma.

Lipoprotein	Apolipoprotein	Density (g/mL)	Size (nm)
Chylomicrons	ApoB-48, Apo C, Apo E, Apo A-I, A-II, A-IV	<0.95	75-1200
Chylomicron remnants	ApoB-48, Apo E	0.930-1.006	30-80
VLDL	ApoB-100, Apo E, Apo C	0.930-1.006	30-80
IDL	ApoB-100, Apo E, Apo C	1.006-1.019	23-35
LDL	ApoB-100	1.019-1.063	18-25
HDL	ApoA-I, ApoA-II, Apo C, ApoE	1.063-1.210	5-12
Lp (a)	Apo (a), ApoB-100	1.055-1.085	25-30

1.5.2 The contribution of lipoproteins to atherogenesis

Different lipoproteins vary with respect to their contribution to atherogenesis. VLDL and LDL exert pro-atherogenic properties by promoting endothelial dysfunction, monocyte infiltration and expression of pro-inflammatory genes (Borén et al., 2020; Ference et al., 2017). More recently, the pro-atherogenic role of Lp (a) has been emphasized, exerting pro-inflammatory and pro-coagulant properties in the subendothelial space (Tsimikas, 2017). In contrast, HDL particles exert anti-atherogenic properties including cholesterol efflux from macrophages, antithrombotic effects and improving endothelial cell function and blood viscosity (Rosenson et al., 2015).

1.5.3 Systemic lipoprotein metabolism: exogenous and endogenous pathways

Lipoprotein metabolism can be divided in exogenous and endogenous pathways. The exogenous lipoprotein pathway starts with intestinal absorption of dietary lipids and assembly into chylomicrons. In the circulation, lipoprotein lipase acts

upon chylomicrons releasing free fatty acids, which are subsequently metabolized by muscle and adipose tissue. The end-product of this process are chylomicron remnants which are cleared from the circulation by the liver. The endogenous lipoprotein pathway begins in the liver with the synthesis of VLDL. The triglycerides carried in VLDL are metabolized in muscle and adipose tissue by lipoprotein lipase releasing free fatty acids. The remaining lipoprotein is now called IDL. The IDL particles are either cleared from the circulation by the liver or further metabolized to LDL by hepatic lipase. LDL on its turn can be taken up in numerous tissues including the liver, the predominant site of uptake, but also by immune cells. The uptake of LDL is mainly mediated by the LDL receptor (LDLR).

Reverse cholesterol transport starts with hepatic and intestinal synthesis of small nascent HDL particles composed of phospholipids and lipoproteins. These small HDL particles can then procure shell components (cholesterol, apolipoproteins and phospholipids) from chylomicrons and IDL. This process is mediated by ATP Binding Cassette Subfamily A Member 1 (ABCA1), also known as the cholesterol efflux regulatory protein, resulting in the formation of mature HDL. Mature HDL can acquire additional cholesterol from cells via ATP Binding Cassette Subfamily G Member 1 (ABCG1), Scavenger receptor B1 (SR-B1), or passive diffusion. The HDL then transports the cholesterol to the liver by directly interacting with hepatic SR-B1 or indirectly by transferring the cholesterol to VLDL or LDL, which is facilitated by cholesteryl ester transfer protein (CETP) (Rosenson, 2019).

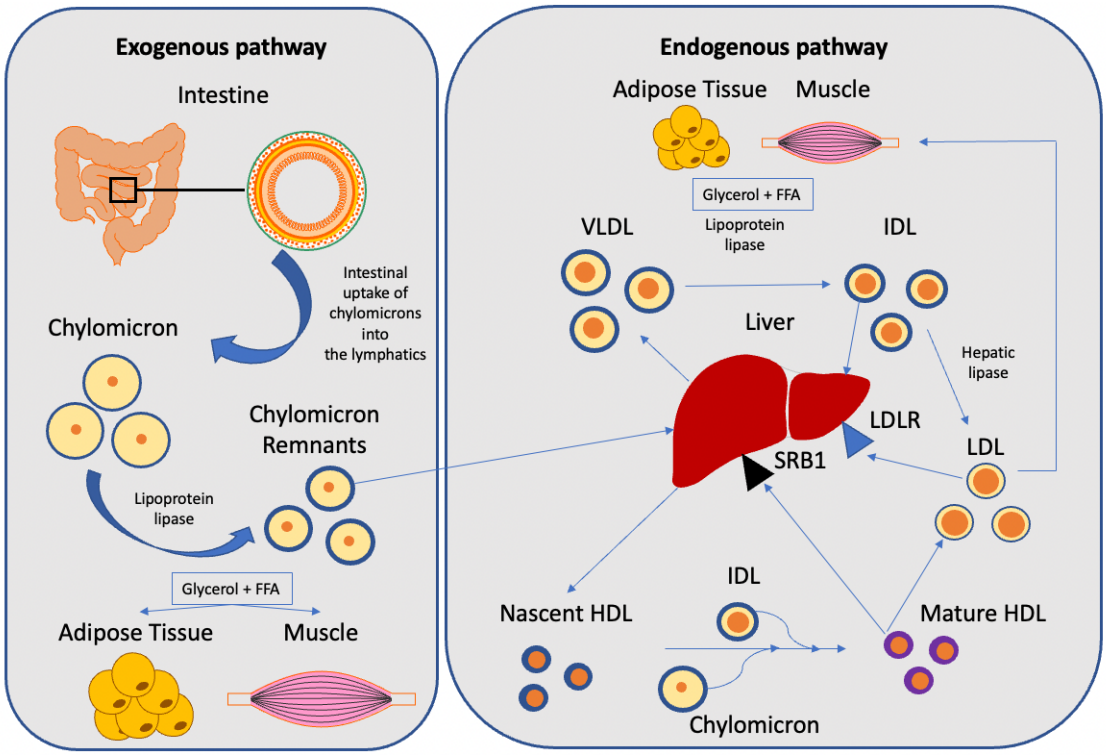

Figure 1.5 | Schematic overview of the exogenous and endogenous lipoprotein metabolism pathway.

Exogenous pathway: In the intestine, free fatty acids and glycerol are absorbed and form triglycerides which are assembled to chylomicrons that are transported into the lymphatic system. Chylomicrons enter the circulation and are hydrolyzed by lipoprotein lipase, releasing triglycerides and free fatty acids, which are metabolized by the tissues. Chylomicron remnants are cleared from the circulation by the liver.

Endogenous pathway: VLDL, which is synthetised by the liver, is cleaved into smaller VLDL remnants called IDL by lipoprotein lipase. IDL is either directly cleared by the liver or hydrolyzed by hepatic lipase to form LDL which can be cleared by the liver through the LDLR. Reverse cholesterol transport starts with synthesis of nascent HDL particles which can be transformed to mature HDL particles through interaction with chylomicrons and IDL. Mature HDL can acquire cholesterol from cells and transports the cholesterol to the liver by directly interacting with hepatic SR-B1 or indirectly by transferring the cholesterol to VLDL or LDL. Abbreviations: ABCA1 = ATP Binding Cassette Subfamily A Member 1; ABCG1 = ATP Binding Cassette Subfamily G Member 1; FFA = Free fatty acid; HDL =

High Density Lipoprotein; IDL = Intermediate Density Lipoprotein; LDL = Low Density Lipoprotein; VLDL = Very Low Density Lipoprotein; LDLR = LDL-Receptor; SRB1 = Scavenger receptor B1.

1.5.4 Cellular cholesterol metabolism: uptake, synthesis and efflux

Cholesterol is the most abundant lipid species in mammalian cells, making up 25% of the plasma membrane lipids. Cholesterol is essential for all cells, as it contributes to membrane integrity, fluidity and biochemical interactions (M. Lee & Bensinger, 2022). However, excess intracellular cholesterol is toxic and can lead to cellular dysfunction and activation of the inflammasome, causing inflammation (Guo et al., 2015). Therefore intracellular cholesterol content is tightly regulated. Cellular cholesterol needs can be met via import through uptake of lipoproteins and intracellular cholesterol synthesis.

Immune cells preferentially utilize imported cholesterol via LDL-receptor mediated internalization of LDL particles. LDLR is expressed on the cell surface and can bind circulating LDL particles, which can be internalized through clathrin-coated vesicles by endocytosis. Next, LDL is hydrolysed by lipases in lysosomes, releasing free cholesterol. Niemann-Pick Type C1 and C2 proteins then export free cholesterol from the lysosomal compartment to cell membrane or the ER for further distribution through the cell (Luo et al., 2020). Alternative uptake mechanisms for cholesterol include uptake of modified LDL particles by scavenger receptors such as scavenger receptor A, CD36 and LOX-1 (Ding et al., 2018). Intracellular cholesterol is sensed in the ER, and regulated by sensor response element binding protein 2 (SREBP-2). SREBP-2 is bound to SREBP cleavage activating protein (SCAP) and insulin-induced gene 1 protein (INSIG). When intracellular cholesterol levels are

low, SREBP2 translocates to the Golgi, where it is cleaved by proteases. Cleaved SREBP2 is transported to the nucleus where it acts as a transcription factor inducing LDLR expression to increase cholesterol uptake, and promotes expression of genes involved in intracellular cholesterol synthesis (Cardoso & Perucha, 2021). Cholesterol is synthesized from acetyl-CoA through a series of enzymatic steps with 3-hydroxy-3-methylglutaryl coenzyme A reductase (HMGCR) as a rate limiting step. When intracellular cholesterol levels are high, cholesterol can be either stored in intracellular lipid droplets or is exported to the circulation. In high cholesterol conditions liver X receptor (LXR) transcription factors are activated, which regulate the expression of cholesterol export molecules ABCA1 and ABCG1 that facilitate efflux (Luo et al., 2020).

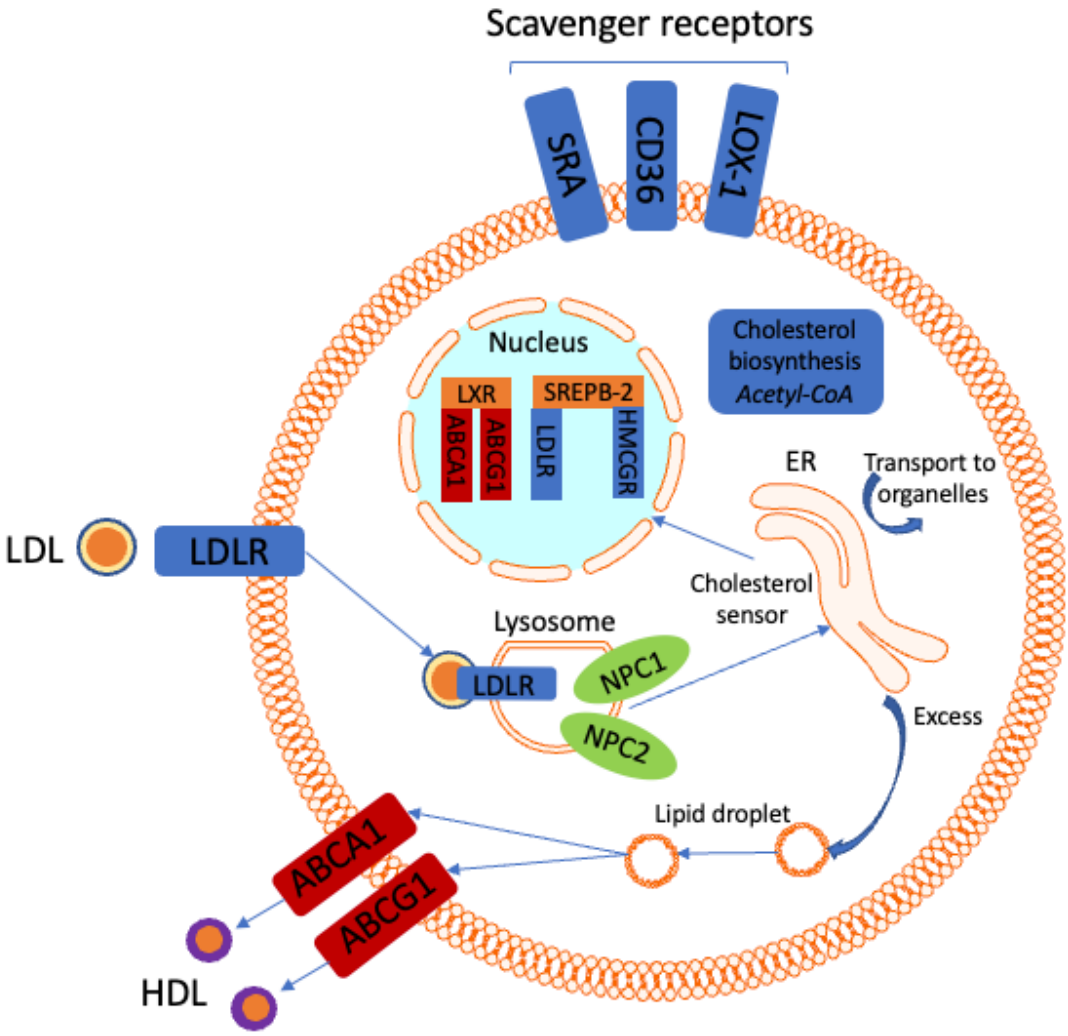

Figure 1.6 | Schematic overview of cellular cholesterol metabolism.
Cellular cholesterol content is tightly regulated. In immune cells cholesterol is mainly acquired through LDL-receptor mediated internalization of LDL particles. Endocytosed LDL is transported to lysosomes, where lipases hydrolyse LDL, releasing free cholesterol. Niemann-Pick Type C1 (NPC1) and C2 (NPC2) proteins then export free cholesterol from the lysosomal compartment to the cell membrane compartment or to the ER for further distribution through the cell. Alternative uptake mechanisms for cholesterol include uptake of modified LDL particles by scavenger receptors such as scavenger receptor A (SRA), CD36 and LOX-1. Intracellular cholesterol is sensed in the ER, and regulated by sensor response element binding protein 2 (SREBP-2). Cleaved SREBP2 is transported to the nucleus where it acts as a transcription factor promoting increased LDLR expression to

enhance uptake of cholesterol, and increased expression of genes involved in intracellular cholesterol synthesis such as 3-hydroxy-3-methylglutaryl coenzyme A reductase (HMGCR). When intracellular cholesterol levels are high, cholesterol can be either stored in intracellular lipid droplets or is exported to the circulation via ABCA1 and ABCG1. ABCA1 and ABCG1 expression are regulated by liver X receptor (LXR) transcription factors, which are upregulated in high cholesterol conditions. Abbreviations: ABCA1 = ATP Binding Cassette Subfamily A Member 1; ABCG1 = ATP Binding Cassette Subfamily G Member 1; AcetylCoA = acetyl coenzyme A; HDL = High Density Lipoprotein; HMGCR = HMG-CoA reductase; LDL = Low Density Lipoprotein; LDLR = LDL-Receptor; LXR = liver X receptor; NPC1 = Niemann-Pick Type C1; NPC2 = Niemann-Pick Type C2; SRA = Scavenger receptor A.

1.6 Hypothesis and Aims

This thesis is built on the following hypotheses:

1. Lipoproteins can bind lipid antigens and hence are involved in lipid antigen delivery to APCs, and subsequent iNKT cell activation.
2. NKT cells in the human atherosclerotic plaque play a pro-atherogenic role.
3. Macrophages, which are known for lipoprotein uptake in the atherosclerotic plaque, are the main APC to interact with iNKT cells in the human atherosclerotic plaque.

The aims for this thesis include:

1. To unravel the role of lipoproteins in lipid antigen binding and delivery to APCs (Chapter 2).
2. To study the relation between human plaque-resident NKT cells, patient characteristics, plaque histomorphology and cardiovascular outcome (Chapter 3).
3. To study the cellular niche of iNKT cells in the human atherosclerotic plaque to identify the APC involved in the APC-iNKT immune synapse (Chapter 4).

2 Lipid antigen delivery to antigen presenting cells

2.1 Introduction

iNKT cells are a specialized subset of T cells that recognize foreign and self lipid antigens presented by the MHCI-like molecule CD1d on APCs (Brennan et al., 2013). Upon activation, iNKT cells exert their immunomodulatory potential through secretion of cytokines, promotion of cytolytic effects, and modulation of the activity of bystander immune cells. (Bendelac et al., 2007; Brennan et al., 2013). Most of the foreign lipid antigens identified so far are hydrophobic glycolipids with a ceramide or glycerol backbone, such as *Sphingomonas*-derived glycosylceramides. These compounds structurally resemble the model iNKT cell antigen α-galactosylceramide (αGalCer) (Kinjo et al., 2011). How lipid antigens are delivered to APCs that regulate iNKT cell activation remains unclear.

Apolipoprotein E (ApoE) is known to facilitate the uptake of lipid antigens by APCs (Allan et al., 2009; Van Den Elzen et al., 2005). Whether ApoE acts alone is currently unknown. The functional characteristics of ApoE yet suggest concerted action with lipoproteins. The vast bulk of ApoE and other apolipoproteins is bound to the phospholipid shell of circulating lipoproteins (Marais, 2019). ApoE binding to lipoproteins coincides with conformational reorganization in functional ApoE monomers, which is essential for optimal ApoE function (Chetty et al., 2017; Garai et al., 2011). Next to their structural role, apolipoproteins act as ligands for lipoprotein receptors. ApoE has a high affinity for the low-density lipoprotein receptor (LDLR), and facilitates LDLR-mediated uptake of very-low density lipoproteins (VLDL) and low density lipoproteins (LDL) by hepatocytes and LDLR-proficient APCs (Marais, 2019). Furthermore, circulating lipoproteins routinely

bind to endogenous glycosylceramides, which are structurally similar to lipid antigens (Iqbal et al., 2017; Scherer et al., 2011). I therefore hypothesized that foreign lipid antigens might do the same, and form complexes with circulating lipoproteins to facilitate lipid antigen transport and delivery to APC.

In this chapter, I used 2-color fluorescence correlation spectroscopy (2c-FCCS) to study complex formation of lipoproteins with the model iNKT cell antigen αGalCer *in vitro* and *in vivo*. Subsequent to uptake and iNKT cell activation experiments *in vitro*, VLDL particles with incorporated αGalCer were used to assess lipid antigen delivery *in vivo*. Finally, peripheral blood mononuclear cells (PBMC) of patients with defined LDLR mutations were used to investigate the relevance of lipoproteins for lipid antigen delivery and iNKT cell activation in humans.

2.2 VLDL and LDL form stable complexes with the model iNKT cell ligand αGalCer

To investigate complex formation of lipoproteins with the prototypic iNKT cell ligand αGalCer, we used 2 color fluorescence cross correlation spectroscopy (2c-FCCS) as an efficient means to assess binding and stability of the complexes (Fig. 2.1) (Krieger et al., 2015; Ries et al., 2010). In 2c-FCCS the sample contains two spectrally distinct fluorophores, whose movements through the observation volume are distinguished with independent detectors. In case of complex formation, diffusion times of the complex components will synchronize, and cross-correlated diffusion of the complex components will occur.

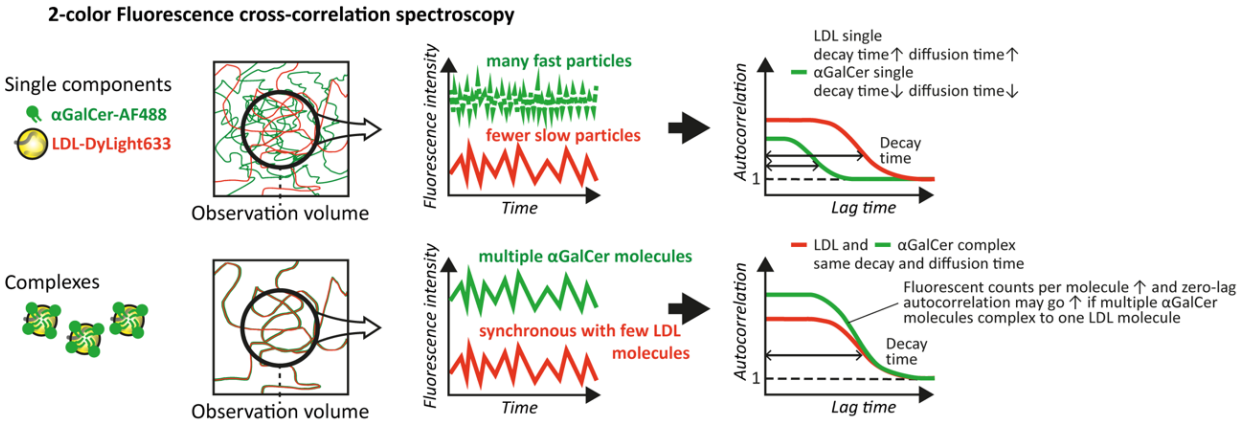

Figure 2.1 | The principle of 2-color fluorescence cross-correlation spectroscopy. Diffusing particles are observed via their fluorescence by two independent detectors. The measured fluorescence fluctuations over time are fitted in an autocorrelation model, which yields a decay time that reflects the average retention time of particles in the observation volume, as well as particle diffusion times. In case of complex formation, decay and diffusion times of the complex components will synchronize, and cross-correlated diffusion of the complex components will occur.

For *in vitro* complex formation a straightforward incubation method was used where Dylight633-labeled lipoproteins were incubated with AF488-labeled αGalCer

in a 1:10 molar ratio at 37°C on a shaker for 1 hour. To assess complexation *in vivo*, fluorescently labeled human LDL and αGalCer were mixed in a syringe and instantly injected in a *Ldlr*$^{-/-}$ mouse. The correlation curve of αGalCer shifted to the right in the *in vitro* and *in vivo* complex samples (Fig. 2.2 A-C), indicating an increased diffusion time of labeled αGalCer due to binding to lipoprotein with a longer diffusion time (Fig. 2.2D). Moreover, high cross-correlation (>1) shows that the complex formation between αGalCer and lipoprotein is highly efficient and specific (Fig. 2.2C). The number of αGalCer particles bound to one LDL particle was extracted from the fluorescence intensity measured in counts per molecule. *In vitro* complexation yielded binding of all αGalCer molecules to human LDL in a 10:1 molar ratio, whereas *in vivo* complexation resulted in a molar ratio of 5:1 (Fig. 2.2E,F). Considering that all αGalCer molecules *in vivo* showed diffusion times similar to lipoproteins (Fig. 2.2D), we assume that any remaining αGalCer has complexed with unlabeled circulating mouse lipoproteins, which are structurally similar to human lipoproteins (Kaabia et al., 2018).

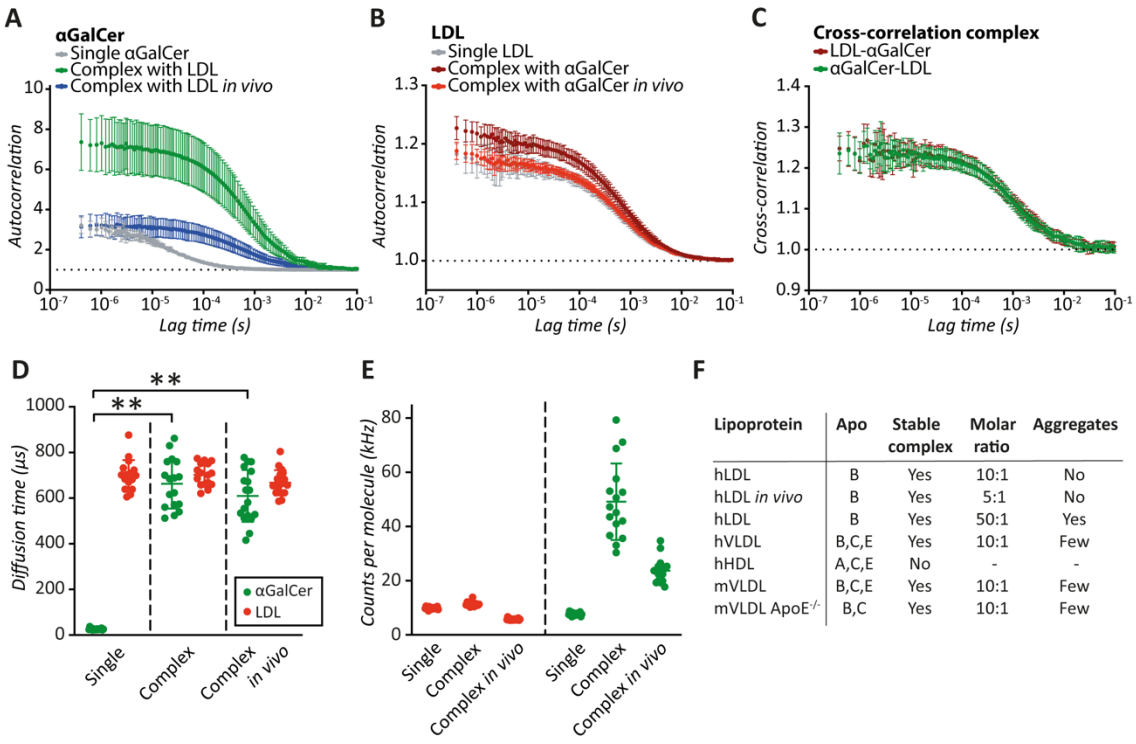

Lipoprotein	Apo	Stable complex	Molar ratio	Aggregates
hLDL	B	Yes	10:1	No
hLDL *in vivo*	B	Yes	5:1	No
hLDL	B	Yes	50:1	Yes
hVLDL	B,C,E	Yes	10:1	Few
hHDL	A,C,E	No	-	-
mVLDL	B,C,E	Yes	10:1	Few
mVLDL ApoE$^{-/-}$	B,C	Yes	10:1	Few

Figure 2.2 | Lipoproteins LDL and VLDL form stable complexes with the prototypic iNKT cell ligand αGalCer. 2c-FCCS was used to assess complex formation of αGalCer with lipoproteins. For *in vitro* complex formation Dylight633-labeled LDL was incubated with AF488-labeled-αGalCer in a 1:10 molar ratio for 1 hour at 37 °C. To assess complexation *in vivo* the serum of mice was collected after injection of fluorescently labeled human LDL and αGalCer were mixed in a syringe and instantly injected in a *Ldlr*$^{-/-}$ mouse. **(A)** Autocorrelation curves of αGalCer single and in complex with human LDL *in vitro* and *in vivo* (*n=15*). **(B)** Autocorrelation curve of LDL, in complex with αGalCer *in vitro* and *in vivo* (*n=15*). **(C)** Cross-correlated diffusion of the αGalCer and LDL complex components (*n=15*). **(D)** Diffusion time of single αGalCer and LDL, compared to complex components *in vitro* and *in vivo*. (*n*=15) **(E)** Fluorescent counts per molecule of single LDL and αGalCer, and complexed components *in vitro* and *in vivo*. The αGalCer counts per molecule *in vivo* were normalized for the lower LDL counts per molecule *in vivo.* (*n=15*) **(F)** Overview of 2c-FCCS studies of lipoprotein-αGalCer complex formation. The results represent 3 biological replicates, each performed in quintuplicates. Apo = apolipoprotein. Statistics: error bars represent mean ± SD. Unpaired *t*-tests (D). * $P < 0.05$; ** $P < 0.01$.

To investigate whether other lipoprotein classes also form complexes with αGalCer, human VLDL, human HDL and mouse VLDL were assessed as well (Fig. 2.3). HDL was the only lipoprotein that did not form complexes with αGalCer (Fig. 2.3C). For subsequent *in vitro* and *in vivo* experiments, we therefore used LDL/VLDL-αGalCer complexes. Finally, to corroborate that lipoprotein-αGalCer complex formation is ApoE-independent, ApoE-deficient mouse VLDL was subjected to complexation *in vitro,* and showed similar complex formation with αGalCer as WT mouse VLDL (Fig. 2.3B). Taken together, LDL and VLDL form stable complexes with the model iNKT cell ligand αGalCer, in an ApoE-independent manner.

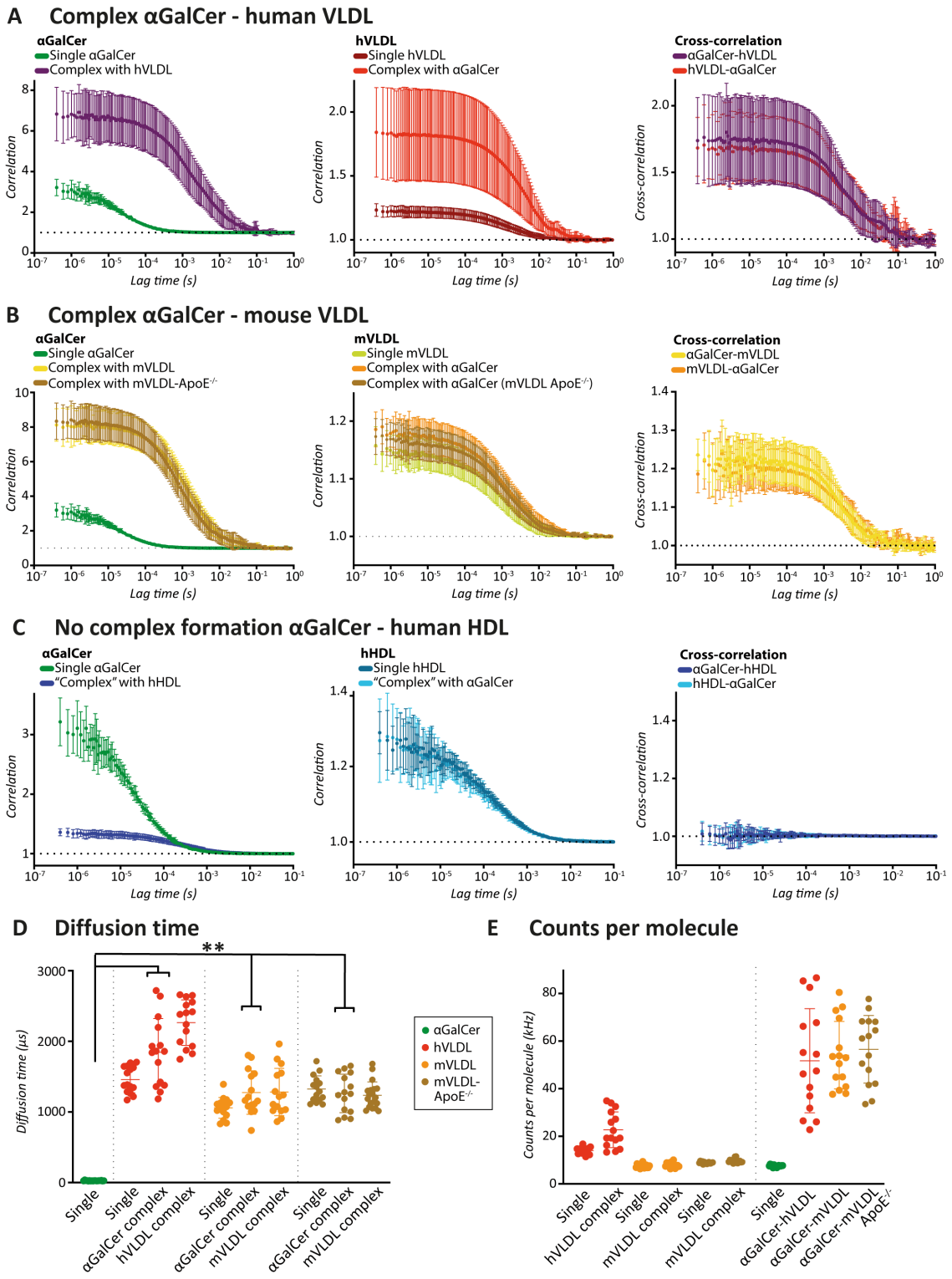

Figure 2.3 | Mouse and human lipoproteins LDL and VLDL form complexes with model lipid antigen αGalCer independent of ApoE. 2c-FCCS was used to assess complex formation of αGalCer with human VLDL, human HDL and mouse VLDL (WT and ApoE$^{-/-}$). **(A)** Autocorrelation and cross-correlation curves of αGalCer-AF488 and Dylight-633 labeled human VLDL, comparing single

components and complexes, indicating complex formation (*n=15*). **(B)** Autocorrelation and cross-correlation curves of αGalCer-AF488, Dylight-633 labeled mouse VLDL, and *ApoE*$^{-/-}$ mouse VLDL (*n=15*), indicating complex formation. **(C)** Autocorrelation and cross-correlation curves of αGalCer-488 and Dylight-633 labeled human HDL. **(D)** Diffusion times of single αGalCer, human VLDL and mouse VLDL, both as single components and in complex (*n=15*). **(E)** Fluorescent counts per molecule of single αGalCer, human VLDL and mouse VLDL, both as single components and in complex (*n=15*). The results represent 3 biological replicates, each performed in quintuplicates. Statistics: error bars represent mean ± SD. Unpaired *t*-tests (D). * P < 0.05; ** P < 0.01.

2.3 LDL-αGalCer complexes are stable after 1 week

To assess stability of complex formation of human LDL and αGalCer, 2c-FCCS was repeated after one week of storage at 4°C. Cross-correlation curves at day 0 and day 7 were compared and showed persistent cross-correlation of labelled αGalCer-488 and labelled human LDL-633, indicating stable complex formation.

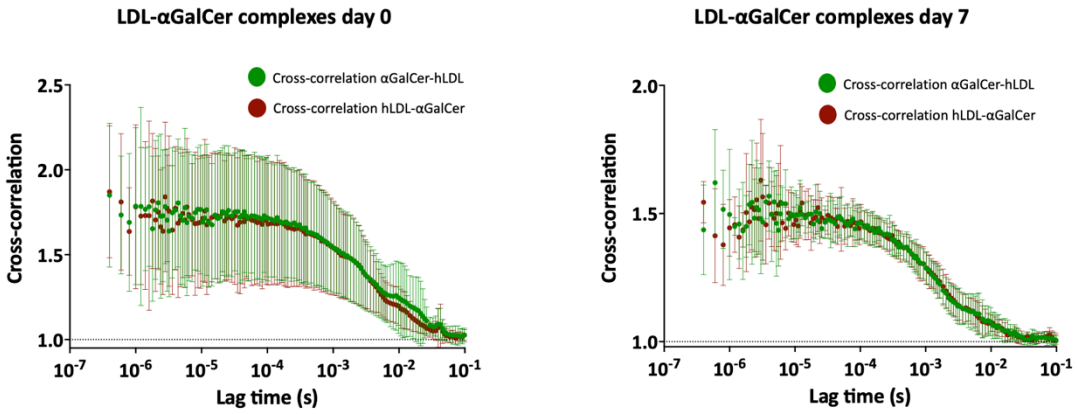

Figure 2.4 | Stability of LDL-αGalCer complexes after 1 week. LDL-αGalCer complexes were stored at 4°C to assess stability of the complexes after 7 days. Cross-correlated diffusion of the αGalCer and human LDL complex components at day 0 (left panel) and day 7 (right panel) (n=15). The results represent the average of 3 biological replicates, each performed in quintuplicates.

2.4 Alternative lipid antigens form complexes with human LDL

To investigate whether complex formation of the model lipid antigen αGalCer with lipoproteins is applicable to alternative lipid antigens, Isoglobotriosylceramide (iGb3), αGalCer analog OCH and glycosphingolipid-1 (GSL-1) were subjected to a similar *in vitro* complexation protocol and analysis as described above. 2c-FCCS showed complex formation for iGb3 and OCH with human LDL (cross-correlation > 1) (Fig. 2.5A,B). There was no complex formation observed for GSL-1 and human LDL (cross-correlation = 1) (Fig. 2.5C).

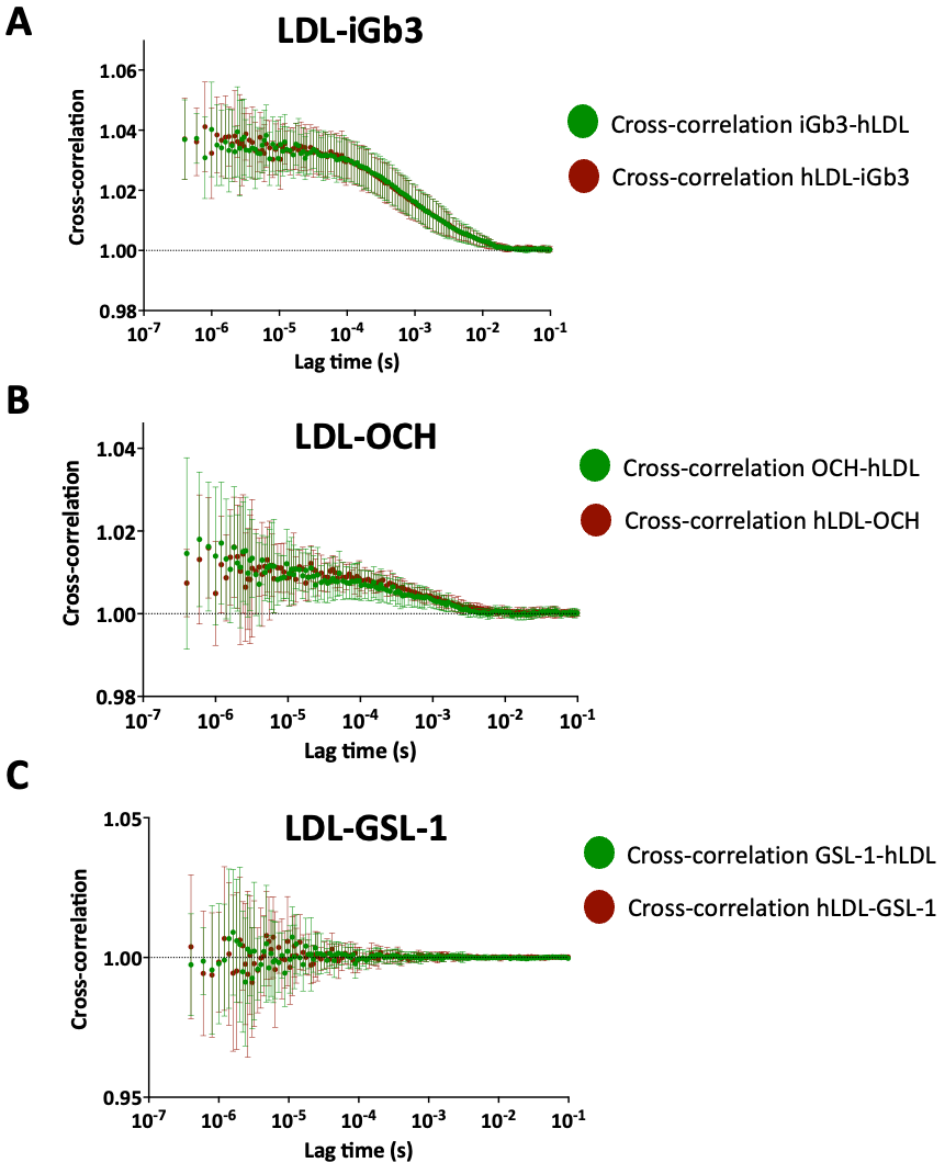

Figure 2.5 | Human LDL forms complexes with alternative lipid antigens iGb3 and OCH. Dylight633-labeled LDL was incubated with AF488-labeled-lipid antigens in a 1:10 ratio for 1 hour. 2c-FCCS was used to assess complex formation of alternative lipid antigens including Isoglobotriosylceramide (iGb3), αGalCer analog OCH and glycosphingolipid-1 (GSL-1). **(A)** Cross-correlated diffusion of iGb3 and human LDL complex components. (n=15). **(B)** Cross-correlated diffusion of OCH and human LDL complex components. (n=15). **(C)** Cross-correlated diffusion of GSL-1 and human LDL complex components. (n=15). The results represent 3 biological replicates, each performed in quintuplicates.

2.5 Uptake of LDL-αGalCer-complexes is LDLR mediated

To study the impact of lipoprotein-αGalCer complexes on iNKT cell activation, we first investigated the uptake of these complexes by APC. αGalCer was used as the model lipid antigen in subsequent experiments, because of its high potency and frequent use in literature. Using flow cytometry we tracked LDLR-mediated uptake of human fluorescently labeled LDL-αGalCer complexes in human THP1 monocytes, which constitutively express LDLR (Hamanaka et al., 1991). Blocking of the LDLR reduced uptake of both the LDL-Dylight633 and αGalCer-AF488 complex components in THP1 monocytes with 80-90%, showing that uptake of LDL-αGalCer complexes is indeed LDLR-dependent (Fig. 2.6 A-B).

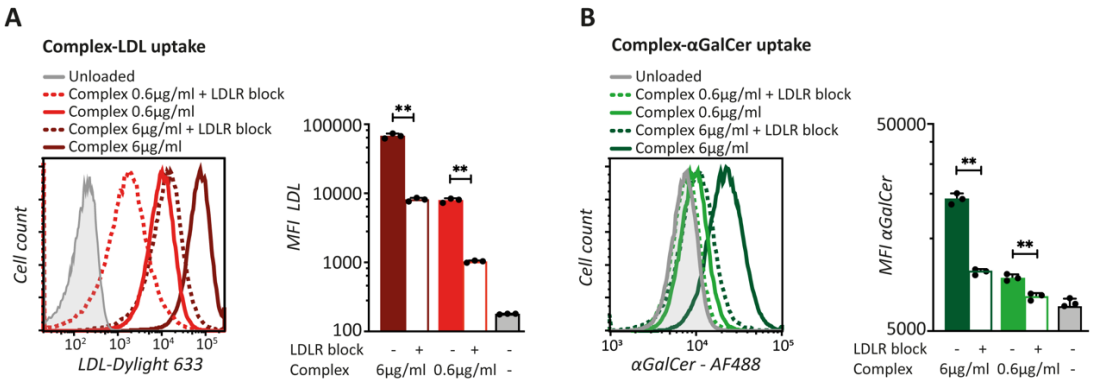

Figure 2.6 | LDLR-mediated uptake of LDL-αGalCer complexes. (A-B) MFI analysis of flow cytometry on THP1 monocytes treated with different concentrations of fluorescently labelled LDL-αGalCer complexes with or without pre-incubation with LDLR blocking antibody (*n=3*). Average of *n=3* biological replicates, each performed in duplicates. Statistics: error bars represent mean ± SD. Unpaired *t*-tests. * P <0.05; ** P < 0.01.

2.6 LDLR-mediated activation of iNKT cells by (V)LDL-αGalCer complexes in vitro

To study whether lipoprotein-αGalCer complexes are functional in their ability to activate human iNKT cells *in vitro*, wildtype THP1 macrophages and THP1 macrophages that overexpress CD1d alone and CD1d and LDLR were loaded with LDL-αGalCer complex, equivalent amounts of LDL, or αGalCer alone, and cocultured with a short-term human iNKT cell line. This resulted in CD1d-dependent activation of iNKT cells, as assessed by IFNγ and IL-4 secretion (Fig. 2.7A). Loading of THP1 macrophages with αGalCer or LDL-αGalCer complexes enhanced the CD1d-dependent activation of iNKT cells, and LDLR overexpression increased the iNKT cell activation by LDL-αGalCer complexes even further (Fig. 2.7A).

To corroborate these findings in a different model, wildtype, *LDLR*$^{-/-}$ and *CD1d*$^{-/-}$ BMDM were loaded with mouse VLDL-αGalCer complexes or equivalent amounts of

VLDL or αGalCer, cocultured with mouse DN32.D3-iNKT cells, and iNKT cell activation was gauged by measuring IL-2 (Fig. 2.7B). Mouse VLDL was used rather than LDL-complexes for practical reasons, as ultracentrifuge-mediated isolation of mouse VLDL is straightforward, and only recombinant VLDL-αGalCer particles were available for the *in vivo* studies (below) (K. Li et al., 2018). Similar to the human coculture experiments, complex-mediated activation of iNKT cells was CD1d and LDLR-dependent (Fig. 2.7B). In conclusion, both human and mouse coculture experiments showed potent complex-mediated activation of iNKT cells *in vitro* in a CD1d- and LDLR-dependent manner.

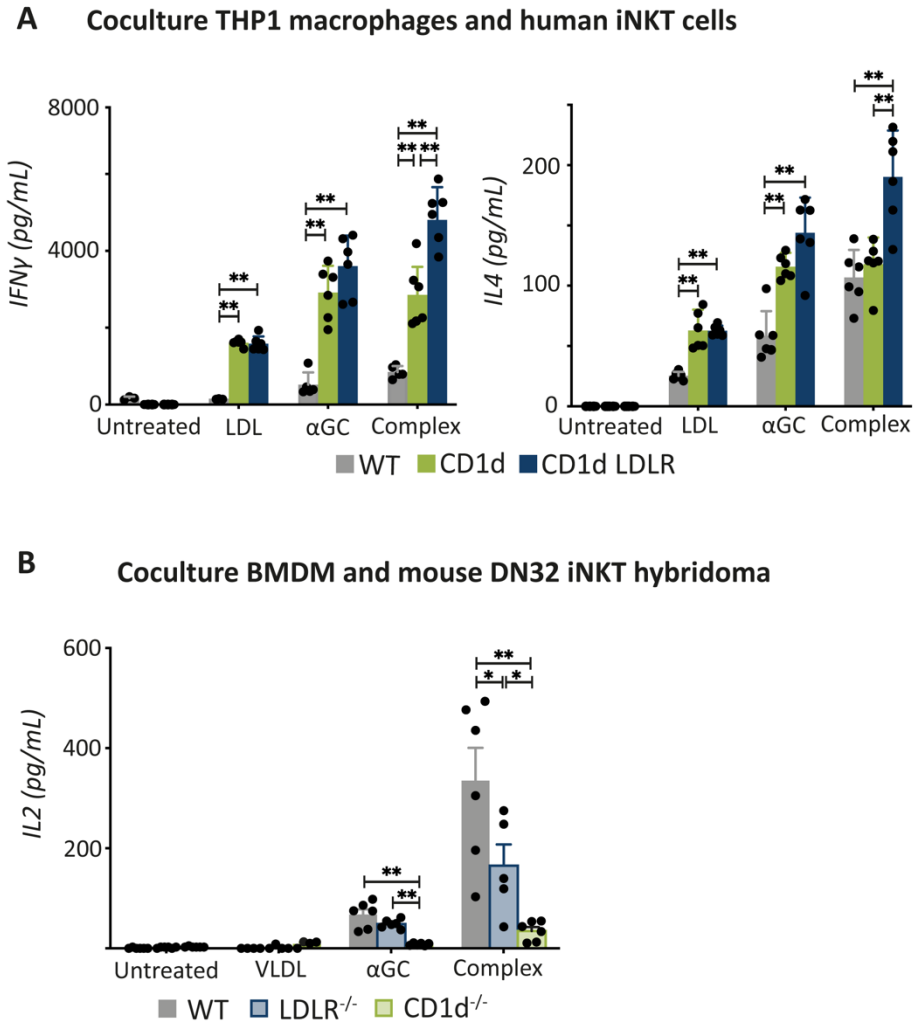

Figure 2.7 | LDLR-mediated uptake of (V)LDL-αGalCer complexes in vitro. (A) IFNγ and IL-4 production in the supernatant of THP1 macrophages in coculture with human iNKT cells. THP1 macrophages were pre-loaded with 6 μg/ml human LDL-αGalCer complex (100 ng/ml αGalCer), or equivalent amounts of LDL or αGalCer, washed and cocultured with iNKT cells overnight (*n=6*). **(B)** IL-2 production in the supernatant of coculture of wildtype, *Ldlr*$^{-/-}$ or *CD1d*$^{-/-}$ mouse BMDM with DN32.D3-iNKT cells. BMDM were pre-loaded with 0.6 μg/ml mouse VLDL-αGalCer complex (10 ng/ml αGalCer), or equivalent amounts of VLDL or αGalCer, washed and cocultured with DN32.D3-iNKT hybridoma overnight (*n=6*). Average of 6 biological replicates. Statistics: ANOVA with Tukey post-hoc analysis and multiple-testing correction to compare groups at single timepoints. * P <0.05; ** P < 0.01. Abbreviations: BMDM = bone marrow derived macrophages.

The modest iNKT cell response to *Ldlr*$^{-/-}$ BMDM *in vitro* nonetheless suggest that other lipoprotein receptors may also contribute to the uptake of VLDL-αGalCer complexes (Fig. 2.7B). Therefore we assessed scavenger receptor A (SRA) as an alternative uptake mechanism for lipoprotein-lipid antigen complexes in absence of LDLR. *Sra*$^{-/-}$ BMDM elicited a reduced cytokine response by DN32.D3-iNKT cells compared to WT BMDM, indicating a role for SRA in the uptake of VLDL-αGalCer complexes (Fig. 2.8).

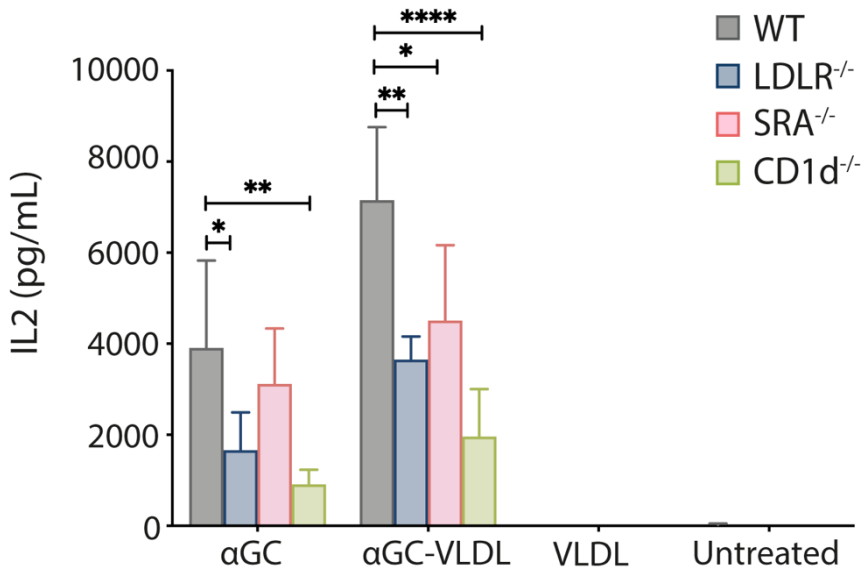

Figure 2.8 | The role of scavenger receptor A in the uptake of VLDL-αGalCer complexes. IL-2 in the supernatant in coculture of wildtype, *Ldlr*$^{-/-}$, *Sra*$^{-/-}$ or *Cd1d*$^{-/-}$ mouse BMDM with DN32.D3-iNKT hybridoma cells. BMDM were pre-loaded with 0.6 µg/ml mouse VLDL-αGalCer complex (10 ng/ml αGalCer), or equivalent amounts of VLDL or αGalCer, washed and cocultured with DN32.D3 overnight (*n*=6). Average of 6 biological replicates. Statistics: ANOVA with Tukey post-hoc analysis and multiple-testing correction to compare groups at single timepoints. * P <0.05; ** P < 0.01; **** P < 0.0001. Abbreviations: BMDM = bone marrow derived macrophages.

2.7 The role of ApoE in complex uptake and activation

ApoE is bound to VLDL and HDL, rather than LDL, and is known to facilitate LDLR-mediated uptake of lipid antigens (Marais, 2019; Van Den Elzen et al., 2005). Previously, we have demonstrated that absence of ApoE does not impair binding of lipid antigen to lipoproteins (Fig. 2.4B). We therefore hypothesized that ApoE would mediate the uptake of VLDL-αGalCer complexes by APC. *ApoE*$^{-/-}$ and wildtype mouse serum was employed to produce ApoE-deficient and proficient VLDL-αGalCer complexes. In accordance with our hypothesis, the uptake of ApoE-deficient VLDL-Dylight633-αGalCer complexes by RAW macrophages was diminished compared to

ApoE-proficient VLDL-αGalCer complexes (Fig. 2.9A). Subsequently, *ApoE*$^{-/-}$ and *CD1d*$^{-/-}$ BMDM were loaded with ApoE-deficient or ApoE-proficient VLDL-αGalCer complexes, or equivalent amounts of αGalCer, followed by a coculture with mouse DN32.D3-iNKT cells. Treatment of BMDM with ApoE-deficient complexes led to decreased CD1d-dependent iNKT hybridoma activation, compared to ApoE-proficient complexes, as assessed by IL-2 secretion (Fig. 2.9B). Taken together, our experiments demonstrated that although ApoE is not necessary for binding of lipid antigens to VLDL, it facilitates uptake of VLDL-αGalCer complexes and subsequent CD1d-mediated iNKT cell activation.

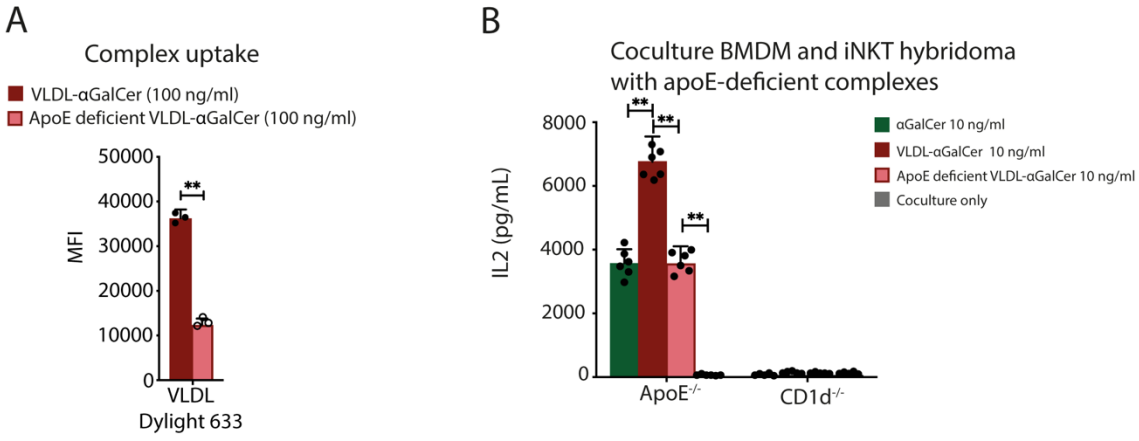

Figure 2.9 | The role of ApoE in uptake of lipoprotein-αGalCer complexes and subsequent iNKT cell activation. VLDL was isolated from serum of WT and ApoE deficient mice to make VLDL-αGalCer complexes and ApoE deficient-VLDL-αGalCer complexes. **(A)** Mean fluorescence intensity comparison of Dylight 633 derived from flow cytometry analysis of RAW cells loaded with 100 ng/ml WT or ApoE free VLDL-Dylight633-αGalCer-488 complexes for 30 minutes (n=3). Average of 3 biological replicates, performed in duplicates. **(B)** Coculture of ApoE-/- and Cd1d-/- mouse BMDM with DN32.D3-iNKT cells. BMDM were pre-loaded with 0.6μg/ml mouse VLDL-αGalCer complex (10ng/ml αGalCer), or equivalent amounts of VLDL or αGalCer (n=6). Average of 6 biological replicates. Statistics: Independent t-test

(panel A). ANOVA with Tukey post-hoc analysis and multiple-testing correction to compare groups at single timepoints (panel B). * P <0.05; ** P < 0.01.

2.8 VLDL-αGalCer complexes activate iNKT cells in vivo in a LDLR-dependent fashion

In vivo experiments allowed us to use recombinant protein-free VLDL particles complexed with αGalCer, which can only bind to ApoE and other exchangeable apolipoproteins in the circulation (Rensen et al., 1997). WT mice with LDLR-proficient hepatocytes generally show rapid clearance of VLDL particles which could limit the uptake by extrahepatic APC (Rensen et al., 1997). We therefore employed bone marrow chimeras of *Ldlr*$^{-/-}$ mice with wildtype and *Ldlr*$^{-/-}$ APCs, to study LDLR-mediated uptake of the VLDL-αGalCer particles (Fig. 2.10).

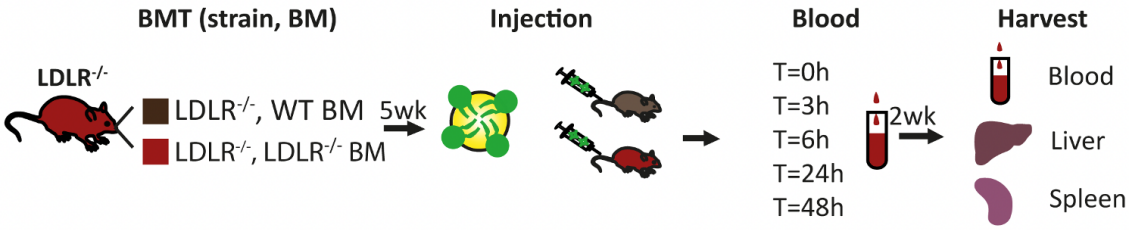

Figure 2.10 | Experimental set-up injection lipoprotein-αGalCer complexes. Bone marrow chimeras were generated of *Ldlr*$^{-/-}$ mice with WT or *Ldlr*$^{-/-}$ bone marrow (*n*=5-6 mice per group; total 11 mice, unless otherwise indicated). After 5 weeks, recombinant VLDL-αGalCer complexes (5 µg αGalCer), free of apolipoproteins, were injected in mice intravenously. Repetitive blood sampling was performed at t = 0h, t = 3h, t = 6h, t = 24h and t = 48h to assess cytokine responses in the serum. 2 weeks later blood, liver and spleen were harvested for assessment of iNKT cell proliferation and phenotype.

The chimeras showed similar numbers of APC, CD1d expression, and circulating iNKT cell numbers pre-treatment, and both groups of mice showed characteristic hypercholesterolemia (Fig. 2.11A-D).

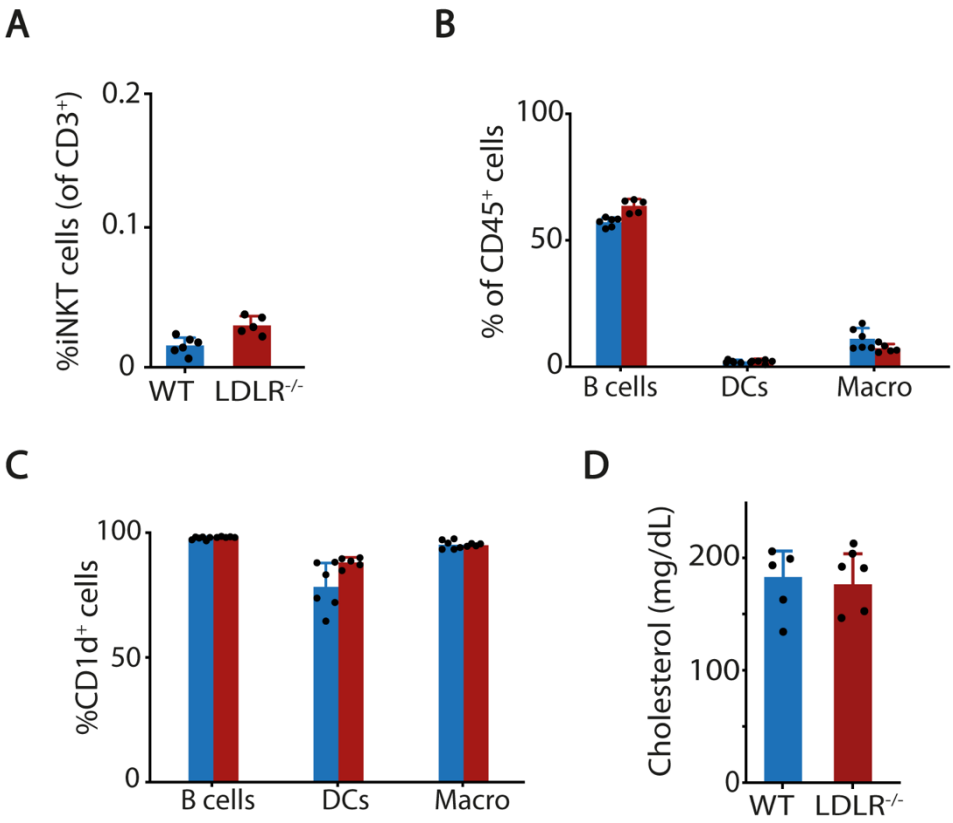

Figure 2.11 | Baseline characteristics of bone marrow chimeras before administration of VLDL-αGalCer complexes. Bone marrow chimeras were generated of *Ldlr*$^{-/-}$ mice with WT or *Ldlr*$^{-/-}$ bone marrow (*n* = 5-6 mice per group; total 11 mice). **(A)** Percentage of circulating iNKT cells in blood before injection with VLDL-αGalCer particles. **(B)** Percentage B cells, dendritic cells and macrophages of CD45^{+} cells in the blood before injection with VLDL-αGalCer particles. **(C)** Percentage of CD1d^{+} B cells, dendritic cells and macrophages in the blood. **(D)** Serum cholesterol levels.

Upon intravenous injection of the recombinant VLDL-αGalCer complexes, both chimeras showed a characteristic iNKT cell response with circulating IL-4 levels

peaking at 3h and IFNγ levels peaking at 6h (Fig. 2.12). *Ldlr*$^{-/-}$ mice with WT APCs showed significantly higher IFNγ and IL-4 levels (Fig. 2.12).

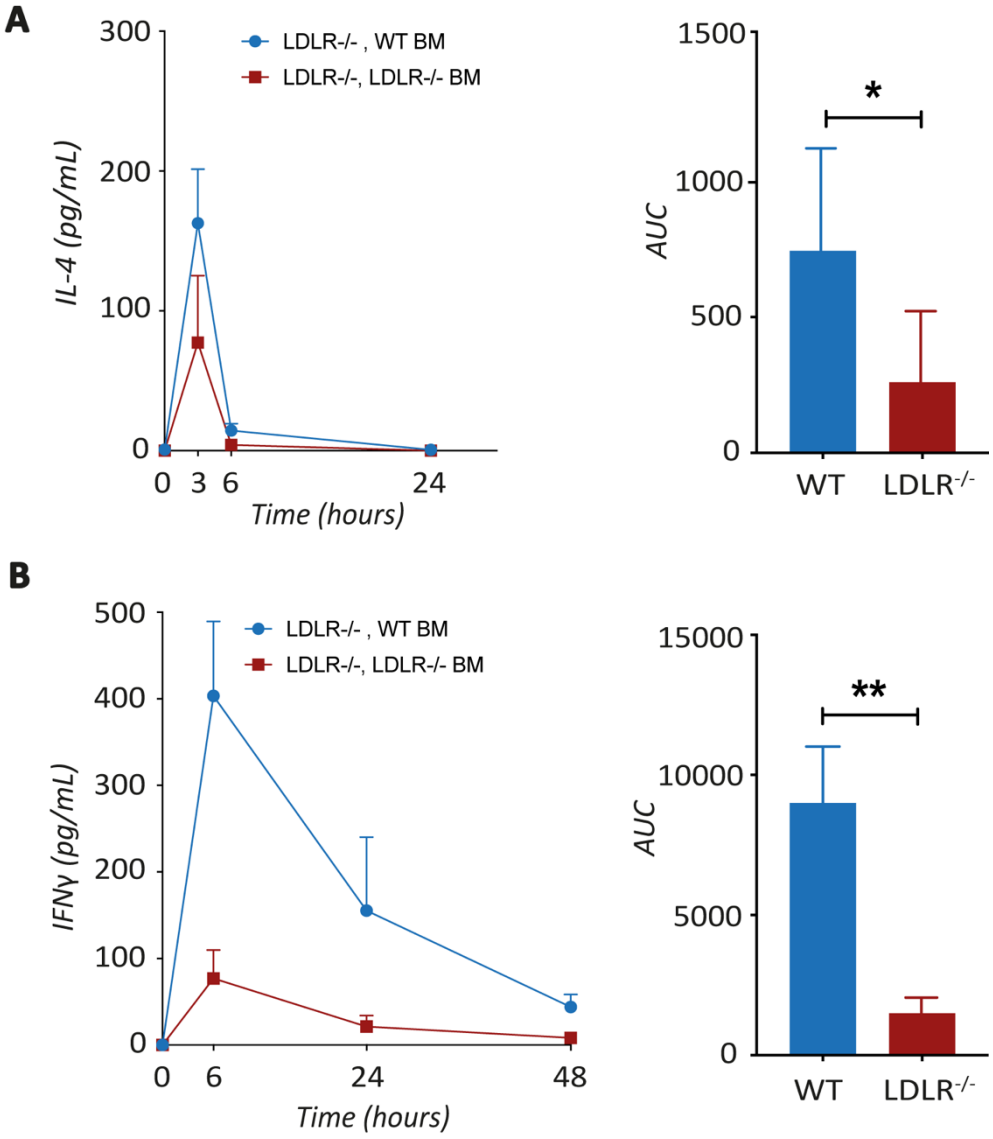

Figure 2.12 | LDLR-proficient antigen presenting cells promote iNKT cell activation by VLDL-αGalCer complexes in hypercholesterolemic mice. (A) Serum IL-4 iNKT cell cytokine responses upon injection with VLDL-αGalCer complexes. **(B)** Serum IFNγ iNKT cell cytokine responses upon injection with VLDL-αGalCer complexes. Total of 22 mice, 10 *Ldlr*$^{-/-}$ WT BM and 12 *Ldlr*$^{-/-}$ *Ldlr*$^{-/-}$ BM. Statistics: Error bars represent mean ± SEM. * P <0.05; ** P < 0.01; *** P < 0.001. Panel A-B Mann-Whitney U test. αGalCer = alpha-galactosylceramide; BM = bone marrow; IFN = interferon.

Two weeks later, iNKT cells were stained with the CD1d tetramer (Fig. 2.13) and the chimeras did not show differences in iNKT cell numbers and phenotype in blood, liver and spleen (Fig. 2.14). Taken together, these experiments showed that VLDL-αGalCer complexes activate iNKT cells *in vivo*. In line with the LDLR-mediated uptake of lipoprotein-αGalCer complexes that we observed *in vitro*, chimeras with LDLR-proficient APC showed the highest iNKT cell cytokine levels. Nonetheless, the presence of an iNKT cell response in chimeras with *Ldlr*$^{-/-}$ APC suggests that the uptake of VLDL-αGalCer complexes by APC *in vivo* does not solely depend on LDLR.

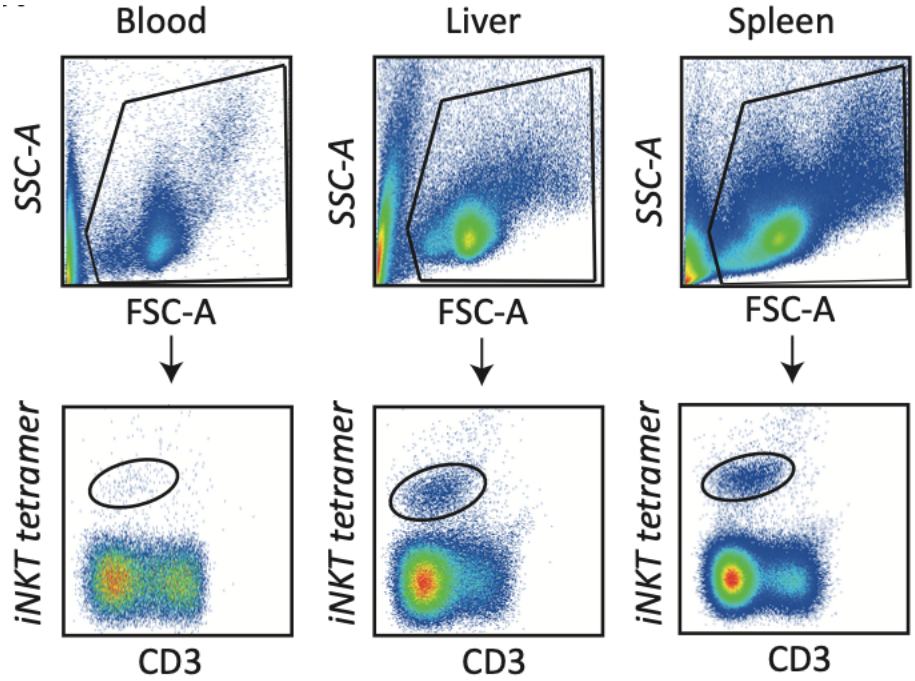

Figure 2.13 | Tetramer staining invariant Natural Killer T cells.
Leukocytes were isolated from mouse blood, liver and spleen and stained with CD3 antibody and CD1d-tetramer for flow cytometry analysis of iNKT cell abundance. Representative plots of iNKT cell gating in the blood, liver and spleen showing CD3 versus iNKT cell tetramer staining.

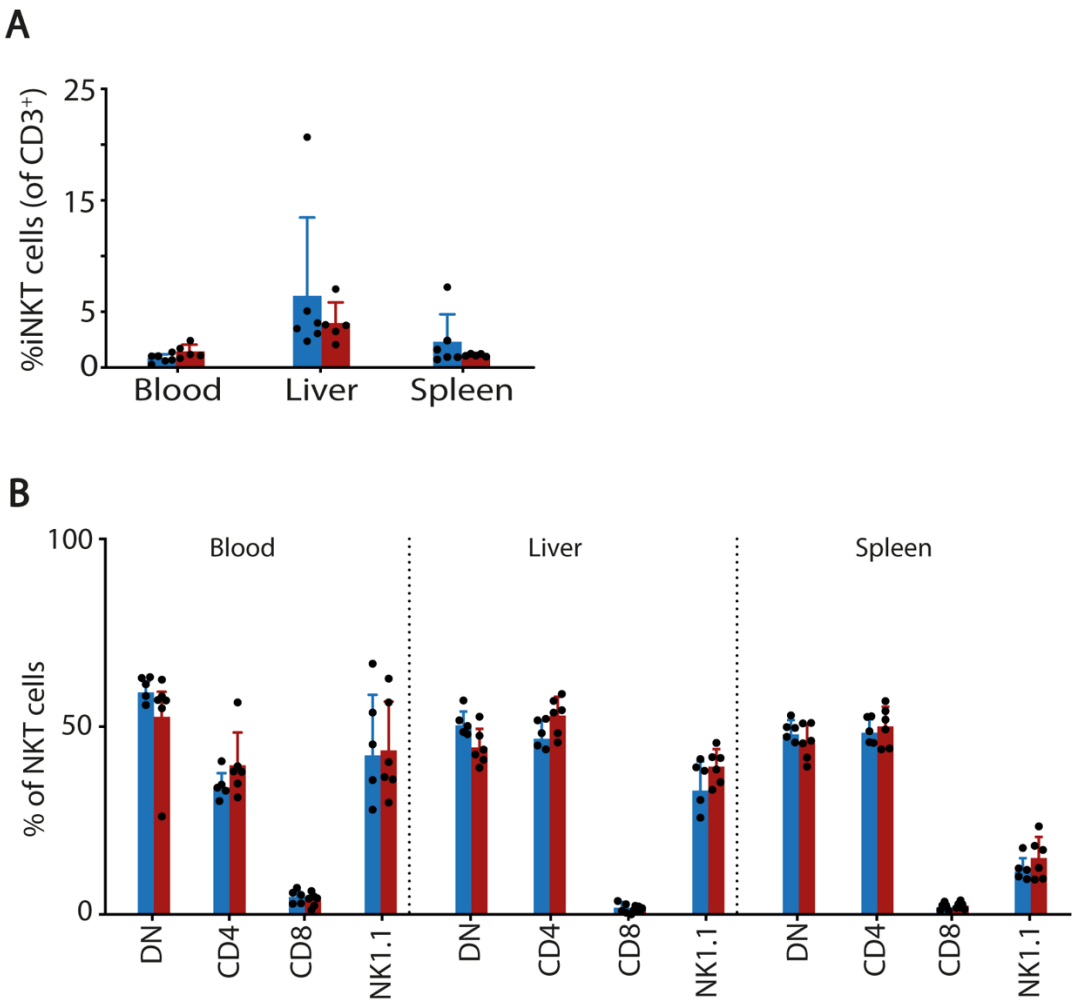

Figure 2.14 | iNKT cell number and phenotype of bone marrow chimeras 2 weeks post-administration of VLDL-αGalCer complexes. (A) Percentage of iNKT cells of $CD3^+$ cells in blood, liver and spleen 2 weeks post injection with VLDL-αGalCer complexes. **(B)** Percentage of $CD4^-CD8^-$ (DN), $CD4^+$, $CD8^+$ and $NK1.1^+$ iNKT cells in blood, liver and spleen 2 weeks post injection with VLDL-αGalCer complexes. Statistics: error bars represent mean ± SD. Unpaired *t*-test when normally distributed based on Shapiro-Wilks test $p > 0.05$. In all other cases, Mann-Whitney U test. *n* = *5-6* mice per group; total 11 mice.

2.9 Human LDLR mutations are associated with impaired iNKT cell activation and proliferation

To investigate the relevance of lipoproteins as a lipid antigen delivery system in humans, PBMCs from patients with receptor-defective or receptor-negative LDLR mutations and controls were collected from a local cardiovascular biobank. The PBMCs were subjected to a standard iNKT cell activation and proliferation assay using αGalCer as the stimulus in the presence of IL-2, assuming that αGalCer would naturally form complexes with the lipoproteins present in serum (Fig. 2.15).

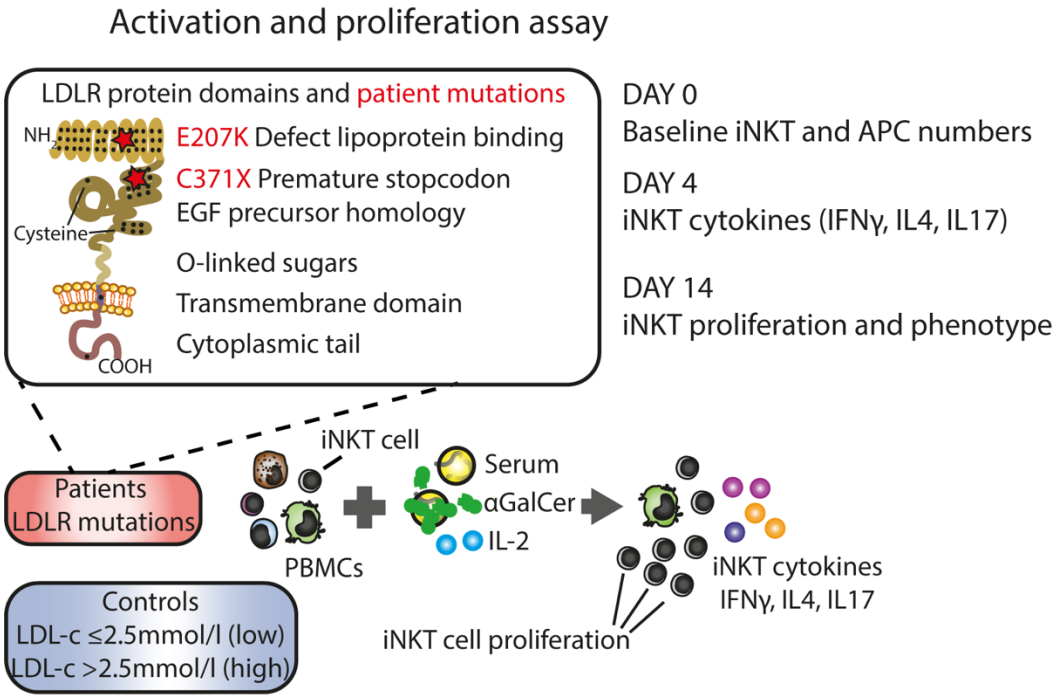

Figure 2.15 | Principle of the human iNKT cell activation and proliferation assay. Schematic overview of the E207K and C371X LDLR-mutations included in the experiment and schematic overview experimental set-up of iNKT activation and proliferation assay. At baseline, no differences in iNKT cell numbers, APC numbers, or CD1d expression were observed between LDLR-mutant PBMCs and controls (Fig. 2.16).

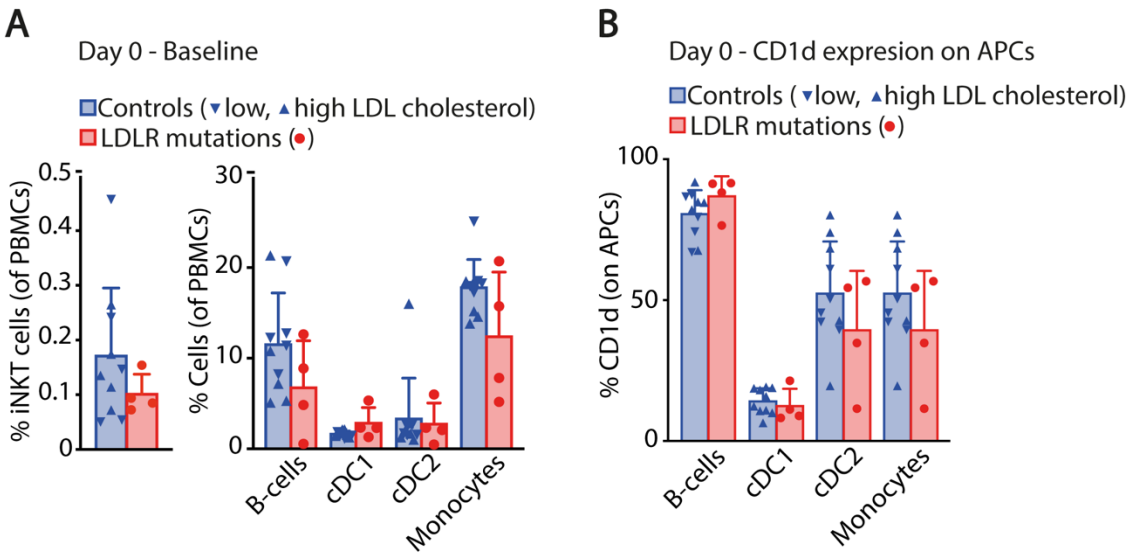

Figure 2.16 | Phenotyping of PBMCs of patients with LDLR mutations and controls. (A) Percentage of iNKT cells (left panel) and APCs including B cells, cDC1, cDC2 and monocytes (right panel), in LDLR-mutated PBMCs and controls at baseline. **(B)** Flow cytometric analysis of CD1d expression on antigen presenting cells in LDLR-mutated PBMCs and controls. Blue downward triangles represent controls with low circulating LDL-cholesterol levels (≤ 2.5 mmol/l, *n = 5*), while blue upward triangles represent controls with high circulating LDL-cholesterol levels (> 2.5 mmol/l, *n = 5*), and red circles represent LDLR-mutated patients (*n = 4*). Statistics: Mann-Whitney U.

On day 4, measurement of iNKT cell cytokines showed significantly reduced secretion of IFNγ by the LDLR-mutant PBMCs. There was no significant difference in IL-4 and IL-17 production between groups (Fig. 2.17).

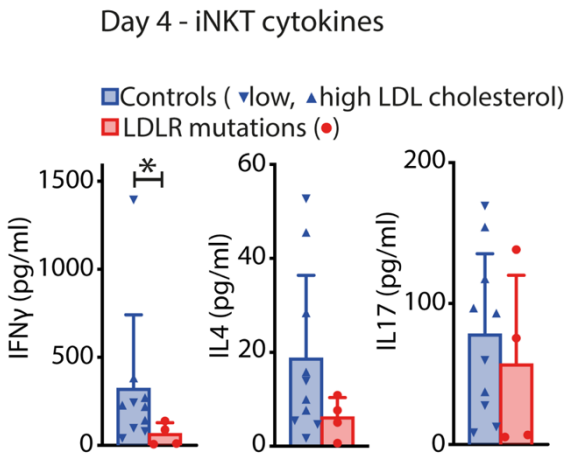

Figure 2.17 | Cytokine production in supernatant PBMCs cocultured with lipoprotein-αGalCer complexes. iNKT cell cytokines IFNγ, IL-4 and IL-17 in the supernatants of LDLR mutated PBMCs and controls on day 4. (*n = 10* controls and *4* patients). Statistics: error bars represent mean ± SD. Mann-Whitney U tests. * P < 0.05.

On day 14, we observed defective iNKT cell proliferation of the LDLR-mutant PBMCs, compared to controls (Fig. 2.18A,B). The impaired iNKT cell activation and proliferation coincided with lower expression of the activation marker CD69 (Fig. 2.18C). The impact of the LDLR-mutations could not be attributed to high patient cholesterol levels, because PBMCs from controls with high and low circulating cholesterol levels showed similar iNKT cell activation and proliferation (Fig. 2.17, 2.18). Taken together, human LDLR mutations are associated with impaired iNKT cell activation and proliferation.

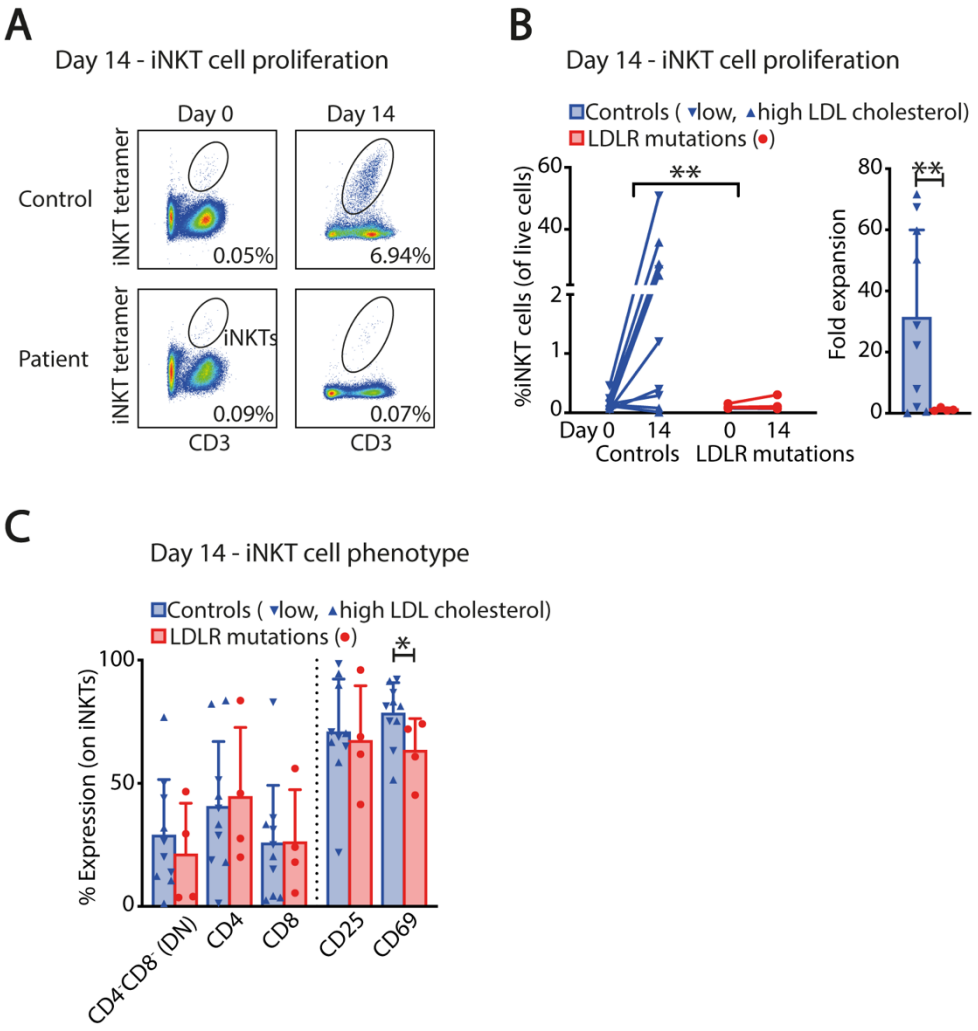

Figure 2.18 | Human LDLR mutations are associated with impaired iNKT cell activation. (A) Representative flow cytometric analysis of LDLR-mutated and control PBMCs on day 0 and 14. Numbers in the graphs indicate the percentage of cells in the iNKT cell gate. **(B)** iNKT cell proliferation on day 14 shown as a percentage of iNKT cells of live cells on day 0 and 14 (left panel), and fold expansion of the iNKT cells after 14 days (right panel). **(C)** Percentage of $CD4^{-}CD8^{-}$ (DN), $CD4^{+}$, $CD8^{+}$, $CD25^{+}$ and $CD69^{+}$ iNKT cells. *n* = 10 controls and 4 patients. Statistics: error bars represent mean ± SD. Mann-Whitney U tests. * $P < 0.05$; ** $P < 0.01$.

In the previous experimental set-up, APCs and iNKT cells from the same donor were used. Therefore, patient iNKT cells had dysfunctional LDLR which may influence activation of these cells. To overcome this limitation, $CD14^{+}$ cells were isolated from

10 patients with LDLR mutations and 10 controls and differentiated to macrophages using MCSF (100 ng/ml) for 5 days. Subsequently, the cells were treated with LDL-αGalCer complexes, αGalCer or LDL for 24 hours. Next, a coculture with healthy donor iNKT cells was started overnight. The following day, measurement of iNKT cell cytokines showed significantly reduced secretion of IFNγ, IL-4 by iNKT cells activated by the LDLR-mutant macrophages compared to controls (Fig. 2.19). These results underscore that human LDLR mutations on APCs are associated with impaired iNKT cell activation.

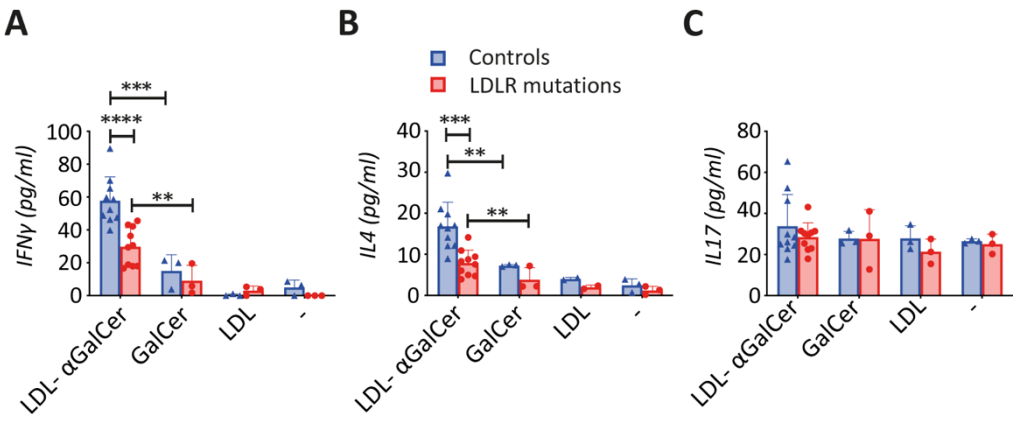

Figure 2.19 | APC specific human LDLR mutations are associated with impaired iNKT cell activation. Monocytes were isolated from the blood of healthy and LDLR mutant donors, and subsequently cultured with 100 ng/ml MCSF for 5 days for differentiation into macrophages. The medium was changed to low serum medium (2% FCS) and cells were treated with LDL-αGalCer, equivalent amounts of αGalCer (100 ng/ml) or LDL overnight and subsequently washed. iNKT cells from a healthy donor were added overnight and cytokine production was measured using ELISA. **(A)** IFNγ in supernatant. **(B)** IL-4 in supernatant. **(C)** IL-17 in supernatant. *n* = 10 controls and 10 patients. Statistics: error bars represent mean ± SD. Mann-Whitney U tests. ** P < 0.01; *** P < 0.001; **** P < 0.0001.

2.10 Discussion

This chapter provides evidence for a distinct role of LDL and VLDL in lipid antigen transport and delivery to APC. Using 2c-FCCS, we demonstrated stable complex formation of the model lipid antigen αGalCer with LDL and VLDL *in vitro* and *in vivo*. Our *in vitro* experiments demonstrated that the uptake of LDL-αGalCer complexes by APC is mediated by the LDLR and facilitated by ApoE. Subsequently, the lipoprotein-lipid antigen complexes propagate iNKT cell activation, as illustrated by the potent iNKT cell response *in vitro* and *in vivo*. The uptake of VLDL-αGalCer complexes *in vivo* was proven to be mediated by LDLR as well. Finally, LDLR-mutant patient PBMCs showed impaired activation and proliferation of iNKT cells, illustrating that LDLR-mediated uptake of lipoprotein-lipid antigen complexes by APCs is also relevant for iNKT cell activation in humans. This study provides new insight into the immunological role of lipoproteins in APC regulated iNKT cell activation.

This study is yet the first to establish the distinct role of lipoproteins in lipid antigen binding and transport. Stable complex formation of ApoE-deficient VLDL and ApoE-free LDL with the prototypic lipid antigen αGalCer revealed that complex formation is ApoE-independent (Fig. 2.9). Similarly, transport of lipoprotein-lipid antigen complexes to APC occurred in an ApoE-independent manner illustrated by the potent iNKT cell response to recombinant apolipoprotein-free VLDL-αGalCer complexes *in vivo* (Fig. 2.12). Our *in vitro* experiments showed that ApoE plays a role in the uptake of VLDL-αGalCer complexes by APC. Together, these findings establish a model of lipoproteins and apolipoproteins acting concertedly in lipid antigen binding, delivery, and uptake. While circulating VLDL and LDL particles can form

complexes with αGalCer and structurally similar foreign lipid antigens to facilitate their transport, apolipoproteins facilitate the LDLR-mediated uptake of lipoprotein-lipid antigen complexes by APC.

Complex formation of lipoproteins and the prototypic lipid antigen αGalCer was assessed using 2-color fluorescence cross-correlation spectroscopy (Fig. 2.1). This technique enables highly accurate detection of complex formation and assessment of complex stability, but does not provide structural analysis of αGalCer binding to lipoproteins (Krieger et al., 2015; Ries et al., 2010). Previous studies showed that glycosylceramides, which are structurally similar to αGalCer, insert into phospholipid rafts (Hall et al., 2010; Hein et al., 2008). Similarly, αGalCer may insert into the phospholipid shell of lipoproteins. This theory could also explain the lack of complex formation of HDL and αGalCer. The phospholipid shell of HDL has a high apolipoprotein content, which decreases lipid fluidity and diffusion of glycosylceramides, and may similarly impair αGalCer binding and insertion (Hall et al., 2010; Massey & Pownall, 1998). In our functional studies, we have therefore focused on LDL and VLDL, rather than HDL. Notably, lack of complex formation *in vitro* does not necessarily imply that HDL cannot transport foreign lipid antigens *in vivo*. Circulating phospholipid transfer protein (PLTP) and cholesteryl ester transfer protein (CETP) have been implicated in transfer of ceramides between human lipoprotein classes (Boon et al., 2013; Iqbal et al., 2017; Yu et al., 2014), suggesting that active transfer of αGalCer and other lipid antigens from VLDL or LDL onto HDL may occur *in vivo*.

Complex formation of human LDL was demonstrated with αGalCer, iGb3 and OCH. Interestingly, there was no complex formation of human LDL with lipid antigen GSL-1. The chemical characteristics of GSL-1 show a highly similar hydrophilic carbohydrate head group to αGalCer, iGb3 and OCH. However, the hydrophobic lipid tail of GSL-1 is much shorter compared to αGalCer, iGb3 and OCH (Appendix Table. 2.1). It has been shown that the binding capacity of lipids is affected by lipid chain length, providing a possible explanation for the lack complex formation with GSL-1 (Dashti et al., 2011; Powl et al., 2007).

The uptake of lipoprotein-αGalCer complexes by APC is LDLR mediated. Our *in vitro* studies showed 80-90% reduction of lipoprotein-αGalCer uptake by THP1 monocyte like cells upon LDLR blocking, and impaired iNKT cell activation in cocultures with LDLR-deficient BMDM, compared to wildtype BMDM (Fig. 2.7). LDLR-mediated uptake of lipoprotein-ligand complexes could have additional benefits for antigen presentation, as complex-derived αGalCer showed greater iNKT cell activation than αGalCer alone (Fig. 2.7 and Fig. 2.19). This is in line with previous studies showing fast LDLR-mediated endocytosis and endolysosomal traversal of lipoprotein-containing cargo, which may accelerate lipid antigen loading and presentation by APCs (Lantz & Bendelac, 1994; Vitols et al., 1990). The modest iNKT cell response in chimeras with *Ldlr*$^{-/-}$ APC and the modest iNKT cell response to *Ldlr*$^{-/-}$ BMDM *in vitro* nonetheless suggest that other lipoprotein receptors also contribute to the uptake of VLDL-αGalCer complexes. We explored this further and showed that SRA has a residual role in the uptake of VLDL-αGalCer complexes. Other alternative uptake mechanisms for lipoprotein-lipid antigen complexes may include sortilin and other members of the LDL receptor family such as LRP1 (Marais, 2004;

Zanoni et al., 2018). In case of LDLR dysfunction or lipoprotein deprivation, cells depend on these alternative uptake mechanisms, next to intracellular cholesterol synthesis, to meet their cholesterol requirements (Marais, 2004; Zani et al., 2015).

The discovery of lipoproteins as a lipid antigen delivery system has several translational implications. For one, it complicates the use of *Ldlr*$^{-/-}$ mice to study the role of iNKT cells in atherosclerosis and other diseases. Mouse models with an intact LDLR pathway for antigen uptake and atherogenic lipid clearance would be preferred. Finally, lipoproteins do not only transport lipid antigens, but have been implicated in transport and LDLR-mediated uptake of lipopolysaccharides and other bacterial lipids as well (Grin et al., 2018; Levels et al., 2005). The emergence of lipoproteins as a delivery system may not end here, as other circulating lipid-based immune mediators might also avail themselves of this delivery route.

In summary, this chapter identified lipoproteins VLDL and LDL as vehicles for lipid antigen delivery and subsequent activation of invariant NKT cells. In the circulation, LDL and VLDL particles bind αGalCer and structurally similar lipid antigens. Subsequent uptake by APCs is LDLR-mediated *in vitro* and *in vivo*. LDLR-mutant APCs of patients with familial hypercholesterolemia are impaired in their ability to activate invariant NKT cells, underscoring the relevance of this lipid antigen delivery system in humans.

3 NKT cells in human atherosclerosis

3.1 Introduction

Plaque rupture is the most common complication of atherosclerosis resulting in cardiovascular events such as myocardial infarction and stroke (Libby & Pasterkamp, 2015). Plaques vulnerable to rupture are characterised by a large necrotic core, macrophage infiltration and lack of collagen and smooth muscle cells to provide stability (Naghavi et al., 2003; Vink et al., 2001). In mice, activation of iNKT cells induces plaque vulnerability through activation of macrophages and upregulation of collagenases in the plaque (Ohmura et al., 2021). Whether results from murine models translate to human atherogenesis remains unknown as only a limited number of studies have assessed NKT cells in human atherosclerosis. The first evidence of NKT cells in the human plaque emerged in 2005 (Bobryshev & Lord, 2005; Chan et al., 2005). Later, CD1d expressing cells were identified in advanced plaques and it was demonstrated that plaque-derived iNKT cells responded to stimulation with αGalCer (Jabir et al., 2017; Kyriakakis et al., 2010). However, the relationship between NKT cells in the human plaque, plaque histomorphology and clinical characteristics remains unknown.

The abundance of NKT cells in tissues has been associated with clinical outcome in several diseases (Lalla et al., 2011; Molling et al., 2007; Tachibana et al., 2005). In colorectal cancer, a higher number of NKT cells in the tumour was an independent prognostic factor for favourable clinical outcome (Tachibana et al., 2005). In patients with hematologic malignancies iNKT cell reconstitution after haemopoietic stem cell transplantation, correlated with remission of disease (Lalla et al., 2011). Defining the relationship between intraplaque NKT cell counts and patient

characteristics could provide valuable insights in the role of NKT cells in human atherogenesis.

To investigate the role of NKT cells in human atherosclerosis, I used atherosclerotic plaque tissue from well characterized patients included in the Athero-Express cohort study. The Athero-Express Biobank collects the carotid plaques from patients who underwent surgical removal of the carotid plaque (carotid endarterectomy), providing a unique opportunity to study human atherosclerosis. Furthermore, patient medical history, blood samples and data on pre-surgical physical examination are collected, and histological assessment of the plaque specimen is performed. Study participants are followed up for a minimum of 3 years to record the occurrence of adverse cardiovascular events such as myocardial infarction and stroke, allowing to study plaque characteristics in relation to cardiovascular outcome (Hellings et al., 2012).

Taken together, the association between NKT cells in the human plaque and clinical characteristics has not been investigated. In this chapter, I study the relation between NKT cell counts in the human atherosclerotic plaque, patient- and plaque characteristics using patient samples and clinical characteristics of patients included in the Athero-Express cohort.

3.2 Study population

A random subset of 97 carotid endarterectomy specimens from the Athero-Express study was included in this study. Upon examination of the quality of the specimens, five specimens were excluded from analysis due to insufficient quality for staining, resulting in a study cohort of 92 patients. The mean age of the patient population was 69 years (SD = 9.98) and 70% was male. The baseline characteristics of the study population are summarized in Table 3.1.

Table 3.1 | Baseline characteristics of patients of Athero-Express Biobank study

Patient characteristics (n = 97)	
Sex, male, *n* (%)	70 (72)
Age in years, mean (SD)	69 (9.98)
History	
Cerebrovascular disease, *n* (%)	80 (82.5)
Coronary artery disease, *n* (%)	25 (25.8)
Peripheral artery disease, *n* (%)	20 (22)
Medication	
Anti-hypertensives, *n* (%)	64 (66)
Lipid lowering drugs, *n* (%)	74 (76.3)
Anti-thrombotics, *n* (%)	82 (84.5)
Oral glucose inhibitor, *n* (%)	12 (12.4)
Risk factors	
Current smoker, *n* (%)	19 (18.6)
Hypertension, *n* (%)	64 (66)
Type 2 diabetes mellitus, *n* (%)	17 (17.5)
BMI, median (IQR)	25.95 (24.09-27.76)
Total cholesterol in mmol/L, mean (SD)	4.26 (1.22)
LDL in mmol/L, mean (SD)	2.43 (1.08)
VLDL in mmol/L, mean (SD)	0.32 (0.24)
HDL in mmol/L, mean (SD)	1.08 (0.34)
Triglycerides in mmol/L, mean (SD)	1.63 (1.20)

3.3 Natural Killer T cell staining on human atherosclerotic plaque

One paraffin embedded 5 µm atherosclerotic plaque section per patient was stained for CD3 and CD56 to identify NKT cells (Fig. 3.1). Stained slides were scanned and the number of CD3 positive cells, number of CD56 positive cells, double positive NKT cells and plaque area were quantified.

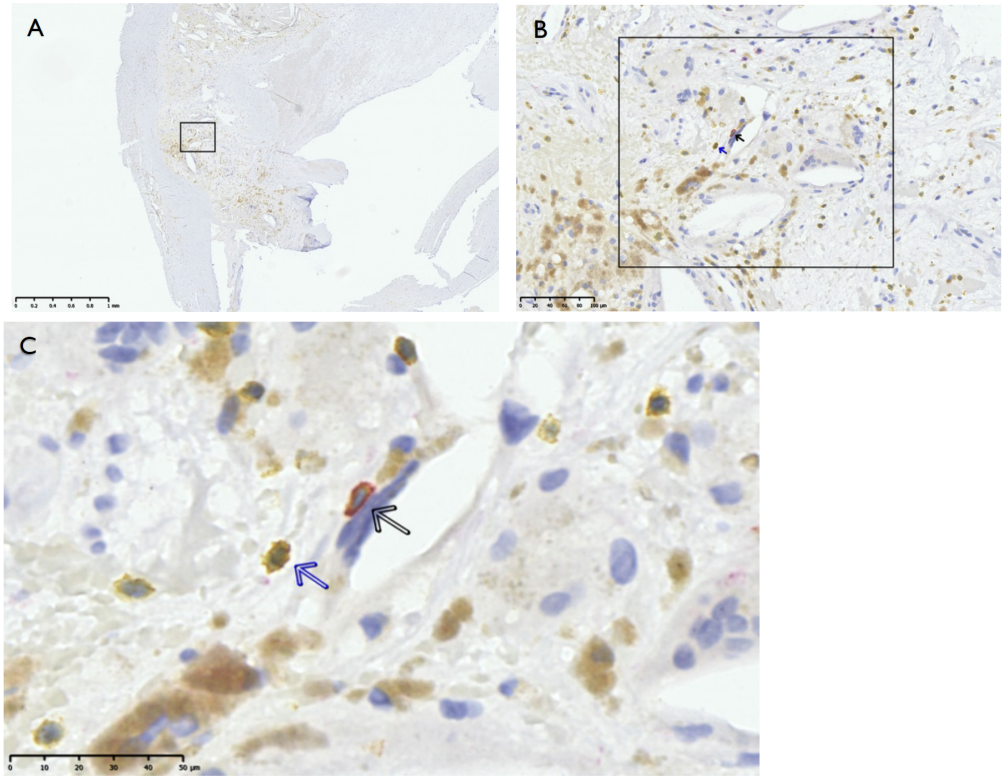

Figure 3.1 | Natural Killer T cell staining in human atherosclerotic plaque. Paraffin embedded human plaque tissue sections were stained with anti-CD3 and anti-CD56 antibody to identify NKT cells. **(A)** Overview of atherosclerotic lesion with rectangle indicating in which area NKT cells are present, magnification 2.5x. **(B)** Higher magnification of rectangle in panel A, magnification 25x. **(C)** Black arrow indicates NKT cell with double positive staining of CD3 (yellow) and CD56 (red). Blue arrow indicates $CD3^+$ cell.

3.4 Natural Killer T cell counts in the human atherosclerotic plaque

The number of NKT cells and T cells per section were counted manually by observer 1 and were assessed for inter-observer reproducibility. Observer 2 counted 30 random slides blinded to the counts of observer 1 (Fig. 3.2). The quantitative analysis of NKT cell number per plaque showed an Intra Class Correlation Coefficient (ICC) of 0.99 (0.983 – 0.996) p<0.001, indicating excellent inter-rater reproducibility (Table 3.2).

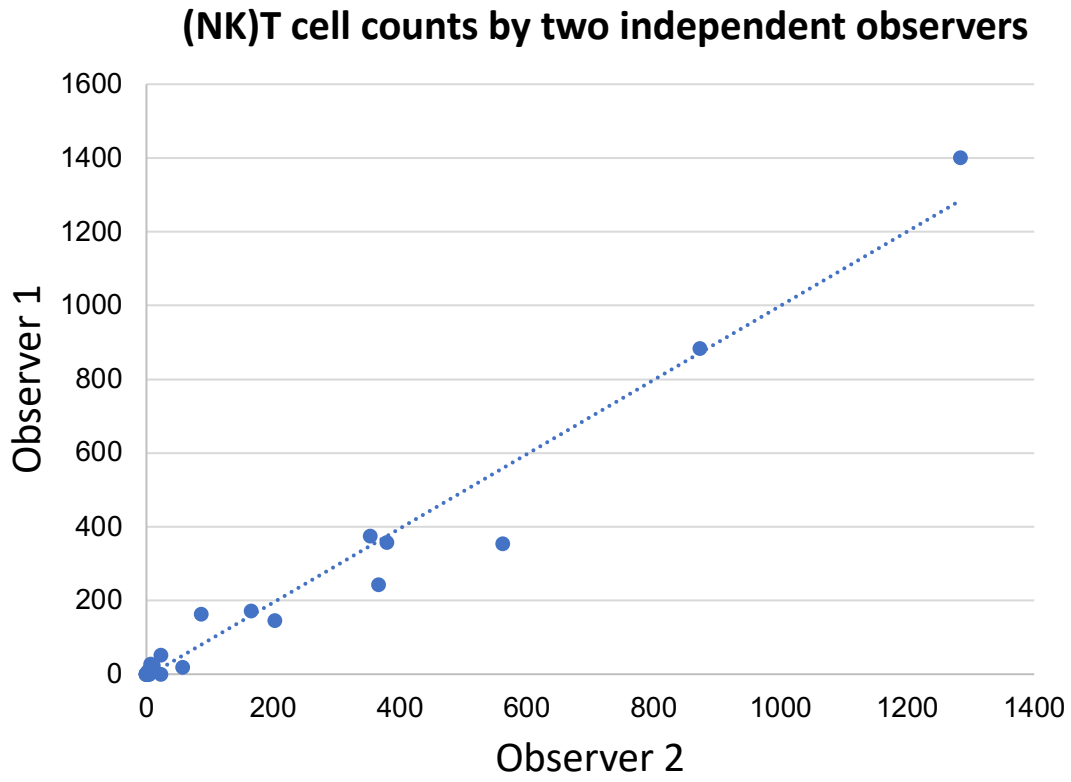

Figure 3.2 | (NK)T cell counts by two independent observers.
The number of (NK)T cells, defined as $CD3^{+}CD56^{+}$ cells, per section were counted manually by observer 1 and were assessed for inter-observer reproducibility. Observer 2 counted 30 random slides blinded to the counts of observer 1.

Table 3.2 | Inter-rater reliability of (NK)T cells counts in human atherosclerotic plaque.

Inter-rater reliability			
Count statistics	**Mean**	**SD**	**N**
Observer 1	147.50	296.99	30
Observer 2	141.57	303.719	30
ICC	**Intraclass correlation**	**95% Confidence Interval**	**P value**
Single Measures	0.984	0.967 – 0.992	<0.001
Average Measures	0.992	0.983 – 0.996	<0.001

In the study population, the absolute NKT cell counts per plaque ranged from 0 to 147. The area of the plaques ranged from 5.3 mm^2 to 73 mm^2. The mean area of the plaque was 28 mm^2 (SD = 13.4). To adjust for differences in plaque area, the number of NKT cells per mm^2 was calculated and ranged from 0 to 8.1. The median NKT cell count per mm^2 was 0.38 per mm^2, and the interquartile interval was 0.063 - 1.19. The median percentage of NKT cells of CD3+ cells was 3.8% (SD = 5.0).

3.5 The location of NKT cells in the human atherosclerotic plaque

Examination of 92 plaques also allowed to study the location of staining of NKT cells in the human plaque and revealed that NKT cells are mainly located in the shoulder of the plaque. Furthermore, it was observed that NKT cell staining was present in the same area of the plaque as CD68 staining (Fig. 3.3), suggesting that myeloid cells may interact with NKT cells in the human plaque.

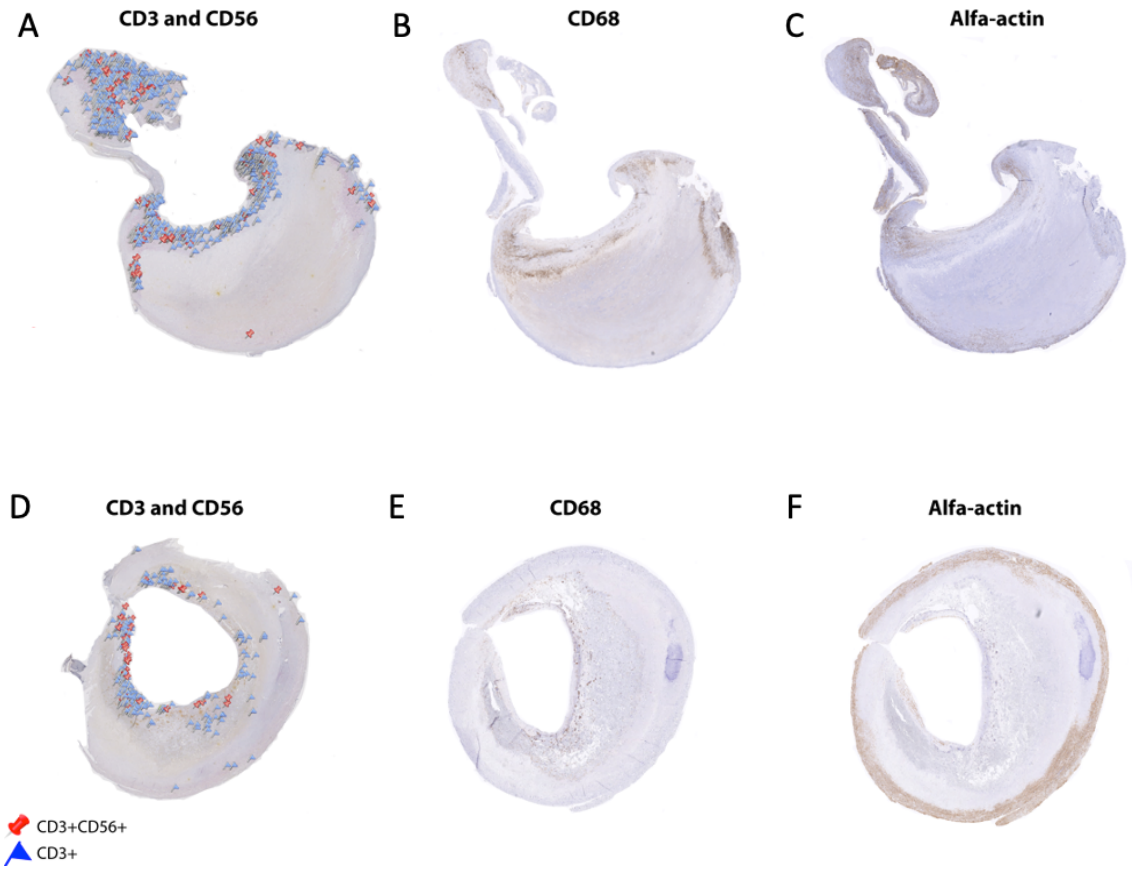

Figure 3.3 | NKT cells and myeloid cells are present in the shoulder of atherosclerotic plaques. Representative examples of human atherosclerotic plaque specimens. **(A,D)** CD3 (yellow) and CD56 (red) staining. Blue flag indicates CD3+ cell, red pin indicates $CD3^{+}CD56^{+}$ cell. **(B,E)** CD68 staining (brown) in adjacent tissue section. **(C,F)** Alfa-actin staining (brown) in adjacent tissue section.

3.6 The relationship between patient characteristics and the number of NKT cells in the human plaque

To assess the relationship between baseline characteristics and NKT cell counts, univariate linear regression was performed. Strikingly, age was negatively associated with the number of NKT cells per mm^2 ($p < 0.001$) (Table 3.3), indicating that older patients had significantly lower NKT cell counts per mm^2 (Fig. 3.4). 19.9% of the variance of NKT cells numbers could be explained by age (Table 3.3). Furthermore, VLDL and Triglyceride levels positively associated with NKT cell

counts (p = 0.03), and 8.3% of variance in NKT cell numbers could be explained by these variables. VLDL levels are calculated by dividing the Triglyceride titers by 5 (Friedewald et al., 1972), and therefore show a similar pattern. However, after Bonferroni correction for multiple testing, associations with VLDL and Triglyceride levels were no longer statistically significant.

Table 3.3 | Univariate linear regression analysis of baseline characteristics with NKT cell counts.

Patient characteristics (n = 92)	**R^2**	**Nominal P-value (α= 0.05)**	**Bonferroni Corrected P-value (α= 0.003)**	**% explained variance**	**Bèta**	**Std. Error**
Sex, male	0.038	0.06	0.06	3.8%	-0.62	0.33
Age in years	0.199	<0.001*	<0.001	19.9%	-0.06	0.01
History						
Cerebrovascular disease	0.004	0.56	0.56	0.4%	-0.24	0.42
Coronary artery disease	0.008	0.40	0.40	0.8%	-0.27	0.32
Peripheral artery disease	0.002	0.69	0.69	0.2%	0.190	0.48
Medication						
Anti-hypertensives	0.026	0.12	0.12	2.6%	0.48	0.31
Lipid lowering drugs	0.001	0.72	0.72	0.1%	0.13	0.36
Anti-thrombotics	0.002	0.65	0.65	0.2%	0.21	0.47
Oral glucose inhibitor	0.001	0.82	0.82	0.1%	-0.09	0.43

Risk factors						
Current smoker	0.004	0.56	0.56	0.4%	-0.21	0.36
Hypertension	0.026	0.13	0.13	2.6%	0.48	0.31
Type 2 diabetes mellitus	0.007	0.44	0.44	0.7%	0.29	0.37
BMI	0.02	0.18	0.18	2%	0.05	0.04
LDL	0.00	0.94	0.94	0%	0.02	0.21
VLDL	0.083	0.03*	0.03	8.3%	1.90	0.89
HDL	0.002	0.73	0.73	0.2%	0.22	0.65
Triglycerides	0.083	0.03*	0.03	8.3%	0.38	0.18

* P < 0.05

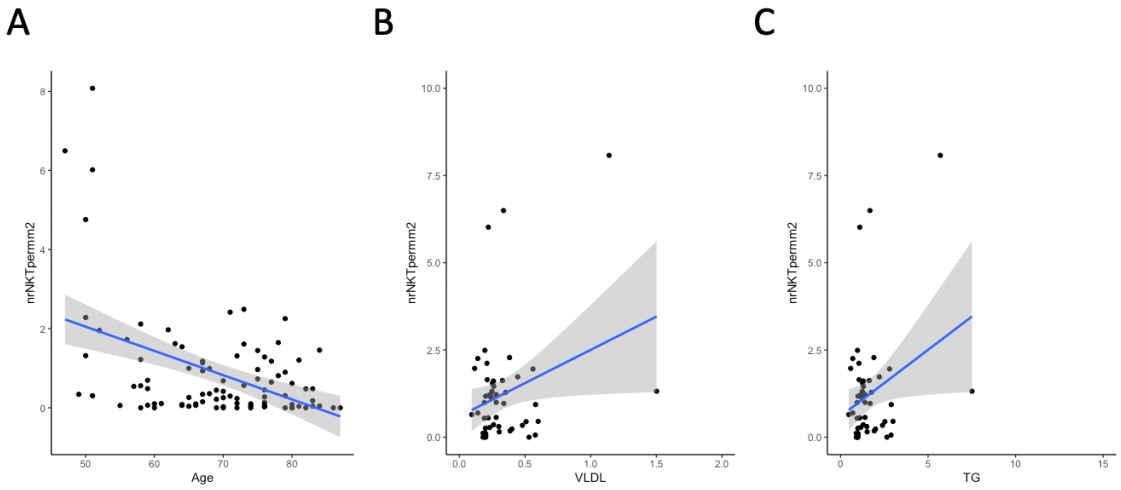

Figure 3.4 | Univariate linear regression between NKT cell counts per mm2 and patient characteristics. (A) Age in association with NKT cell counts per mm^2 (*n = 92)*. **(B)** VLDL in association with NKT cell counts per mm^2 (*n = 92)*. **(C)** Triglycerides in association with NKT cell counts per mm^2 (*n = 92)*. The blue line represents the linear regression accompanied by the 95% confidence interval in grey. Abbreviations: VLDL: Very Low Density Lipoprotein; TG: Triglycerides.

3.7 The relationship between clinical outcome and NKT cell numbers in the human plaque

During the median follow-up time of 3.0 (IQR 2.7 – 3.2) years, 14 patients (15%) reached the composite cardiovascular endpoint defined as non-fatal myocardial infarction, coronary interventions, non-fatal stroke, peripheral vascular interventions and cardiovascular death (Table 3.4 and Fig. 3.5). Univariate linear regression was used to analyze the relationship between occurrence of the cardiovascular endpoint (yes/no) and NKT cell counts in the plaque. There was no association observed between cardiovascular outcome and NKT cell numbers (Table 3.5).

Table 3.4| Definition of clinical endpoint

Composite cardiovascular endpoint	Non-fatal myocardial infarction, coronary interventions, non-fatal stroke, peripheral vascular interventions and cardiovascular death.
Cardiovascular death	Death from stroke, myocardial infarction, congestive heart failure, rupture of abdominal aortic aneurysm or sudden death (unexpected death within 1 hour after onset of symptoms).
Non-fatal myocardial infarction	At least two of the following: (1) Chest pain for at least 20 min, not disappearing after administration of nitrates; (2) ST-elevation >1 mm in two following leads or a left bindle branch block on the ECG; (3) CK elevation of at least two times the normal value of CK and a MB fraction >5% of the total CK.
Coronary interventions during follow-up	Including Percutaneous coronary atherectomy (PCA) and Coronary Artery Bypass Graft Surgery (CABG).
Non-fatal stroke	Relevant clinical features which have caused an increase in handicap of at least one grade on the modified Ranking scale,

	accompanied by a fresh infarct or a hemorrhage on a repeat CT scan.
Vascular intervention	Any vascular intervention to treat clinically relevant ischemic disease in coronary, carotid, iliacal, femoral and crural arteries that was not yet planned at inclusion.

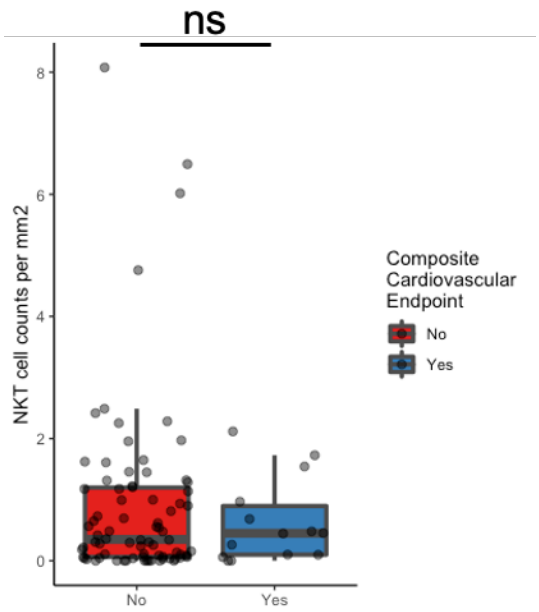

Figure 3.5 | Relation between Composite Cardiovascular Endpoint and NKT cell counts.

Relationship between occurrence of the cardiovascular endpoint (yes/no) and NKT cell counts per mm2 in the plaque. Statistics: independent t-test.

3.8 The relationship between plaque histomorphology and NKT cell numbers

All atherosclerotic plaques were assessed by the Athero-Express team for staining of collagen content (no/minor or moderate/heavy), macrophage content (no/minor or moderate/heavy), smooth muscle cells content (no/minor or moderate/heavy) and fat in the plaque (binned at 10% of the plaque area). Univariate linear regression analysis revealed that smooth muscle cell content was positively

associated with plaque NKT cell counts ($p < 0.006$) (Fig. 3.6). Plaques with moderate/heavy smooth muscle cell staining were associated with higher NKT cell counts (Table 3.5). Fat content in the plaque was negatively associated with plaque NKT cell counts ($p < 0.001$). Higher fat content (>10%) was associated with lower NKT cell counts (Table 3.5).

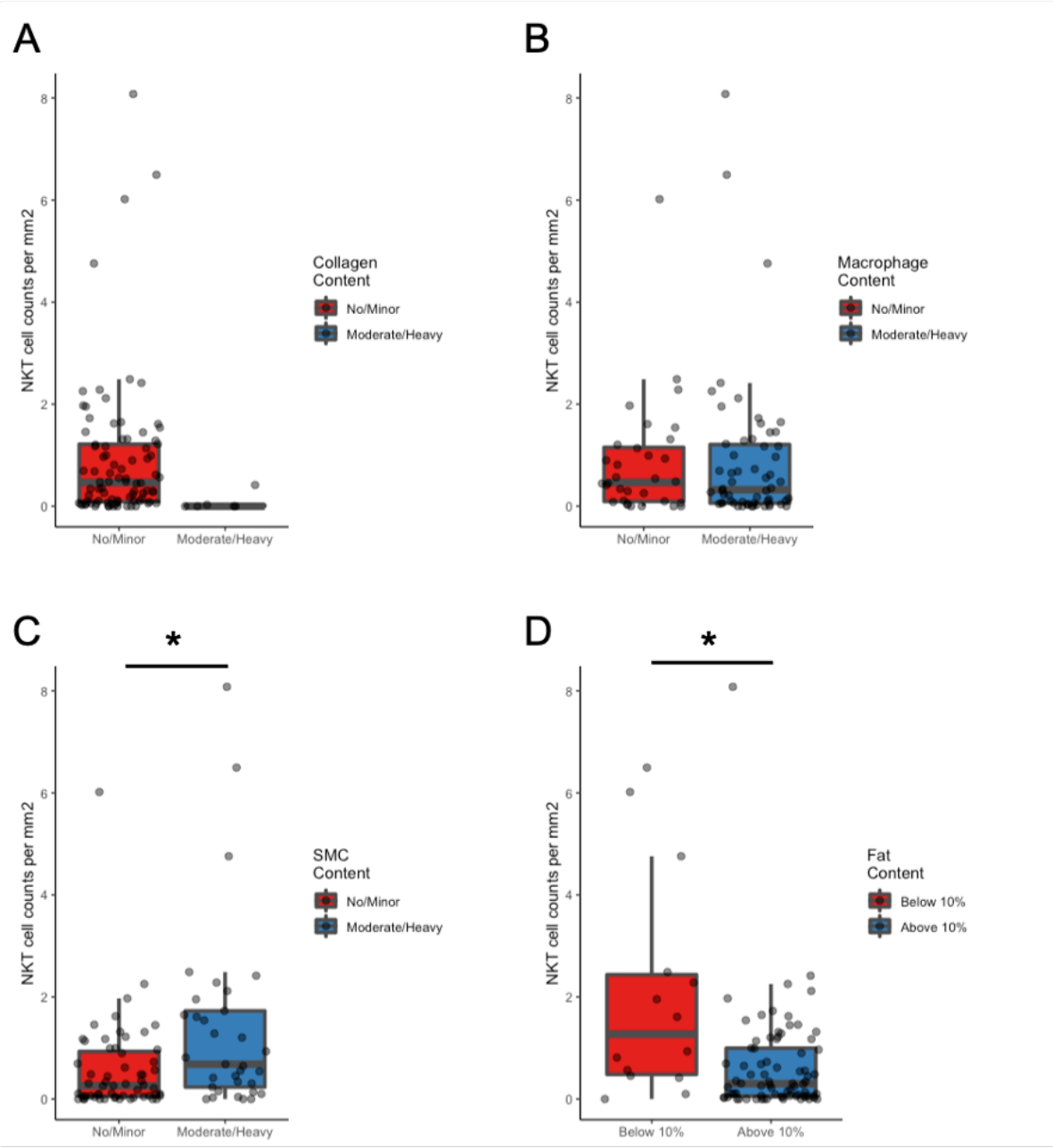

Figure 3.6 | Relation between plaque characteristics and NKT cell counts. (A) Collagen content in relation to NKT cell counts per mm² (*n = 92).* **(B)** Macrophage content in relation to NKT cell counts per mm² (*n = 92).* **(C)** Smooth muscle cell

content in relation to NKT cell counts per mm² (*n = 92).* **(D)** Fat content binned at 10% in relation to NKT cell counts per mm² (*n = 92).* Abbreviations: NKT cell = Natural Killer T cell; SMC = Smooth muscle cell. Statistics: independent t-test. * P <0.05.

To calculate the previously validated plaque vulnerability index, each plaque characteristic that defines a stable plaque (no/minor macrophages, moderate/heavy collagen, moderate/heavy smooth muscle cells and <10% fat) was given a score of 0. Plaque characteristics defining a vulnerable plaque (moderate/heavy macrophages, no/minor collagen, no/minor smooth muscle cells and ≥10% fat) were given a score of 1 (B. Verhoeven et al., 2005). Univariate linear regression analysis indicated that the plaque vulnerability index was negatively associated with NKT cell counts per mm² (p = 0.01). In other words, vulnerable plaques were associated with lower NKT cell counts (Fig. 3.7).

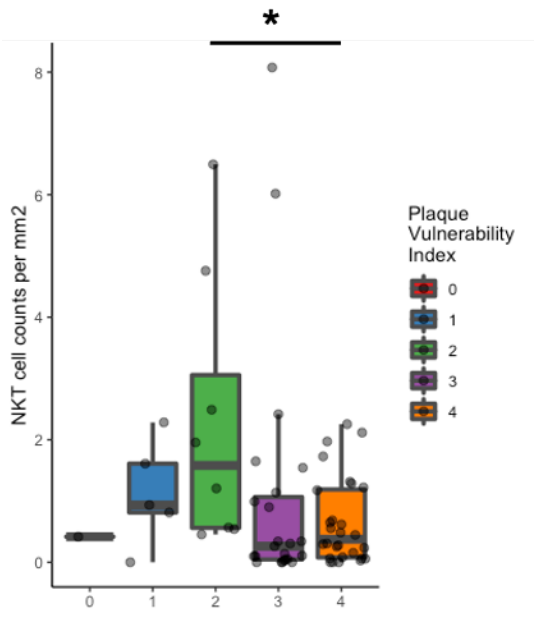

Figure 3.7 | Relation between Plaque Vulnerability Index and NKT cells per mm².

To calculate the plaque vulnerability index, each plaque characteristic that defines a stable plaque (no/minor macrophages, moderate/heavy collagen, moderate/heavy smooth muscle cells and <10% fat) was given a score of 0. Plaque characteristics defining a vulnerable plaque (moderate/heavy macrophages, no/minor collagen, no/minor smooth muscle cells and ≥10% fat) were given a score of 1. This plot shows the relation between plaque vulnerability divided from 0 to 4 and NKT cell counts per mm^2. Statistics: ANOVA with Tukey post-hoc analysis.

Table 3.5 | Univariate linear regression analysis of plaque histomorphology and clinical outcome with NKT cell counts.

Univariate linear regression	R^2	Nominal P-value (α=0.05)	Bonferroni Corrected P-value (α=0.01)	% explained variance	Bèta	Std. Error
Composite cardiovascular endpoint	0.005	0.495	0.495	0.5%	-0.27	0.40
Macrophages	0.000	0.88	0.88	0%	0.045	0.306
Collagen	0.024	0.143	0.143	2.4%	-0.852	0.576
Smooth muscle cells	0.082	0.006*	0.006	8.2%	0.81	0.228
Fat in the plaque	0.137	<0.001*	<0.001	13.7%	-1.407	0.372
Plaque vulnerability index	0.072	0.01*	0.01	7.2%	-0.24	0.09

* P < 0.05

3.9 Discussion

In this chapter, I have investigated NKT cells in the human atherosclerotic plaque in relation to patient characteristics, plaque histomorphology and cardiovascular outcome. Several new observations were made.

First, this study revealed that NKT cell numbers decrease with age in the human plaque. This may be a result of decreased NKT cell numbers in the circulation. In PBMCs of healthy donors, a reduction of 3.4% in iNKT cell numbers was observed per increasing year of age (Molling et al., 2005). Another study confirmed the decrease in iNKT cell numbers in the blood of elderly patients and showed that this was accompanied by an increase in the proportion of $CD4^+$ iNKT cells compared to double negative iNKT cells (Jing et al., 2007). Furthermore, increased IL-4 production was observed upon stimulation with αGalCer in elderly donors compared to young donors, indicating a Th2 shift with aging (Jing et al., 2007). Although the mechanism behind these observations have yet to be unraveled, the reduction of NKT cells could be attributed to changes in CD1d expression. The studies by Molling et al. and Jing et al. did not report CD1d expression, yet skin biopsies show reduced CD1d expression with age (Adly et al., 2006). Further experiments assessing CD1d expression on plaque derived APCs in relation to age, and iNKT cell phenotyping in the human plaque should be performed to provide further inside on the role of immune-aging in iNKT cell biology.

NKT cell count was negatively associated with the plaque vulnerability index. This was driven by the association of low lipid- and high VSMC content with high NKT cell counts in the plaque. VSMCs are the main cellular component of the fibrous cap

which protects the plaque against rupture. Plaque rupture is inversely correlated with the number of VSMC, and increased apoptosis of VSMCs is observed in unstable versus stable plaques (Davies et al., 1993). VSMCs contribute to plaque stability through the production of extracellular matrix component such as collagen that provide strength to the plaque tissue (Harman & Jørgensen, 2019). In addition, they play a role in lipid retention in early stages of plaque formation through interaction of LDL apolipoproteins with VSMC-derived proteoglycans (Skålén et al., 2002). One study examined the interaction between plaque-derived VSMCs and NKT cells *in vitro*, showing that VSMCs enhance iNKT cell proliferation via CD40/CD40L interaction, which may explain the association of high smooth muscle cell content with increased NKT cells in our study (Chan et al., 2005). Furthermore, it was demonstrated that iNKT cells induce VSMC apoptosis *in vitro*, which may act a negative feedback mechanism to prevent overgrowth of VSMCs in the plaque (Chan et al., 2005). The balance between VSMC induced iNKT cell proliferation and iNKT cell induced VSMC apoptosis could determine plaque stability. In mice, increased plaque vulnerability was observed upon αGalCer mediated iNKT cell activation via macrophage activation and upregulation of collagenases (Ohmura et al., 2021). However, translation of mouse studies to humans in the context of plaque vulnerability is complicated because plaque rupture occurs in much lower frequency in mice compared to humans, and the rupture occurs at the brachiocephalic artery in mice compared to the carotid artery in humans (Schwartz et al., 2007). Further *in vitro* studies using cocultures of plaque derived NKT cells and VSMCs are required to investigate causality in the context of plaque vulnerability.

In this study there was no association between LDL and VLDL levels with NKT cells counts in the plaque. In chapter 2 of this thesis, the role of LDL and VLDL in iNKT cell activation and proliferation was identified. A possible explanation for the absence of associations between NKT cell numbers with lipid levels in this study, is the use of lipid lowering drugs by the majority of patients. Patients included in this cohort were well monitored and low target levels of LDL and VLDL were achieved (Table 3.1), perhaps masking the possible associations between lipid levels and NKT cells numbers in the plaque.

There are several limitations to this study. This is an observational study and as such can only identify associations rather than confirm causality. NKT cells were defined as CD3+CD56+ cells, which does not exclude a small portion of Mucosal-associated invariant T (MAIT) cells and Type II NKT cells. Moreover, it should be taken into consideration that one section per patient was stained for NKT cells, which does not provide information on the whole plaque. Finally, although manual counting of NKT cells showed excellent reproducibility, it is highly time consuming and therefore limited the cohort size. The next step is automation of the NKT cell counts using Cellprofiler and slideToolKit software to be able to substantially increase the cohort size and improve the power of the study for cardiovascular outcome assessment (Nelissen et al., 2014).

In summary, this is the first study to quantify NKT cells in the human atherosclerotic plaque, indicating a decrease of NKT cells counts with age. For the first time, the relationship between NKT cell numbers in the plaque, plaque composition and clinical follow-up was studied in a well characterized cohort. We observed that

markers of plaque stability including low lipid content and high smooth muscle cell content, are associated with higher NKT cell numbers in the human plaque, which may suggest a role for NKT cells in plaque stability. These observations call for further investigation of the cellular niche of NKT cells in the human plaque (chapter 4), specifically examination of the biological mechanisms behind the relationship between NKT cells and VSMCs, a hallmark of plaque stability.

4 Spatial mapping of the APC-INKT axis in the human atherosclerotic plaque

4.1 Introduction

Atherosclerosis is a chronic inflammatory disease, involving the innate and adaptive immune system, with response to anti-inflammatory therapies such as canakinumab and colchicine in clinical trials (Nidorf et al., 2020a; Ridker et al., 2017a; Tardif et al., 2019). Understanding the complex interplay between immune cells in atherosclerotic plaque remains a substantial challenge, and is essential to identify new therapeutic targets.

The immune cell landscape of the human atherosclerotic plaque has been identified in several studies using single-cell techniques such as cytometry by time of flight (Helios CyTOF) and single-cell RNA sequencing. These studies brought a comprehensive description of the different cell types in the plaque and highlighted the heterogeneity of vascular leukocytes in atherosclerotic lesions (Depuydt et al., 2020b; Fernandez et al., 2019). However, they require isolation of the cells from the tissue and therefore lack spatial mapping which would allow to reveal tissue context and cellular interactions. Tissue context and cellular interactions are specifically important for the establishment of an immune response within the vascular wall (Engelen et al., 2022; Leistner et al., 2020). In the plaque, iNKT cells depend on interaction with APCs for activation (Getz & Reardon, 2017). Little is known about the micro-environment where APC meet iNKT cells in the atherosclerotic plaque. Specifically, the identity of the APC interacting with iNKT cells in the atherosclerotic plaque remains elusive.

In the past decades, immunohistochemistry has been used for tissue-specific localization of protein expression in atherosclerotic plaque tissue. These methods use antibodies conjugated with fluorophores or enzyme reporters that generate colored pigments, allowing for staining using 1 to 3 antibodies on one sample. The number of antibodies on one sample is limited by spectral overlap and the small number of possible donor species of the antibodies, and has prevented a multiplex IHC approach to identify multiple immune cell subsets and their interactions in the human plaque (Chen et al., 2016; Lee et al., 2018).

To overcome these limitations, I validated the use of Hyperion Imaging Mass Cytometry (IMC) on human atherosclerotic tissue. This technique combines subcellular resolution imaging capability and CyTOF mass cytometry technology, including all advantages of the metal ion-labelling of mass cytometry such as overcoming auto fluorescence and spectral overlap, while preserving tissue architecture (Ali et al., 2020; Giesen et al., 2014). Hyperion IMC allows up to 40 parameters to be visualized in a single tissue section. The tissue is ablated using a 1 µm laser, which scans a selected region of interest. The ablation leads to formation of plumes of tissue matter which are aerosolized, atomized, and ionized, and then transferred into a time-of-flight mass spectrometer for analysis of isotope abundance. For location on the tissue, the isotope abundance can then be mapped back to the original coordinates (Giesen et al., 2014). The use of metal-labelled antibodies is specifically beneficial in atherosclerosis because of its high autofluorescence, which has limited the use of fluorescence based immunohistochemistry techniques (Fitzmaurice et al., 1989; Haeckel et al., 2021; Monici, 2005).

In this chapter, I highlight the potential of multiplexed single-cell technology to characterize the plaque microenvironment to understand the complex immune cell landscape in atherosclerosis.

4.2 Development of an antibody panel to characterize the human atherosclerotic plaque microenvironment

4.2.1 Validation of antibody affinity and specificity on human tonsil tissue

To develop an antibody panel that could elaborately characterize human atherosclerotic plaque morphology and immune cell subsets, antibodies commonly used for immunohistochemistry were optimised for Hyperion IMC. The antibodies were initially validated on human tonsil tissue to confirm binding affinity and specificity (Fig. 4.1). To provide insight in tissue structure, the panel included collagen I for collagen depositions, ACTA2 for smooth muscle cells and CD31 for endothelial cells. For identification of different immune cell subtypes, we included, CD3, CD4, CD8a, iNKT tetramer, TBET and IFNγ for T cell subsets. For B cell identification CD19, CD20, CD38 were included, and HLA-DR, CD64, CD14, CD16, CD68, TREM1, TREM2, CD1d and CD163 for identification of myeloid cells. Nuclei were stained using Histone 3 antibody and iridium nuclear intercalator solution (Fig. 4.1).

Raw Hyperion IMC images were visualized in the MCD viewer software (Std. Biotools) and for each of the markers the staining pattern and coexpression were assessed to evaluate binding specificity. Due to high cellularity of tonsil tissue leading to overlap of nuclei in the images, detailed assessment of coexpression on a single-cell level was hampered. Therefore, the histological structure of tonsil tissue

was used for antibody validation as well. Germinal centers showed high expression of CD19 and CD20 positive B cells as expected. The tissue surrounding the germinal centers showed predominantly CD3 positive staining coexpressing CD4 or CD8 for T cells, and CD163 positive macrophages (Fig.4.2).

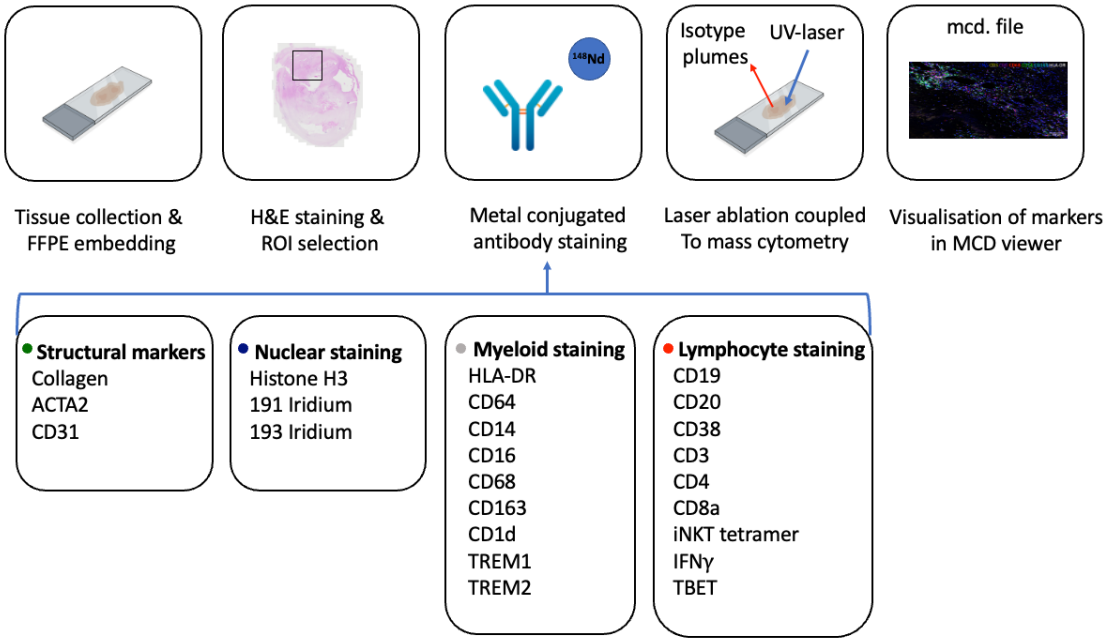

Figure 4.1 | Schematic overview of the workflow used for Hyperion Imaging Mass Cytometry. Tissue sections 5 µm thickness were stained for H&E to define the region of interest based on cellularity. A consecutive tissue section was stained with a cocktail of 22 antibodies labelled with metal isotopes. The tissue was ablated using a 1 µm laser, scanning a selected region of interest of 1.5 mm^2. The ablation leads to formation of plumes of tissue matter which are aerosolized, atomized, and ionized, and then transferred into a time-of-flight mass spectrometer for analysis of isotope abundance per pixel mapped to the location on the section, resulting in mcd file constructing a single image per patient with each of the individual markers.

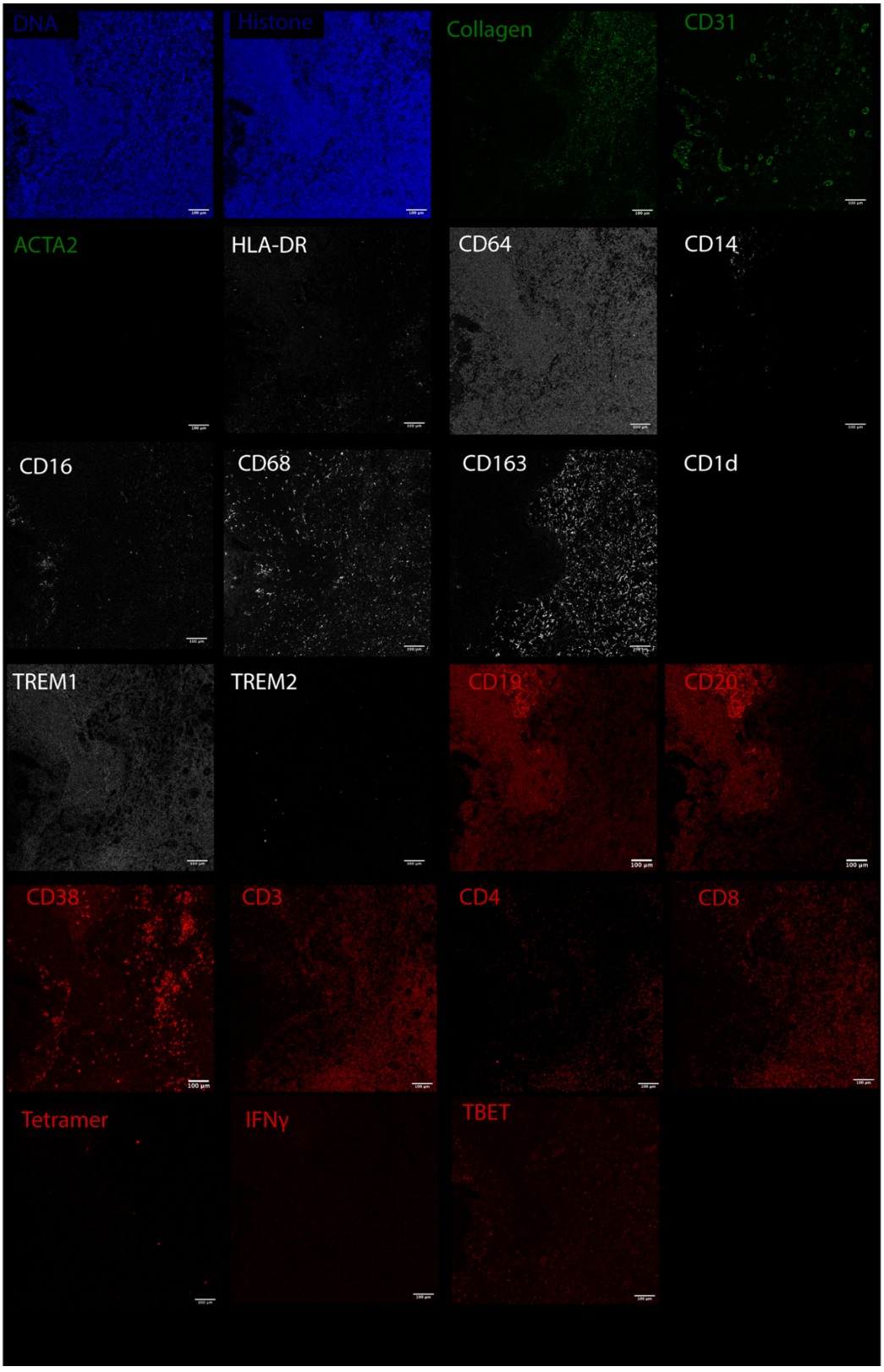

Figure 4.2 | Hyperion IMC panel to characterize the human tonsil microenvironment. Representative images of human tonsil stained with nuclear- (blue), structural- (green), myeloid- (white), and lymphocyte (red) markers. Scale bar 100 µm.

4.2.2 Validation of antibody affinity and specificity on human atherosclerotic plaque tissue

Next, the antibody panel was validated on human atherosclerotic plaque tissue derived from patients who underwent carotid endarterectomy and were included in the Athero-Express cohort study. To determine the optimal antibody concentration for each antibody in the panel, the antibody staining was performed in four dilutions (1:50, 1:100, 1:200 and 1:400) on adjacent tissue sections (Fig. 4.3). In the examples in Figure 4.3 a dilution of 1:100 was selected for the CD8 antibody, 1:200 for the CD68 antibody, 1:50 for the Tetramer, 1:200 for the CD14 antibody, 1:400 for the ACTA2 antibody and 1:100 for the HLA-DR antibody.

Antibody specificity was assessed by visual analysis of marker expression in MCD viewer (Std. Biotools). For example, CD4 and CD8 were mutually exclusive, while coexpressed with CD3. IFNγ was coexpressed with CD3, and CD14 and CD68 showed coexpression as expected. Histone 3 coexpressed with iridium staining suggesting that the iridium staining is a suitable marker for cell segmentation (Fig. 4.4).

4.2.3 Establishment of tetramer based selective staining for iNKT cells

Unique to this panel, is the tetramer staining for identification of iNKT cells. The αGalCer loaded CD1d tetramer staining is specific for iNKT cells and is the gold standard for iNKT cell identification in cell suspension (Chapter 2). In tissues, coexpression CD3 and CD56 or CD3 and CD161 is used to identify iNKT cells (Bobryshev & Lord, 2005). However, this does not exclude a small portions of mucosal-associated invariant T (MAIT) cells and type II NKT cells (Dias et al., 2017).

Using Hyperion IMC, the αGalCer-CD1d-tetramer was validated to identify iNKT cells. To confirm the specificity of the tetramer staining, we assessed coexpression of CD3 and CD56. As expected on iNKT cells, tetramer positive cells, coexpressed CD3 and CD56 (Fig. 4.4C).

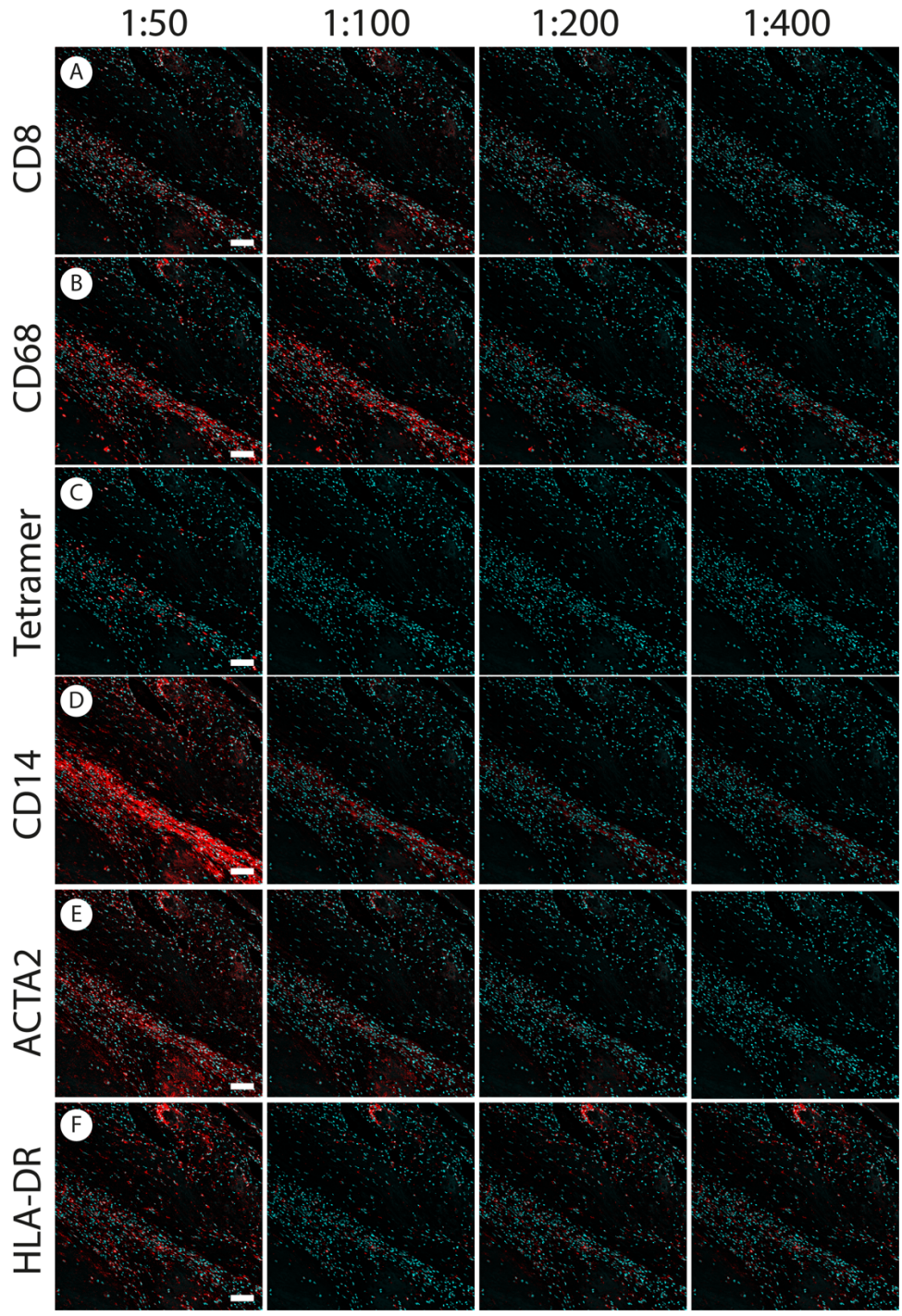

Figure 4.3 | Antibody titration on human atherosclerotic plaque tissue. This figure shows representative images of human atherosclerotic plaque tissue with nuclear (cyan) and cell lineage marker staining (red). Each antibody in the panel was tested in four dilutions to determine the optimal antibody concentration for human atherosclerotic plaque tissue. **(A)** DNA (cyan), CD8 (red). **(B)** DNA (cyan), CD68 (red). **(C)** DNA (cyan), Tetramer (red). **(D)** DNA (cyan), CD14 (red). **(E)** DNA (cyan), ACTA2 (red). **(F)** DNA (cyan), HLA-DR (red). Scale bar 100 µm.

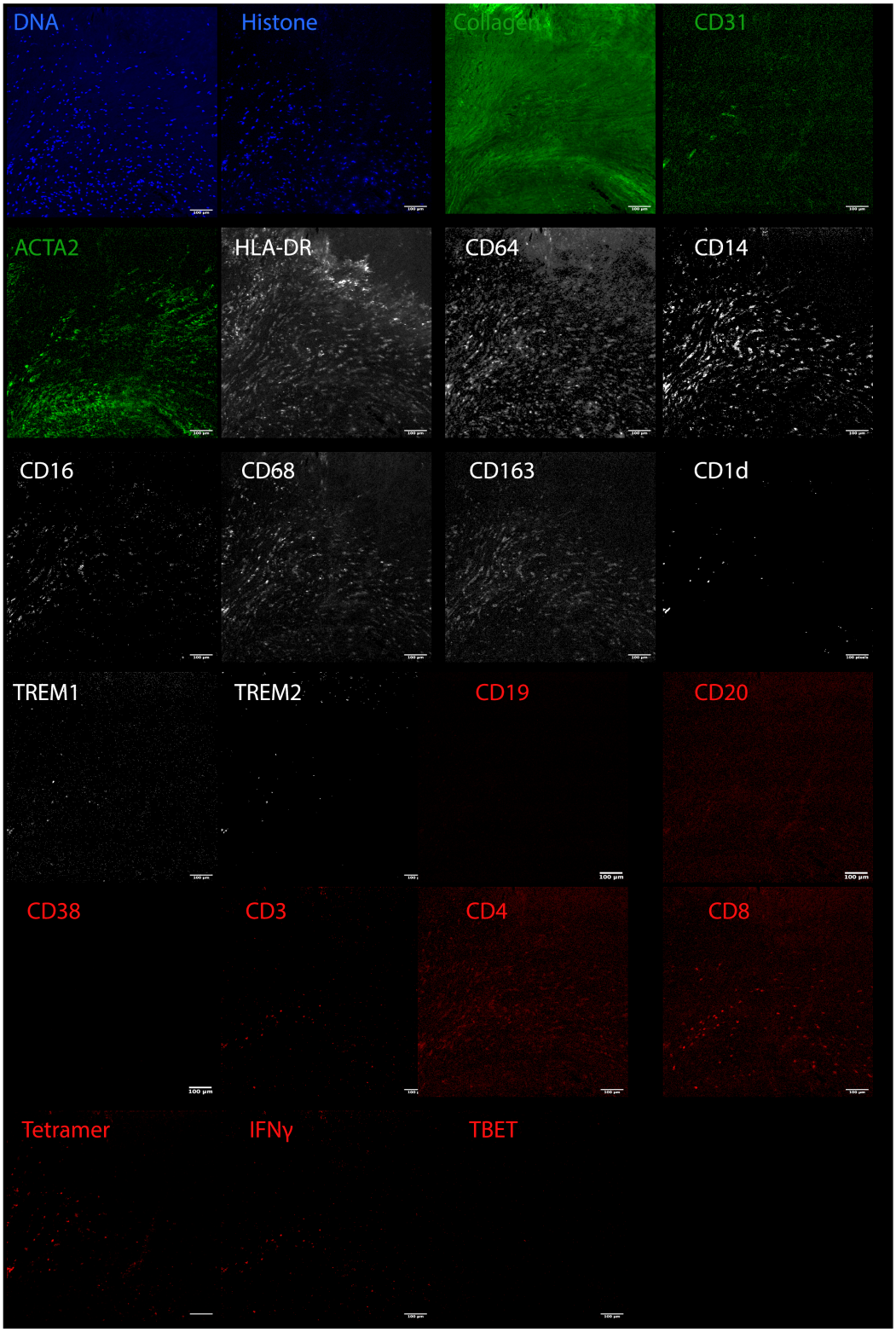

Figure 4.4 | Hyperion IMC panel to characterize the human atherosclerotic plaque. Representative images of human atherosclerotic plaque stained with nuclear (blue), structural (green), myeloid (white), and lymphocyte (red) markers. Scale bar 100 µm.

Evaluation of multi-color images led to the identification of a variety of immune cell subsets such as macrophages, T cells and iNKT cells (Fig. 4.5A, C). The structural marker panel provided insight in plaque histomorphology by identification of collagen deposits, smooth muscle cells and intra-plaque vessels (Fig. 4.4B).

Taken together, the optimized antibody panel provided markers to identify several immune cell subsets including T cells, iNKT cells, B cells, macrophage/monocyte subsets, endothelial cells, smooth muscle cells and collagen depositions.

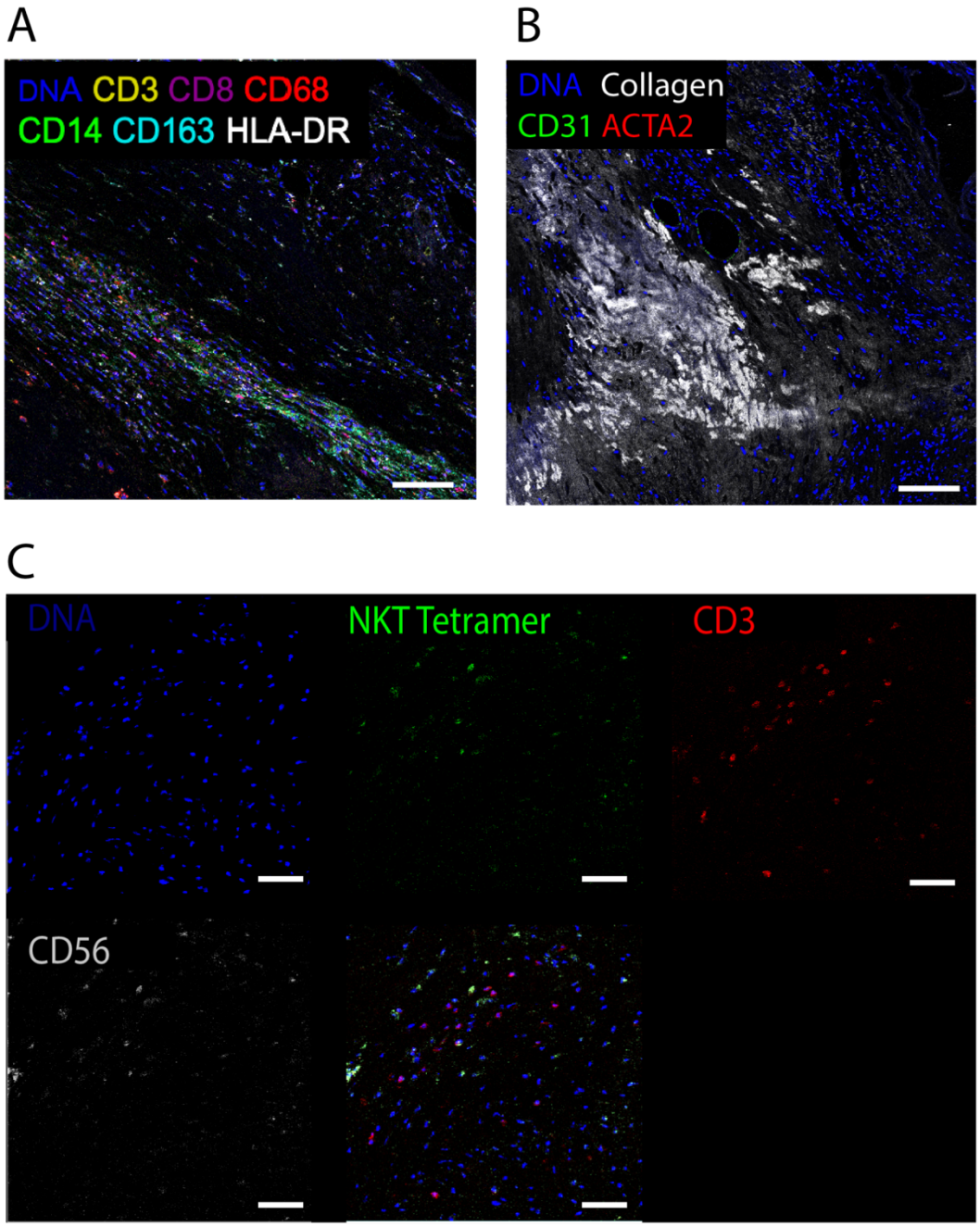

Figure 4.5 | Multiplex imaging of human atherosclerotic plaque tissue to identify immune cell subsets in human atherosclerotic plaque tissue using Hyperion IMC. (A) Image obtained from human atherosclerotic plaque tissue showing DNA, CD3, CD8, CD68, CD14, CD163 and HLA-DR staining. Scale bar 175 µm. **(B)** Image obtained from human atherosclerotic plaque tissue showing DNA, collagen, CD31 and ACTA2 staining. Scale bar 150 µm. **(C)** Invariant Natural Killer T cell staining in human showing coexpression of tetramer staining with CD3 and CD56, both markers for NKT cells. Scale bar 100 µm.

4.3 Image analysis identified distinct immune cell subsets in human atherosclerotic plaque tissue

To assess the microenvironment of the atherosclerotic plaque, five atherosclerotic plaque sections derived from patients who underwent carotid endarterectomy were stained with our optimised antibody panel (Fig. 4.1). Regions of interest of 1.5 - 5 mm^2 were acquired using the Hyperion Imaging Mass Cytometer (Std. Biotools). The images were visualized in the MCD viewer software (Std. Biotools) to assess marker signal intensity, which resulted in the exclusion of one patient sample from the analysis because of poor image quality.

4.3.1 Extraction of single-cell data

To convert the raw IMC images into single-cell data, images were converted to TIFF format and segmented into single cells using CellProfiler (Fig. 4.6A). Nuclear channels iridium 191 and iridium 193 were used to identify cell nuclei, which served as the basis for cell segmentation (Fig. 4.6B). To assess the quality of cell segmentation, raw images were compared with the cell masks and were largely in agreement with the staining pattern. The cell masks were exported as TIFF files and used for signal quantification (Fig. 4.6C). The mean intensity of signal per marker and X and Y coordinates per single cell were exported from CellProfiler for further single-cell analysis. Cells with expression of all markers, identified by row variance analysis, were excluded from analysis after visual comparison of the staining pattern confirmed they were artifacts. Cells that exclusively stained for Iridium without Histone 3 staining or other marker staining, were excluded from further analysis as well, resulting in a total of 5,062 cells.

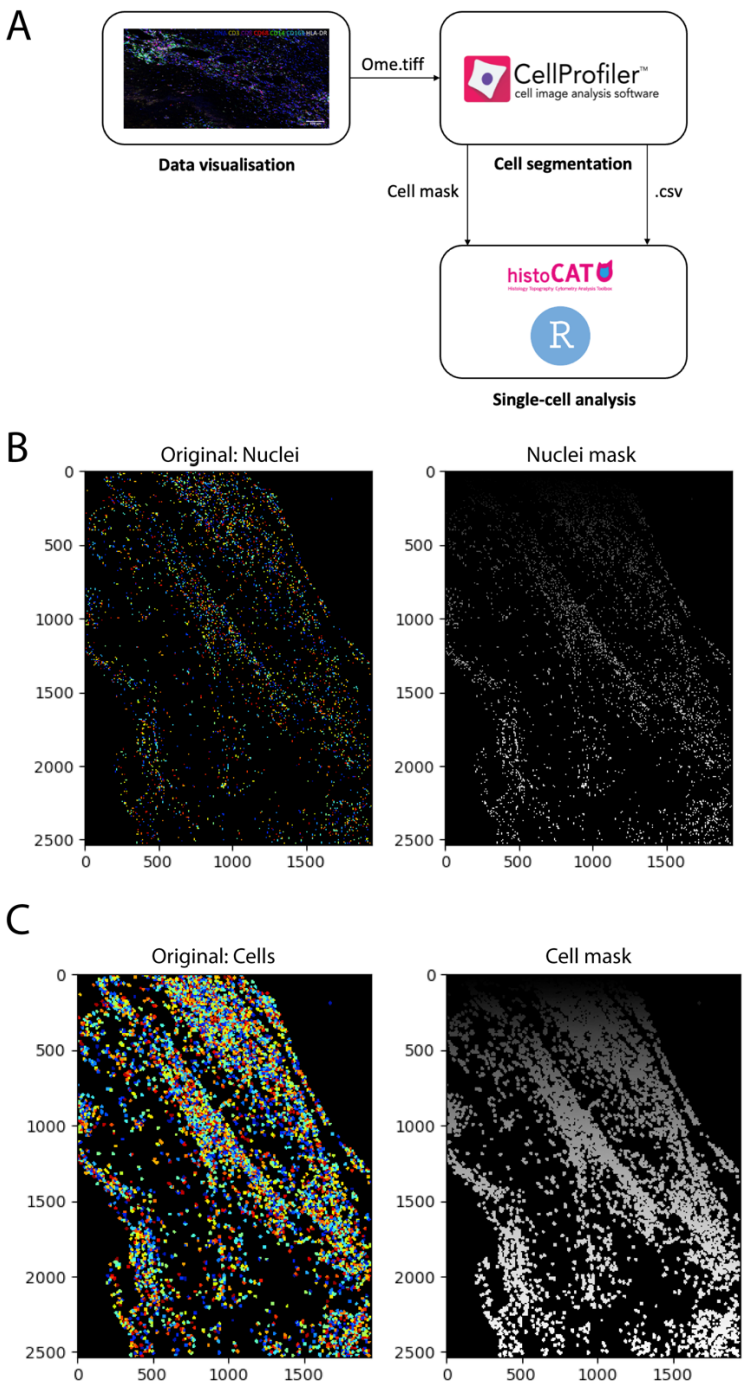

Figure 4.6 | Establishing an image analysis pipeline to characterize the human atherosclerotic plaque microenvironment.

(A) Overview of analysis workflow. Cells were segmented in CellProfiler to identify cell location and marker expression. Subsequent single-cell analysis was performed in HistoCAT and R studio. **(B)** Representative image obtained from human atherosclerotic plaque tissue showing nuclei identification based on Iridium 191 and Iridium 193 DNA staining (left panel) and nuclei mask generation by

CellProfiler cell segmentation software (right panel). **(C)** Representative image of predicted cells generated by CellProfiler software (left panel) and corresponding cell mask (right panel).

4.3.2 Cell type clustering of immune cell subsets in human atherosclerotic plaque

Having identified single cell marker expression, phenograph clustering was performed and resulted in 7 clusters identifying smooth muscle cells (cluster 5), CD8+ T cells (cluster 2), dendritic cells (cluster 4), macrophages (cluster 6) and iNKT cells (cluster 8) (Fig. 4.7A,C). Cells with expression patterns not distinctive for a specific immune cell subset were classified as unclassified. The Uniform Manifold Approximation and Projection (UMAP) algorithm was used to project all cells (Fig. 4.7B). To assess the quality of the cell classification, raw images were compared with the identified clusters and showed agreement in staining pattern.

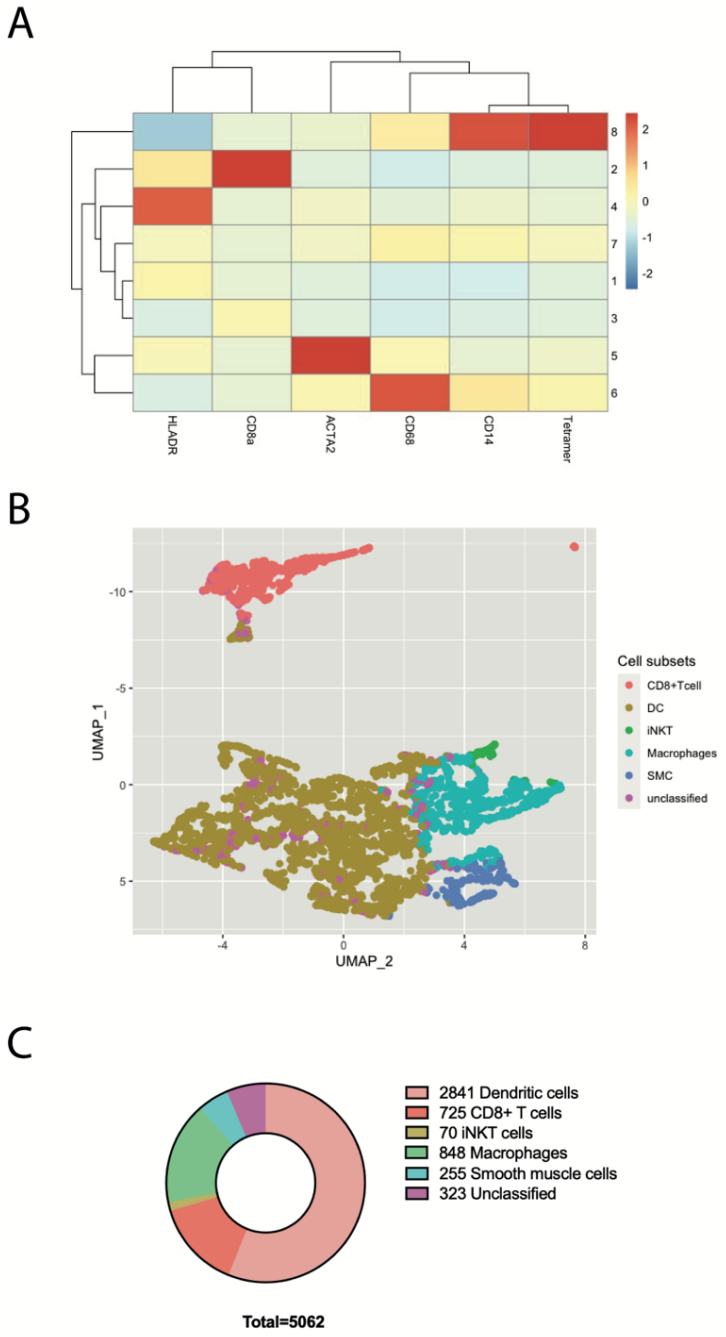

Figure 4.7 | High dimensional cellular profiling via clustering analysis. Using Phenograph clustering cells were classified into 7 cell clusters based on expression of cell lineage markers. Cells with expression patterns not distinctive for a specific cell subset were named unclassified. **(A)** Heatmap of the mean intensity of each identity marker for each cluster. Mean intensity is calculated per cell type from the normalized mean expression per cell. **(B)** UMAP projection of cell clustering of 5,062 cells using expression of 6 cell linage markers. Each dot represents a single cell. **(C)** Total number of cells in each identified cell cluster.

4.3.3 *Macrophages are the APC subset residing in the closest proximity to iNKT cells in the human atherosclerotic plaque*

To study the spatial features of the human atherosclerotic plaque, for each sample the previously identified cell clusters were spatially mapped, providing insight in cell distribution through the tissue (Fig. 4.8). The median distance between cell subsets was calculated in R studio (igraph package) to assess which cells are present in the cellular niche of iNKT cells (Fig. 4.9A). The smallest distances were observed among iNKT cells. Next, macrophages were in closest proximity to iNKT cells, suggesting that macrophages are involved in the APC-iNKT axis in human atherosclerotic plaque tissue (Fig. 4.9). Smooth muscle cells, DCs and $CD8^+$ T cells showed larger distances from iNKT cells.

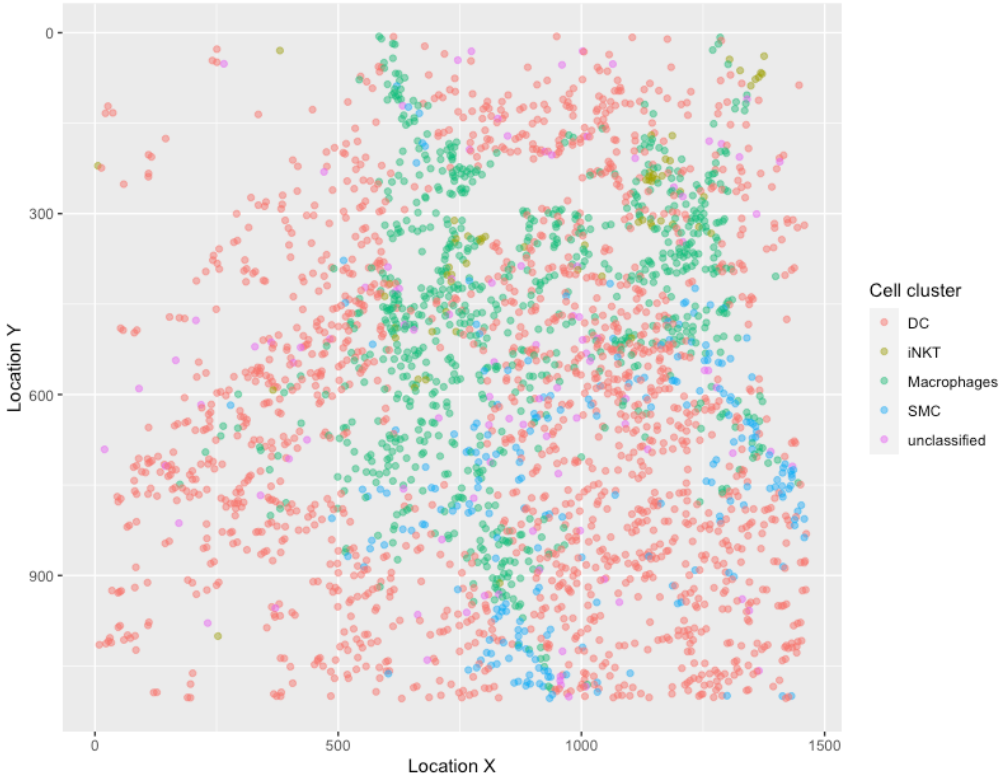

Figure 4.8 | Spatial representation of cell clusters in human atherosclerotic plaque tissue. Spatial graph of 1 ROI indicating the location of 2,069 cells and 6 cell clusters, with each dot representing an individual cell.

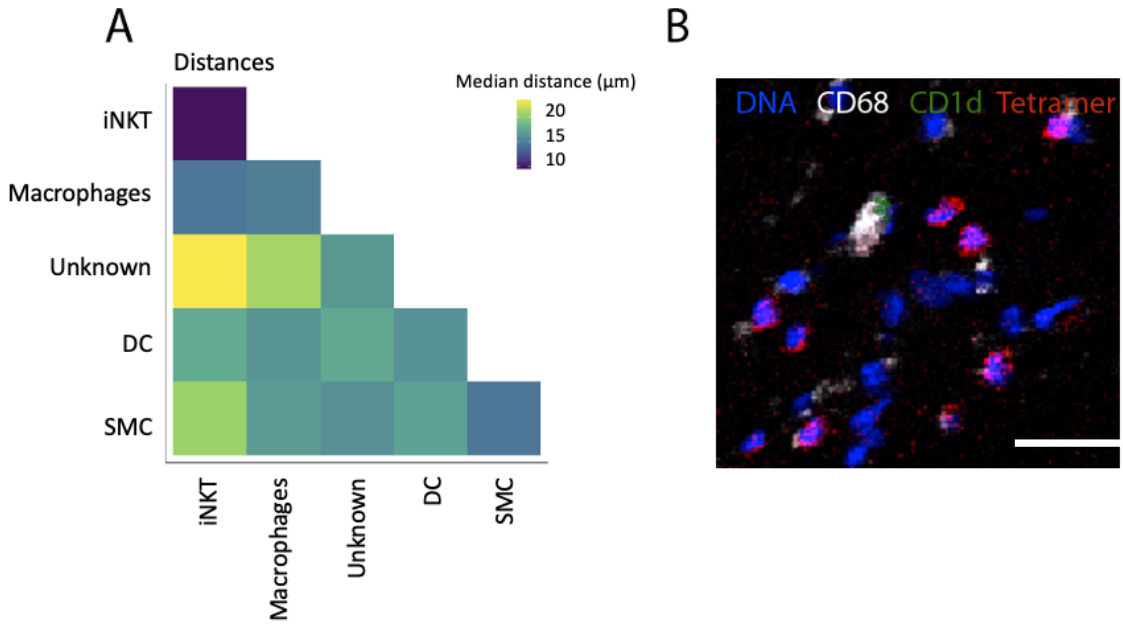

Figure 4.9 | Macrophages reside in close proximity to iNKT cells in the human atherosclerotic plaque.

(A) Heatmap showing the median distance in micrometers between cell subsets in 6 ROIs derived from 4 patient samples. **(B)** Representative image showing DNA (blue), CD68 (white), CD1d (green) and Tetramer (red) staining. CD1d expressing macrophages (CD68) and iNKT cell (Tetramer) reside in close proximity. Scale bar: 20 µm. Abbreviations = ROI: Region of interest.

4.4 Discussion

In this chapter I show, for the first time, that highly multiplexed tissue imaging using Hyperion Imaging Mass Cytometry is feasible in human atherosclerotic plaque tissue. I developed a staining protocol specific for human atherosclerotic plaque tissue resulting in simultaneous staining of 22 markers on 1 tissue section, which is unique in the field of atherosclerosis. The panel allowed for the identification of several immune cell subsets including T cells, iNKT cells, macrophages, endothelial cells, smooth muscle cells and collagen depositions. Next, a first analytical effort towards single-cell clustering and spatial analysis resulted in the identification of macrophages as the APC in closest proximity to iNKT cells, suggesting macrophages are the key antigen presenting cell in the APC-iNKT axis in the human plaque.

4.4.1 Validation of Hyperion Imaging Mass Cytometry on human atherosclerotic plaque tissue

To validate the use of Hyperion Imaging Mass Cytometry on human atherosclerotic plaque tissue I designed a broad antibody panel enabling identification of the main immune cell subsets. A major advantage of Hyperion IMC is that the conjugation of antibodies with metal isotopes is straightforward and therefore a wide variety of IHC tested antibody can be included in the panel. Previous studies have validated the conjugation of antibodies and indicated that the conjugation process does not affect antigen binding properties and IMC staining patterns could be reproduced by IHC (Giesen et al., 2014; Ijsselsteijn et al., 2019). In this study, iNKT cells were defined by tetramer staining and co-expression of CD3 and CD56. In chapter 3, coexpression of CD3 and CD56 was used for identification of iNKT cells. However, this does not exclude a small portion of MAIT cells and type II NKT cells. The

establishment of tetramer staining, which is specific for the invariant TCR of iNKT cells, allowed for more accurate identification of iNKT cells in tissue.

Cell segmentation is the most challenging step in multi-plex image analysis and requires further optimisation. Although successful cell segmentation was achieved for the majority of cells, cells in densely packed immune infiltrates in the plaque showed inaccurate segmentation. Overlapping cells were interpreted by the software as one cell, leading to the identification of an iNKT cell cluster with both Tetramer and CD14 expression, while visual inspection of the staining pattern showed that the expression of Tetramer and CD14 belonged to different cells in close proximity to each other. This issue has been reported in a study by Bodenmiller et al. as well, resulting in a T-B cell cluster in their analysis (Jackson et al., 2020). Furthermore, the heterogeneity of immune cell morphology in the plaque complicates cell segmentation, with cells varying from small round T cells (5-7 μm) to elongated smooth muscles cells (5 μm x 200 μm). Improved cell segmentation pipelines using artificial intelligence and H&E staining of adjacent slides are currently being developed by collaborators to be incorporated in future analysis, which could allow more detailed clustering of immune cell subsets.

In this study, one patient sample was excluded due to overall insufficient signal intensity, possibly due to older age of the tissue section. In future experiments signal intensity could be improved by using freshly cut FFPE tissue or fresh frozen samples, however the latter would require additional optimisation of the staining protocol. In case one or two markers show specifically dim expression, signal amplification could be employed to enhance signal (Rana et al., 2019).

4.4.2 Identification of the APC-iNKT axis in the human atherosclerotic plaque

This data indicates that CD1d expressing macrophages are the APC subset residing in closest proximity to iNKT cells in the human atherosclerotic plaque, suggesting that macrophages are the key APC involved in iNKT cell activation in this tissue. This is relevant, because the APC involved in lipid antigen presentation to iNKT cells differs in an organ-dependent fashion with implications for the iNKT cell cytokine response. In the liver for example, CD1d expressing specialized macrophages called Kupffer cells are involved in CD1d dependent the activation of iNKT cells (Schmieg et al., 2005). In the spleen, B cells are the main APC interacting with iNKT cells in the marginal zone, and dendritic cells fulfill this role in the red pulp (P. Barral et al., 2008; Schmieg et al., 2005). Specifically, DC-mediated lipid antigen presentation induces a more pro-inflammatory iNKT cell cytokine response, compared to iNKT cell responses mediated by Kupffer cells, indicating that the APC subset involved in the APC-iNKT cell axis determines its activation profile towards either a pro- or anti-inflammatory response (Schmieg et al., 2005). The mechanism behind this has not been investigated, but there may be a role for costimulatory molecules in this process as it has been shown that PD-1 blockade can skew iNKT cells towards a Th1 cytokine profile and CD86 blockade resulted in Th2 skewing of iNKT cells (Pál et al., 2001; Wang, Bhave, et al., 2020). As shown in chapter 2 (Fig. 2.7), coculture of αGalCer-treated THP1 derived macrophages with iNKT cells leads to potent iNKT cell activation *in vitro*. Future experiments employing coculture of human plaque derived macrophages treated with or without CD1d antagonist DPPE-DPPE-PEG_{350} and human primary iNKT cells could explore the effect of plaque derived macrophage mediated iNKT cells activation further. *In vivo* studies using a mouse

strain with *Cd1d1*$^{-/-}$ vascular macrophages in comparison to WT mice could explore the effect of this interaction on atherogenesis.

Taken together, I validated the use of Hyperion Imaging Mass Cytometry on human atherosclerotic plaque tissue, allowing single-cell profiling of the plaque micro-environment, while preserving spatial information. This allowed for the identification of macrophages as the APC in closest proximity to iNKT cells, suggesting that macrophages are the key APC involved in iNKT cell activation in the human atherosclerotic plaque. Profiling of the plaque micro-environment will further our understanding of atherogenesis and could potentially enable patient stratification and therapeutic target identification for the development of novel immunotherapies in CVD.

5 Final discussion

Atherosclerosis, the major cause of cardiovascular disease, is a chronic inflammatory disease triggered by the accumulation of cholesterol-containing low-density lipoprotein (LDL) particles in the arterial wall (Libby, 2012). NKT cells operate at the interface of lipids and the immune system, as they are activated by lipid antigens presented on CD1d by APCs. Upon activation NKT cells rapidly produce Th1, Th2 and Th17 cytokines and cytotoxins. Although relatively few (0.1-1% of T lymphocytes) in absolute number, their response is robust and leads to activation of bystander immune cells. NKT cells are considered pro-atherogenic, mainly based on murine studies (Getz & Reardon, 2017). However, fundamental aspects of NKT cell biology remain unclear including the mechanisms involved in lipid antigen delivery and NKT cell activation and their role in human atherosclerosis.

5.1 Summary

5.1.1 Lipoproteins act as vehicles for lipid antigen delivery to APCs and iNKT cell activation

I identified lipoproteins very-low-density- (VLDL) and low-density (LDL) as vehicles for lipid antigen delivery and subsequent activation of invariant NKT cells. Previous experiments showed a role for ApoE on lipoprotein particles for the activation of iNKT cells. However, the identity cognate receptors for ApoE on the APCs side is not ascertained. Using 2c-FCCS, I demonstrated stable complex formation of the model lipid antigen αGalCer with lipoproteins *in vitro* and *in vivo* in the circulation (Fig. 2.1). My *in vitro* experiments demonstrated that the uptake of LDL-αGalCer complexes by APC is predominantly mediated by LDLR (Fig. 2.6).

Subsequently, the (V)LDL-αGalCer complexes propagate robust iNKT cell activation, demonstrated *in vitro* and *in vivo* (Fig. 2.7, Fig. 2.12). The uptake of VLDL-αGalCer complexes *in vivo* was proven to be mediated by LDLR as well. LDLR-mutant PBMCs of patients with familial hypercholesterolemia showed impaired in activation and proliferation of invariant NKT cells, illustrating that LDLR-mediated uptake of lipoprotein-lipid antigen complexes by APCs is also relevant for iNKT cell activation in humans (Fig 2.17, Fig. 2.18). This study showed that lipoproteins can act as vehicles for lipid antigen delivery and that iNKT cell activation in mice and humans is dependent on the LDLR, providing new insights into the immunological abilities of lipoproteins.

5.1.2 NKT cells in human atherosclerotic plaques are associated with plaque stability

I studied the relationship between NKT cell counts in the human atherosclerotic plaque and patient- and plaque characteristics and clinical outcome in the well characterized Athero-Express cohort of patients who underwent carotid endarterectomy. It is the first study that quantified NKT cells in the human atherosclerotic plaque. Markers of plaque stability, including low lipid content and high smooth muscle cell content, were associated with higher NKT cell numbers in the human plaque, which suggest a protective role for NKT cells in plaque stability in human atherosclerotic plaque tissue (Table 3.3). These findings are at odds with the literature in murine models of atherosclerosis. However, these studies mainly measured lesions size and fibrous cap thickness, which are not the only determinants in humans of cardiovascular outcomes. Endogenous lipid antigens involved in NKT cell activation in human atherosclerosis, which have yet to be

identified, might skew NKT cells towards a more anti-inflammatory profile contributing to plaque stability, compared to αGalCer induced iNKT cell activation used in mouse models. My findings, if confirmed encourage further research on the biology of NKT cells in human atherogenesis. Investigation of the biological mechanisms behind the relationship between NKT cells and plaque stability are required to determine causal relations.

5.1.3 Spatial mapping of the APC-iNKT axis in the human atherosclerotic plaque

Finally, I validated the use of Hyperion Imaging Mass Cytometry on human atherosclerotic plaque tissue, allowing single-cell profiling of the plaque micro-environment, while preserving spatial information. I developed an antibody panel including 22 markers characterizing human atherosclerotic plaque morphology and immune cell subsets including T cells, iNKT cells, B cells, macrophage/monocyte subsets, endothelial cells, smooth muscle cells and collagen depositions (Fig. 4.3). I made a first effort towards cell segmentation and single cell analysis of Hyperion IMC images which allowed the identification of macrophages as the APC in closest proximity to NKT cells, suggesting that macrophages are involved in the APC-iNKT cell axis in the human plaque (Fig. 4.10). This finding is in line with Chapter 1 where I demonstrate that macrophages have the ability to activate invariant NKT cells via LDLR-mediated uptake of lipoproteins. Future studies using Hyperion IMC can benefit from improved cell segmentation pipelines using artificial intelligence and H&E staining of adjacent slides which are currently in development by collaborators.

5.2 Future perspective

The big question that remains in the field of NKT cells in atherosclerosis is which endogenous lipid antigens trigger NKT cell activation in atherosclerosis. The identification of lipid antigens would enable development of new therapeutics such as lipid antigen neutralizing antibodies. In this thesis, I have established how model lipid antigens are transported to APCs, which guided the search of lipid antigens to VLDL and LDL particles. CD1d sortagging is a potential strategy to identify endogenous lipid antigens derived from these lipoproteins. Culture of LDL with THP1 cells expressing CD1d with a sortase tag, enables site-specific cleavage and biotin labelling of CD1d-lipid complexes. CD1d-lipid complexes can be subsequently captured on streptavidin beads and processed for lipid antigen identification by mass spectrometry.

Implementation of immunophenotyping of human atherosclerotic plaques using Hyperion IMC can help identify patients with vulnerable plaques, who are at high risk of recurrent cardiovascular events. Currently, 4 plaque determinants are used to assess plaque vulnerability: fat-, macrophage-, collagen- and smooth muscle cell-content. Deep immunophenotyping strategies can enhance the identification of vulnerable lesions and select patients who would benefit from additional monitoring or specific therapeutics.

5.3 Concluding remarks

In conclusion, this thesis defines the mechanism of lipid antigen delivery to APCs by circulating lipoproteins, and its fundamental role in invariant NKT cell activation. It proposes innovative imaging modalities to study the APC-iNKT axis in the human

plaque, and associates NKT plaque-abundance with plaque stability for the first time. Gaining a better understanding of the interplay of lipids and the immune system, is essential for identification of novel targets to tackle inflammation in atherosclerosis and improve patient outcome.

6 Material and Methods

6.1 List of antibodies and buffers

Antibodies used in experiments are listed in Tables 6.3 – 6.5. Buffers and solutions made in-house are listed in Table 6.6.

6.2 Study approval

Animal studies were performed according to UK Home Office regulations and European directive 2010/63/EU. Human studies were approved by the Medical Research Ethics Committee of the University Medical Center Utrecht (protocol numbers 11-183, 19-081 and TME/C-01.18), and complied with the Declaration of Helsinki. All patients provided written informed consent.

6.3 Patient samples

6.3.1 Peripheral blood mononuclear cells

Peripheral blood mononuclear cell (PBMC) samples of 4 patients with LDLR mutations and 10 age-matched controls were provided by the Ucorbio Cardiovascular Biobank of the University Medical Center in Utrecht, The Netherlands (clinicaltrials.gov identifier NCT02304744). Patients: 3 men and 1 woman, mean age 58 years, circulating LDL-cholesterol levels 1.4-6 mmol/l, LDLR mutations C371X or E207K. Controls: 6 men and 4 women, mean age 60 years, of whom 5 with normal circulating LDL-cholesterol levels (<2.6 mmol/l) and 5 with high circulating LDL-cholesterol levels (≥2.6 mmol/l).

6.3.2 Atherosclerotic plaque tissue

Paraffin embedded atherosclerotic plaques sections were provided by Athero-Express Biobank of the University Medical Center in Utrecht, The Netherlands. The samples were donated by patients who underwent carotid endarterectomy according to local clinical guidelines.

6.3.3 Tonsil tissue

Paraffin embedded tonsil sections obtained from 5 patients who underwent tonsillectomy were provided by the Oxford Radcliffe Biobank (protocol number 19/SC/0173) and used for antibody validation (Hyperion Imaging Mass Cytometry).

6.4 Animal work

6.4.1 Mouse maintenance

Male LDLR-deficient (*Ldlr*$^{-/-}$) mice on a C57BL/6 background and male C57BL/6 control mice (WT) were purchased from Jackson laboratories, bred in-house under specific-pathogen free conditions and fed a standard chow diet.

6.4.2 Genotyping

Genomic DNA was extracted from tissue derived from ear biopsies using REDExtract-N-Amp™ Tissue PCR Kit (Sigma-Aldrich). The tissue was added to 25 µl of Extraction solution and 5.25 µl of Tissue Preparation solution. This mixture was vortexed and incubated for 10 minutes at room temperature. Subsequently, the samples were incubated at 95°C for 3 minutes. Next, 25 µl of Neutralisation solution B was added. The samples were vortexed and stored at 4°C until used for Polymerase Chain Reaction (PCR).

6.4.3 Polymerase Chain Reaction (PCR)

Extract-N-AmpTM PCR ReadyMixTM (Sigma-Aldrich) was used according to the manufacturer's instructions to detect genomic DNA. Genomic DNA bands were visualised in a 1% agarose gel (ThermoFisher Scientific) with SYBR DNA gel stain (ThermoFisher Scientific) in TAE buffer. Primer sequences and PCR reaction conditions are listed in Table 6.8.

6.4.4 Generation of bone marrow chimeras

To create bone marrow chimeras, 10-12 weeks old CD45.2 *Ldlr*$^{-/-}$ underwent irradiation and transfer of either CD45.1 *Ldlr*$^{-/-}$ or WT bone marrow cells. Using X-ray irradiation recipient mice were irradiated twice with a 4-hour interval (Gulmay; 1.8 Gy/min, 210 kV, 113mA for 3 min, height: 4 cm). 1 hour after the second dose of irradiation, 4 million bone marrow cells were injected by tail vain injection. The mice received autoclaved 1% Baytril drinking water for 14 days to reduce the risk of infection during the immunosuppressed phase upon irradiation.

6.4.5 Immunization with VLDL-αGalCer complexes

Mice were immunized with lipoprotein-αGalCer by intravenous injection of VLDL-like particles containing 1 mg of triglycerides and 5μg of αGalCer (Rensen et al., 1997). Next repetitive blood sampling was performed at 0, 3, 6, 24 and 48 hours for determination of serum cytokine levels. The iNKT cell response cytokines IL-4 and IFNγ were measured in serum using ELISA (Biolegend) according to manufacturer's instructions. After two weeks, the mice were sacrificed and blood, spleen and liver were harvested for further analysis of iNKT cell numbers and phenotype using flow cytometry.

6.4.6 Isolation of mouse leukocytes and flow cytometry

Blood leukocytes: Murine blood was collected by cardiac puncture and centrifuged at 13.000 rpm for 20 minutes at 4°C in a Heraeus Primo R centrifuge (Thermo Scientific) to separate the serum. Blood samples were incubated at room temperature for 2 minutes with red blood cell lysis buffer (Sigma) and subsequently washed using RPMI including 2% FCS and Penicillin/streptomycin (Gibco).

Splenic leukocytes: Spleens were minced through a 70 µm mesh strainer (Falcon), collected in red blood cell lysis buffer for 2 minutes, and washed in RPMI including 2% FCS and Penicillin/streptomycin (Gibco).

Liver leukocytes: Livers were dissected into small pieces and dissociated using an enzyme mix including 0.5 mg/ml collagenase IV (Sigma C5138) and 0.01 mg/ml DNase I (Sigma/Roche) for 40 minutes at 37°C. Subsequently, dissociated livers were minced over a 70 µm mesh filter (Greiner), liver leukocytes were harvested using Ficoll-Hypaque (Sigma) density centrifugation (20 min at 2300 rpm on lowest ramp) and washed in RPMI including 2% FCS and Penicillin/streptomycin (Gibco).

Bone marrow: Mouse femurs and tibias were harvested and disinfected in 70% ethanol for 45 seconds. The epiphysis of the bones were removed and bone marrow was flushed out with medium using a 25-gauge needle and a syringe. Subsequently, the cells were washed twice with RPMI, filtered through a 70 µm cell strainer (Greiner Bio-One) and erythrocytes were lysed using Red Cell Lysis Buffer (Sigma-Aldrich). In case the bone marrow was used for transplantation the erythrocyte lysis step was not performed.

Flow cytometry: Mouse leukocytes were washed in FACS buffer (2% FCS, 2 mmol/l EDTA and 0.1% NaN_3 in PBS), preincubated with 10% rat serum in FACS buffer to block non-specific binding, and stained with viability dye (Biolegend) and mAbs specific for CD3, CD4, CD8, CD25, CD45.1, CD45.2, NK1.1, and a CD1d tetramer (NIH) for iNKT cell phenotyping, and mAbs specific for CD1d, CD11b, CD11c, CD19, CD45.1, CD45.2, CD64, F4/80, Ly6C, and MHCII for APC phenotyping (Table 6.3). Cells were acquired using an LSR II flow cytometer (BD Biosciences) with FACS-Diva software (BD Biosciences), and data was analyzed with FlowJo software v10 (Tree Star Inc).

6.5 Cell culture

6.5.1 Cell culture mouse bone marrow

Mouse bone marrow cells were cultured in RPMI-1640 (Gibco), 10% FBS, 1% Penicillin/Streptomycin (Gibco) and 50 µM 2-mercaptoethanol (Gibco), together with 100 ng/ml MCSF (Peprotech) for 5 days for differentiation into macrophages. 100.000 cells per well were cultured in a flat bottom 96-well plate. On day 6, cells were treated with lipid antigen or lipid antigen lipoprotein complexes for 4 hours and subsequently washed to remove all remaining treatment.

6.5.2 Cell culture of DN32.D3 mouse NKT hybridoma

DN32.D3 cells were cultured in a flask at 0.75-1.0 x 10^6/ml in RPMI-1640 supplemented with: 10% heat-inactivated FBS, 1% Penicillin/streptomycin, 10 mM HEPES, Glutamax, 50 µM 2-mercaptoethanol.

6.5.3 Generation of human primary iNKT cell line

Blood cones from healthy donors were purchased from the NHS blood service at the John Radcliffe Hospital in Oxford. Blood was diluted in HBSS to a total volume of 40 ml. Subsequently, PBMCs were isolated using lymphoprep (Sigma) centrifugation. 20 mL of blood was layered on top of 20 ml of lymphoprep and centrifuged for 25 minutes at 2300 rpm without brake. Part of the PBMCs were placed aside and irradiated (30 Gray, 210 kV, 13.0 mA, 8:30 min), and were used as feeders in the iNKT cell culture. Lymphocytes were isolated from PBMCs by counter current centrifugal elutriation (CCE). CCE separates cells based on size and density by changing the balance of inward fluid velocity, driving the cells towards the center of rotation, and outward centrifugal force. Lymphocytes elute first, followed by monocytes and granulocytes. The lymphocytes were filtered through an 0.30 µm mesh filter to remove cell clumps. iNKT cells were separated by bead-based cell separation (Miltenyi) according to the manufacturer's instructions. $1x10^6$ cells/ml iNKT cells were cultured in a 1:1 ratio in a 24-well plate with feeder cells in RPMI-1640 supplemented with: 10% hiFBS, 1% Penicilline/streptomycin, 15 mM, Glutamax, 50 µM 2-ME including 100ng/ml αGalCer and IL2 $2x10^6$IU/ml. After 2 weeks, 50% of the medium was replaced every 3-7 days in fresh medium including IL-2 100 IU/ml. Cells were split in a 1:2 ratio in the event of confluency of the well. Purity of the primary cell lines were determined by CD1d-tetramer staining using flow cytometry. Cell lines with >60% purity were used in coculture assays.

6.6 Serum or lipid related assays

6.6.1 Serum cholesterol assay

Murine blood was collected by cardiac puncture and centrifuged at 13.000 rpm for 20 minutes at 4°C in a Heraeus Primo R centrifuge (Thermo Scientific). The serum was collected and stored at -80°C. The Randox total cholesterol kit (CH200) was used to measure cholesterol levels according to the manufacturers instructions. Absorbance was measured at 540 nm and 640 nm wavelengths using the SPECTROstar Nano (BMG Labtech) plate reader. The standard curve was used to determine the cholesterol concentrations of sample wells in mg/dL. The mean values from two wells of each dilution were used for calculations.

6.6.2 Lipoprotein isolation

Lipoproteins were isolated from human serum (NHS blood donation service, London) and mouse serum using established ultracentrifugation protocols (Gelissen & Brown, 2017). In short, the density of the serum was adjusted to 1.25 g/ml by adding 3.85 g Potassiumbromide (KBr) per 10 ml of serum. Sterile KBr solutions of 1.225 g/ml and 1.100 g/ml in NaCl/EDTA solution were prepared. A sterile tube was filled with 7.4 ml of 1.25 g/ml plasma, 4.2 ml of 1.225 g/ml KBr solution, 8.4 ml of 1.1 g/ml KBr solution and 6.3 ml of NaCl/EDTA solution to set up discontinuous density gradients (Fig. 6.1). Upon completion, the gradients were centrifuged in the Sorvall Evolution RC with Surespin 630 ultracentrifuge at 105,000 g for 20 hours without brake. After centrifugation the clearly separated lipoprotein fractions were isolated by needle aspiration (Fig. 6.1). The different lipoprotein fractions were washed with PBS over Amicon spin colums: HDL (10 kDa MWCO), LDL and VLDL (50 kDa MWCO). The samples were passed through a 0.22

µm filter to sterilise and remove aggregates. The sample concentration was determined after filtration by bicinchoninic acid (BCA) assay, and adjusted to 2.0 mg/ml with sterile PBS, after which the LDL was stored in aliquots at 4°C.

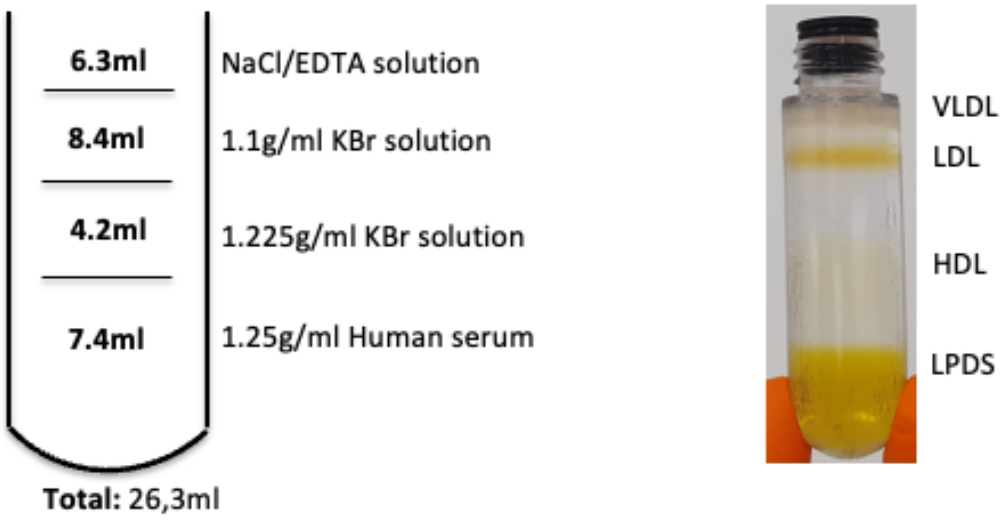

Figure 6.1 | Lipoprotein isolation from human serum. After density-gradient ultracentrifugation of human serum, lipoprotein fractions separate into different bands. Very low density lipoprotein (VLDL) is found in the top layer. The next layer is the low density lipoprotein layer (LDL). Further down, a band of high density lipoprotein (HDL) is found. On the bottom of the well the remaining lipoprotein depleted serum (LPDS) is found.

6.6.3 Fluorescent labeling of lipoproteins

Isolated lipoprotein fractions were fluorescently labeled using a Dylight633 NHS-ester (ThermoFisher). The NHS Ester and DMF (N,N-dimethylformamide, Sigma) were first equilibrated to room temperature. 50 µg of Dylight633 was dissolved in 50 µl of DMF (1mg/ml), vortexed, sat for 5 minutes at room temperature, and vortexed again. 20x Borate buffer (Pierce) was dissolved in LDL to 1x. The LDL in borate buffer and the Dylight633 in DMF were mixed and incubated for 1 hour at

room temperature on a shaker. Next, the mixture was dialyzed against 4 L PBS using dialysis columns with a 10 kDa MW cut-off (Generon). The labeled lipoprotein fraction was protected from light and stored at 4°C for up to 2 weeks.

6.6.4 Synthesis of AF488-labeled αGalCer

AF488-labeled αGalCer was synthesized by the Besra Group (Birmingham) following reported procedures (Jervis et al., 2013). The fluorescent label was introduced at the α- position of the acyl chain of αGalCer via Click chemistry which is a class of biochemical reactions used in bioconjugation that allows binding of two substrates with specific biomolecules (Devaraj & Finn, 2021). Firstly, AF488-PEG4-alkyne was synthesized by stirring a solution of AF488-NHS ester (ThermoFisher A20000) (1.0 mg, 1.6 μmol) and amino-PEG4-alkyne (SigmaAldrich 764248) (0.4 mg, 1.6 μmol) in DMF (0.5 ml) overnight. Concentration of the reaction substrate under reduced pressure, followed by trituration with diethyl ether (2 x 0.5 ml) afforded AF488-PEG4-alkyne in quantitative yield. Secondly, $CuSO_4$ solution (6 μL of a 0.5 M solution, 3 μmol) and a sodium ascorbate solution (13 μL of a 1.0 M solution, 13 μmol) were added to a solution of the 2-azide derivative of αGalCer (1.3 mg, 1.6 μmol) and the AF488-PEG4-alkyne (1.2 mg, 1.6 μmol) in a t-BuOH/H_2O mixture (0.5 ml, 1:1) at room temperature. The reaction mixture was heated for 10 h at 50°C, diluted with $CHCl_3$ (5 ml), and washed with brine (1.5 ml). The phases were separated, and the aqueous layer was extracted with $CHCl_3$ (2 × 2.5 ml). The combined organic layers were dried over Na_2SO_4, and the volatiles were removed under reduced pressure. Purification of the residue by flash column chromatography ($CHCl_3$/MeOH/H_2O, 65:25:4) afforded AF488-labeled αGalCer.

6.6.5 Fluorescent labeling of iGb3, OCH and GSL-1

iGb3, OCH and GSL-1 were labeled labelled using a Dylight488 NHS-ester (ThermoFisher). The NHS Ester and DMF (N,N-dimethylformamide, Sigma) were first equilibrated to room temperature. 50 µg of Dylight488 was dissolved in 50 µl of DMF (1mg/ml), vortexed, sat for 5 minutes at room temperature, and vortexed again. The lipid antigen, triethylamine and NHS ester were mixed in a 1.3 : 1.0 : 1.0 ratio and incubated for 1 hour at room temperature on a shaker protected from light. The labeled lipid antigens were stored at 4°C protected from light for up to 48 hours.

6.6.6 Lipoprotein-lipid antigen complex formation

For complex formation, lipoproteins were incubated with lipid antigens in a 1:10 molar ratio at 37°C on a shaker for 1 h. For example, 1 ml of human LDL (apolipoprotein content 2 mg/ml, approx. 4 µM) was incubated with 34 µl αGalCer (dissolved in 1 mg/ml in DMSO or sucrose/L-histidine/Tween, approx. 40 µM).

6.7 2-Color Fluorescence Cross-Correlation Spectroscopy (2c-FCCS)

Dylight633-labeled lipoproteins, AF 488-labeled αGalCer, and lipoprotein-αGalCer complexes were 100x diluted in PBS with 0.1% FCS, and separately loaded on 8-well chambered coverslips (Ibidi). *In vitro* complex formation has been described above. For *in vivo* complexation, 200 µl of Dylight633-labeled human LDL (2mg/ml) and AF488-labeled αGalCer were mixed in a 1:10 molar ratio and instantly injected intravenously in a *Ldlr*$^{-/-}$ mouse. After 30 min, serum was harvested and 20x diluted in PBS, and loaded on the chambered coverslip. Samples were warmed to 37°C before measurement on a Zeiss LSM880 Inverted Confocal Microscope System,

using a designated 2c-FCCS Plan Apochromat 40x/1.2 NA Water objective, and Zen Black 2.1 SP3 LSM software with 2c-FCCS module (Zeiss). Laser alignment and pinhole position were optimized for 2c-FCCS, and using a 488/633 laser power of ≈3-4 µW set to prevent photobleaching. All samples were measured in 3 runs of 6 repetitive measurements of 10 seconds. Upon exclusion of measurements with aggregates, 15 representative correlation measurements G(τ) per sample underwent curve fitting to extract diffusion times, τ_D , and counts per molecule, using a model for free diffusion in 3D with one diffusive species and a triplet state with a fixed decay time τ_F = 5 µs in the Zen software FCS module (Zeiss).

$$G(\tau) = \frac{< I(t)I(t+\tau) >}{< I(t) >^2} - 1 = \frac{1}{< N >}\left(\frac{1 - T + Te^{-\frac{\tau}{\tau_F}}}{(1-T)}\right)\left(\frac{1}{\left(1+\frac{\tau}{\tau_D}\right)\left(1+\frac{\tau}{S^2\tau_D}\right)^{\frac{1}{2}}}\right)$$

Where <I(t)> is the mean intensity in the focal volume, <N> is the average number of molecules in the focal volume, T is the relative fraction of the triplet state and S = ω_z/ ω_{xy} is the ratio of axial to radial ($1/e^{-2}$) radii of the measurement volume. For our measurements we set S = 5. The counts per molecule were calculated from <I(t)>/<N>.

6.8 Uptake of lipoprotein-αGalCer complexes by THP1 cells

THP1 cells, known for their constitutive LDLR expression (Hamanaka et al., 1991), were cultured in RPMI-1640 (Gibco) supplemented with 10% heat-inactivated FCS (ultra-low endotoxin, Biosera), 4 mmol/l Glutamax (Gibco), 5 mmol/l Sodium Pyruvate (Sigma), and Penicillin/streptomycin (Gibco). For the uptake experiments, THP1 cells were washed in PBS, and 100.000 THP1 cells were seeded in 100 µl Optimem (Gibco) on a 96-well plate (Corning). Upon 30 minutes pre-incubation

with 5 µg/ml LDLR (AF2148, R&D Systems) blocking antibody. THP1 cells were incubated for 4 h with 0.3 µl (6 µg/ml) or 0.03 µl (0.6 µg/ml) fluorescently labeled lipoprotein-αGalCer complexes per well, respectively containing 100 ng and 10 ng αGalCer. Finally, uptake of the Dylight633-lipoprotein and AF488-αGalCer was assessed on a FacsCanto II flow cytometer (BD Biosciences) with FACS-Diva software (BD Biosciences), and data was analyzed with FlowJo software v10 (Tree Star Inc).

6.9 Cocultures of antigen presenting cells and NKT cells

6.9.1 THP1 macrophage like cells in coculture with human primary iNKT cells

THP1 cells were in cultured in RPMI-1640 supplemented FBS, 1% Penicillin/streptomycin, Glutamax and Sodium pyruvate together with PMA for 48 hours with a density of 100.000 cells per well in a 96-well plate (flat bottom). After washing, the cells were incubated with human LDL, αGalCer (100 ng/mL) or complex (100 ng/mL αGalCer) for 4 hours and then washed with PBS. 50.000 human primary iNKT cells were added per well for overnight incubation, followed by harvesting the supernatant for determination of cytokine levels of IL-4 and IFNγ using ELISA according to manufacturer's instructions (Biolegend).

6.9.2 Mouse BMDM in coculture with iNKT hybridoma

Bone marrow cells of C57BL/6, *Ldlr*$^{-/-}$, *Sra*$^{-/-}$ and *Cd1d*$^{-/-}$ mice were differentiated into bone marrow derived macrophages (BMDM) over 5 days using 100 ng/ml murine MCSF (Peprotech). Upon differentiation, BMDM were loaded for 4 h with 0.6 µg/ml mouse VLDL, 0.6 µg/ml VLDL-αGalCer complex (containing 10 ng/ml αGalCer) or αGalCer (10 ng/ml) in Optimem (Gibco), and washed with PBS. Next,

1.5 x 10^5 BMDMs per well were cocultured with 1.5 x 10^5 mouse DN32.D3 iNKT hybridoma cells for 16 h in culture medium. Co-culture supernatants were harvested and analyzed for mouse IL-2 levels using ELISA according to manufacturer's instructions (R&D Systems).

6.9.3 Human iNKT cell activation and proliferation assay

PBMCs of 4 patients with LDLR mutations and 10 age-matched controls were subjected to a standard iNKT cell activation and proliferation assay (Exley et al., 2017). PBMCs were incubated with 10% heat-inactivated human AB serum, 100 ng/ml αGalCer, and 100 IU/ml human IL2 (R&D Systems) in standard T cell medium (Table 6.6). On day 0, baseline APC and iNKT cell phenotypes were assessed using flow cytometry (Table 6.4). On day 4, a small supernatant fraction of 60 µl was harvested to measure the iNKT cell cytokines IL-4, IFNγ and IL-17 using a multiplex immunoassay (Luminex). On day 14, iNKT cell proliferation and phenotype were assessed again using flow cytometry (Table 6.4).

6.10 Athero-Express Cohort Study

6.10.1 Study design

The Athero-Express study is a prospective cohort study conducted in the Netherlands in two hospitals: the University Medical Center Utrecht (UMCU) and the St. Antonius Hospital in Nieuwegein. Patient enrolment commenced in April 2002 and continues until present. All patients who underwent primary carotid endarterectomy were asked to participate in the study. In summary, carotid plaques of patients undergoing carotid endarterectomy were collected and subjected to histological examination. Patients were asked to complete a questionnaire before

admission to the hospital including questions about their medical history, symptoms of cardiovascular disease (coronary artery disease, peripheral artery disease, cerebral ischaemia and abdominal aneurysm), risk factors (smoking, alcohol intake, hypertension, diabetes mellitus, hyperlipidemia, physical activity, and medication use. Blood samples were drawn from patients before surgery, including serum, EDTA plasma and red blood cell free citrate plasma which were stored at 80°C to assess cholesterol, hs-CRP, glucose and triglyceride levels. Standard pre-operative physical examination was performed including height, weight, body mass index and blood pressure measurements. Cohort members were followed up for carotid restenosis for 2 years and for a minimum of 3 years to record the occurrence of adverse cardiovascular events.

6.10.2 Patients

A random subset of 97 carotid endarterectomy specimens from the Athero-Express Biobank was included. Carotid endarterectomy was indicated when colour Doppler assisted duplex investigation showed a diameter reduction of >70% on at least one side. In asymptomatic patients with stenosis >70%, the indication for surgical therapy depended on co-morbidity and vertebral-basilar sufficiency. Patients with a terminal malignancy and those who are not living in the Netherlands permanently were excluded from the study.

6.10.3 Sample procurement

Atherosclerotic plaque samples were collected without delay from the operating theatre in RPMI-1640. Subsequently, the plaque was dissected in parts of 0.5 cm. The middle section was fixated in formaldehyde 4%, decalcified in

ethylenediaminetraacetic acid for 8 hours, and transported to the pathology department for paraffin embedding. Of each paraffin embedded segment 5 µm sections were cut on a microtome for histological staining.

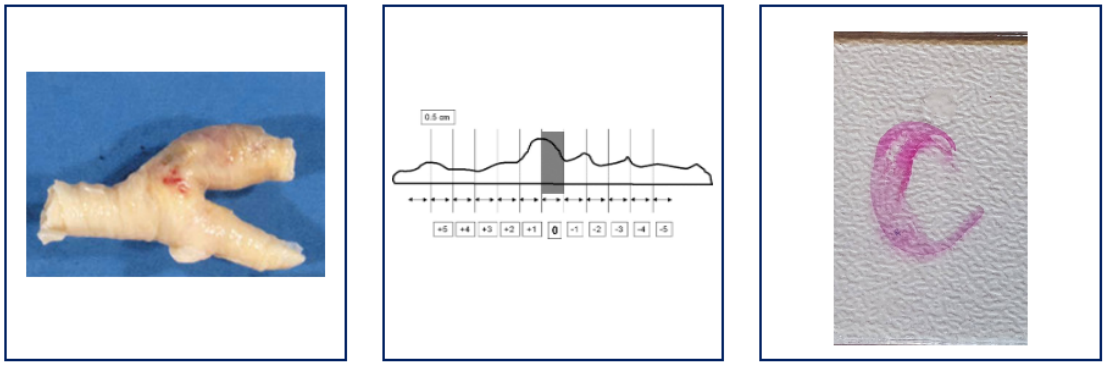

Figure 6.2 | Human atherosclerotic plaques from the Athero-Express cohort. **(A)** Representative image of atherosclerotic plaque tissue. **(B)** Schematic overview of plaque sections. **(C)** H&E stained plaque section.

6.10.4 Plaque phenotyping

Immunohistochemical phenotyping of the plaques included in the Athero-Express cohort have been described previously (B. A. N. Verhoeven et al., 2004). In short, 5 µm sections were stained by the Athero-Express Study pathology team to assess for fat content (Picro Sirius red) macrophage content (CD68 staining, clone KP1), and smooth muscle cell content (ACTA2 staining, clone 1A4). Intraplaque haemorrhage was assessed based on the H&E staining and was classified as either absent or present.

6.10.5 Immunohistochemical staining of Natural Killer T cells

Paraffin embedded atherosclerotic plaque sections were deparaffinized in xylene and rehydrated in graded alcohol series (100%, 95%, 80%, 75%) by the Athero-Express pathology team. Slides were washed in deionized water and antigen

retrieval was conducted with Tris-EDTA (pH 9) at 96°C on a heat block. Tissue sections were blocked with UltraVision Protein Block (Thermo Scientific) for 10 minutes and incubated with CD56 antibody overnight. CD56 antibody was detected by BrightVision alkaline phosphatase goat anti-rabbit antibody (Immunologic) and liquid Permanent Red (DAKO) was used as a chromogenic substrate. Slides were washed in PBS and blocked with hydrogen peroxide for 15 minutes. The tissues were incubated with CD3 antibody for 1 hour. CD3 antibody was detected by BrightVision horseradish peroxidase goat anti-rabbit secondary antibody (Immunologic) and high definition yellow (Enzo Life Sciences) was used as a chromogenic substrate. Both secondary antibodies were incubated for 30 minutes. Sections were washed with PBS between all incubation steps and hematoxylin staining, which is described previously, was used as a counterstain. Besides atherosclerotic plaque tissue, tissue microarrays (TMA) containing liver, tonsil, intestine and neural tissue in duplicate were added to all microscopic slides serving as control tissue.

Table 6.1 | Antibodies for staining of Natural Killer T cells

Target	Clone	Isotope	Company
CD3	Polyclonal	rIgG1	Agilent
CD56	MRQ-42	rIgG1	Sigma-Aldrich

6.10.6 Image processing, counting and reproducibility

Stained sections were scanned (slide scanner, Hamamatsu Photonics) and visualized using NDP.view2 (Hamamatsu Photonics). The number of CD3+ and CD3+CD56+ cells per section were manually counted by observer 1. Cells were excluded from the counts when located inside the lumen of a blood vessel, on the

border of the tissue or in folded tissue. To determine interobserver reproducibility observer 2 counted 30 slides without access to the counts of observer 1.

6.10.7 Study endpoints

The primary endpoint includes all adverse cardiovascular events and interventions during follow-up including (Table 3.2): cardiovascular death, non-fatal myocardial infarction, non-fatal stroke and vascular interventions.

The secondary endpoint includes the plaque vulnerability score. The plaque vulnerability score was defined as previously described by van Keulen et al (van Keulen et al., 2021). In short, macrophages, collagen and smooth muscle cell content were semi-quantitatively defined as no/minor or moderate/heavy. Plaque fat content was binned at 10%. Plaque characteristics that contribute to a stable plaque were given a score of 0 including no/minor macrophages, moderate/heavy collagen, moderate/heavy smooth muscle cells and <10% fat. Plaque characteristics contributing to a vulnerable plaque were given a score of 1 including: moderate/heavy macrophages, no/minor collagen, no/minor smooth muscle cells and ≥10% fat (Table 6.2).

Table 6.2 | Plaque vulnerability index

	0 points	**1 point**
Macrophages	No/minor	Moderate/heavy
Collagen	Moderate/heavy	No/minor
Smooth muscle cells	Moderate/heavy	No/minor
Fat	< 10%	> 10%

6.11 Hyperion Imaging Mass Cytometry

6.11.1 Antibody panel

An antibody panel was designed to identify different immune cell subsets including antigen presenting cells and iNKT cells as well as structural characteristics to visualize histological landmarks. Marker and clone information are available in Table 6.5.

6.11.2 Metal-conjugation of antibodies

Metal conjugated antibodies were purchased from Standard BioTools Inc. The unconjugated antibodies were conjugated-in house using the Maxpar X8 Metal labelling kit (Standard Biotools Inc.). Metal conjugation was performed for the following antibodies: IFNγ, PLIN2, CD1d, TREM2, CD1d Tetramer, CD66a, TREM1, CD56, CD64, CD161 and CD3. Antibodies were stored at 4°C in Antibody Stabilizer PBS in a Protein LoBind tube.

6.11.3 Haematoxylin and Eosin (H&E) staining and selection of region of interest

For each patient one atherosclerotic plaque section (5 µm) was stained for Haematoxylin and Eosin (H&E) to visualise plaque morphology and cell infiltration. This was used for selection of the region of interest for Imaging Mass Cytometry (Hyperion) data acquisition on consecutive tissue sections. The staining procedure was performed by the histopathology facility at the Kennedy Institute of Rheumatology using the Tissue-Tek Prisma/Film automated slide stainer (Sakura) and Glas™ g2 coverslipper (Sakura). Cell rich areas located around the shoulder of the atherosclerotic plaque were selected as the region of interest for Imaging Mass

Cytometry (Hyperion) data acquisition. The size per region of interest was 1.5 – 5 mm^2.

6.11.4 Hyperion tissue staining and antibody validation

Paraffin embedded atherosclerotic plaque sections were deparaffinized in xylene and rehydrated in graded alcohol series (100%, 95%, 80%, 75%). Slides were washed in Maxpar Water and antigen retrieval was conducted with Tris-EDTA (pH 9) carefully kept at 96°C for 30 minutes on a heat block. Slides were cooled down on the bench to 70°C, washed with MaxPar water and Maxpar PBS for 10 minutes each and incubated for 45 minutes with blocking solution with 3% BSA to block unspecific binding. The samples were then stained for 2 hours at room temperature for CD1d, Tetramer, IFNγ, CD3 and CD8 and overnight at 4°C with the full antibody panel including 21 markers (Table 6.5). Slides were washed in 0.2% Triton-X100 in Maxpar PBS for 8 minutes and subsequently washed in Maxpar PBS. The tissue was stained with Intercalator-Ir in Maxpar PBS (1:400 dilution) for 30 minutes at RT in a hydration chamber. Slides were washed in Maxpar Water for 5 minutes and air-dried for 20 minutes. The slides were stored in a dust-free slide box at RT until ablation. Antibody concentration and specificity were evaluated by visual inspection of IMC images of atherosclerotic plaque and tonsil tissue.

6.11.5 Imaging Mass Cytometry data acquisition

Images were acquired using the Hyperion Imaging Mass Cytometry System (Standard Biotools Inc.) coupled to a Helios mass cytometer (Standard Biotools Inc.). Tissue sections were ablated with a laser at a resolution of 1 µm and acquired

at 200 Hz. ROIs of 1.5 - 5 mm^2 were acquired. The acquired data was exported as MCD files and visualized using Standard Biotools Inc. MCD™ viewer.

6.11.6 Cell segmentation

Cells were segmented using CellProfiler v.4.2.1. Ir191, Ir193 and Histone 3 channels were used to identify nuclei for segmentation. Primary objects a diameter between 4 and 15 pixels were identified as nuclei. In this workflow circumferential pixel expansion of 5 pixels around the segmented nuclei was used to identify cells. Cell masks were generated and were used to extract the mean expression level markers and spatial features for each cell.

6.11.7 Data transformation and visualisation

Mean marker expression intensities were normalized per cell by log transformation and scaling for each channel using R's scale() function. Cells with expression of all markers, identified by row variance analysis, were excluded from analysis after visual comparison of the staining pattern confirmed they were artifacts. Cells that exclusively stained for Iridium without Histone 3 staining or other marker staining, were excluded from further analysis as well (MatrixStats package, R studio).To visualise the data, high-dimensional single-cell data were reduced to two dimensions using a nonlinear dimensionality reduction algorithm t-SNE in HistoCAT.

6.11.8 Cell clustering and spatial analysis

The lineage markers ACTA2, HLA-DR, CD14, CD68, CD8a and Tetramer were used for the initial classification. PhenoGraph clustering resulted in generation of 7

clusters of which 5 clusters were biologically relevant. Smooth muscle cells were defined by high ACTA2 expression, CD8+ T cells were defined by high CD8a expression, dendritic cells by high HLA-DR expression, macrophages by high CD68 expression and iNKT cells by high tetramer expression. Clusters with expression patterns not distinctive for a specific immune cell subset were named unclassified. Clusters were merged when they corresponded to the same set of rules. The distance between neighbouring cells with respect to cell types across all samples was calculated using the components function of the igraph R package.

6.12 Statistics

Data are presented as mean plus standard deviation, unless otherwise indicated. The Shapiro-Wilk test was used to assess normality of the data. The null hypothesis (H_0) was that the data was normally distributed. Variables with a Shapiro-Wilk test with $p > 0.05$ were considered normally distributed. Statistical significance between two groups was determined using unpaired *t* tests for parametric data, and Mann-Whitney U tests for nonparametric data. Associations between the number of NKT cells with clinical outcome, patient- and plaque- characteristics were asses using univariate linear regression. Bonferroni correction was used to correct for multiple comparisons. The intraclass correlation coefficient (ICC) was calculated in order to assess interobserver reproducibility. Determinants with $P < 0.05$ or a 95% CI not including 1 were regarded as statistically significant. Statistical analyses were performed using Prism 8 for MacOS (Graphpad Software) or SPSS statistics v27.

Table 6.3 | Fluorochrome-conjugated antibodies used for Flow Cytometry on mouse leukocytes.

Target	Fluor	Clone	Isotype	Company	Cat #
NKT panel					
Tetramer	PE			NIH	
CD45.1	FITC	A20	rIgG2a,κ	Biolegend	110706
CD4	PE/Cy	RM4-5	rIgG2a,κ	BD	552775
CD3	PerCP	145-2C11	hIgG	Biolegend	100326
NK1.1	APC	PK136	mIgG2a,κ	Biolegend	108710
CD25	BV421	PC61	rIgG1l	Biolegend	102043
CD279 (PD1)	BV510	29F.1A12	rIgG2a,κ	Biolegend	135241
CD8	BV785	53-6.7	rIgG2a,κ	Biolegend	100750
APC panel					
CD21-25	FITC	7E9	rIgG2a,κ	Biolegend	123407
CD23	PE	B3B4	rigG2a,κ	Biologend	101607
CD64	PE/Cy7	X54-5/7.1	mIgG1,κ	Biolegend	139314
CD19	PerCP/Cy5.5	1D3	rIgG2a,κ	Biolegend	152406
CD1d	AF647	1B1	rIgG2b,κ	Biolegend	123511
MHCII	BV421	M5/114.15.2	rIgG2bv	BD	562564
CD11b	BV510	M1/70	rIgG2b,κ	Biolegend	101263
F4/80	BV605	BM8	rIgG2a,κ	Biolegend	123133
CD45.1	BV605	30-F11	rIgG2b,κ	Biolegend	103139
CD11c	BV711	N418	hIgG	Biolegend	117349
CD45.2	BV785	30-F11	rIgG2b,κ	Biolegend	103149

Abbreviations: APC: Antigen Presenting Cell, NIH: National Institutes of health, NKT: Natural Killer T cell.

Table 6.4 | Fluorochrome-conjugated antibodies used for Flow Cytometry on human PBMCs.

Target	**Fluor**	**Clone**	**Isotype**	**Company**	**Cat #**
NKT panel					
CD3	AF700	HIT3a	mIgG2a, κ	Sony Biotech	2101620
CD1d-tetramer-loaded with PBS-57	BV421			NIH tetramer core facility	
CD4	PE-Cy7	L200	mIgG1, κ	BD	560644
CD8	APC-Cy5	RPA-T8	mIgG1, κ	BD	555368
CD25	Pe-Cy7	2A3	mIgG1, κ	BD	335789
CD69	APC	FN50	mIgG1, κ	BD	560711
APC panel					
CD19	BV711	HIB19	mIgG1, κ	Biolegend	302246
CD14	APC-Cy7	MφP9	mIgG2b, κ	BD	554656
CD16	V500	3G8	mIgG1, κ	BD	561394
HLA-DR	FITC	LN3	mIgG2b, κ	eBioscience	15506656
CD11c	BV450	3.9	mIgG1, κ	BD	565911
CD11b	AF700	M170	mIgG2b, κ	BD	557960

Table 6.5 | Metal-conjugated antibodies validated for Imaging Mass Cytometry on human atherosclerotic plaque tissue.

Metal	Target	Clone	Company
141 Pr	CD38	EPR4106	Standard Biotools Inc.
142 Nd	CD19	6OMP31	Standard Biotools Inc.
143 Nd	IFNγ	B27	Biolegend
144 Nd	CD14	EPR3653	Standard Biotools Inc.
145 Nd	TBET	D6N8B	Standard Biotools Inc.
146 Nd	CD16	EPR16784	Standard Biotools Inc.
147 Sm	CD163	EDHu-1	Standard Biotools Inc.
149 Sm	CD11b	EPR1344	Standard Biotools Inc.
151 Eu	CD31	EPR3094	Standard Biotools Inc.
152 Sm	PLIN2	HPA016607, poly	Merck
154 Sm	CD11c	EP1347	Standard Biotools Inc.
155 Gd	ACTA 2	1A4	Standard Biotools Inc.
156 Gd	CD4	EPR6855	Standard Biotools Inc.
158 Gd	CD1d	NOR3.2	Abcam
159 Tb	CD68	KP1	Standard Biotools Inc.
160 Dy	TREM2	LS-B16999	LSBio
161 Dy	CD20	H1	Standard Biotools Inc.
162 Dy	CD8a	C8/144B	Standard Biotools Inc.
163 Dy	CD66a	CD66aB1.1	Thermofisher
164 Dy	Tetramer	NIH	NIH
168 Er	TREM1	EPR22060-229	Abcam
169Tm	Collagen	Polyclonal	Standard Biotools Inc.
170 Er	CD56	MRQ-42	Merk
171Yb	Histone	D1H3	Standard Biotools Inc.
172 Yb	CD64	OTI3D3	Abcam
174 Yb	HLA-DR	LN3	Standard Biotools Inc.
175 Lu	CD25	EPR6452	Standard Biotools Inc.
176 Er	CD3	Polyclonal	Agilent

Table 6.6 | Other metal-conjugated antibodies tested for Imaging Mass Cytometry on human atherosclerotic plaque tissue.

Metal	Target	Clone	Company
148 Nd	CD278/ICOS	D1K2T	Standard Biotools Inc.
150 Nd	PD-L1	E1L3N	Standard Biotools Inc.
152 Sm	PLIN2	HPA016607, poly	Merck
152 Sm	CD45	D9M8I	Standard Biotools Inc.
160 Dy	TREM2	LS-B16999	LSBio
163 Dy	CD66a	CD66aB1.1	Thermofisher
165 Ho	PD-1	EPR4877	Standard Biotools Inc.
167 Er	Granzyme B	EPR20129-217	Standard Biotools Inc.
168 Er	TREM1	EPR22060-229	Abcam
170 Er	CD3	Polyclonal	Standard Biotools Inc.
175 Lu	CD25	EPR6452	Standard Biotools Inc.
176 Yb	Perforin	dG9	Standard Biotools Inc.

The antibody list above did not result in specific staining.

Table 6.7 | Buffers, media and solutions made in-house.

Solution	Composition
FACS buffer	PBS with 2% FBS and 0.1% Sodium Azide
MACS buffer	PBS with 0.5% FBS and 2 mM EDTA
50x TAE buffer	242 g Tris-base, 57.1 ml Glacial Acetic Acid, 18.6 g, 100 mM EDTA in 1 L distilled H2O.
NaCl/EDTA solution	0.9% w/v NaCl / 1 mM EDTA.
HEK293T culture medium	DMEM (Gibco 11995-065, 4.5g/L glucose, l-glut, sodium pyruvate), supplemented with: 1% Penicillin/streptomycin, 10% heat-inactivated FBS, glutamax.
DN32.D3 Hybridoma culture medium	RPMI-1640 supplemented with: 10% heat-inactivated FBS, 1% Penicillin/streptomycin, 10 mM HEPES, Glutamax, 50 µM 2-mercaptoethanol.

THP1 medium	RPMI-1640 supplemented with: 10% heat-inactivated FBS, 1% Penicillin/streptomycin, Glutamax, Sodium pyruvate (Sigma 8636-100ml).
Human NKT cell medium	RPMI-1640 supplemented with: 10% hi FBS, 1% Penicilline/streptomycin, 15 mM, Glutamax, 50 µM 2-ME, 100ng/ml αGalCer, IL2 $2x10^6$IU/ml.
Mouse BMDM culture medium	RPMI-1640 supplemented with: 10% heat-inactivated FBS, 1% Penicillin/streptomycin.

Abbreviations: BMDM: bone marrow derived macrophages, DMEM: Dulbecco's Modified Eagle Medium. EDTA: Ethylenediaminetetraacetic acid, FBS: Fetal Bovine Serum, PBS: Phosphate buffered saline.

Table 6.8 | Mouse strains used in experiments.

Mouse strain	Source	Used for
Ldlr$^{-/-}$ CD45.1	Bred in-house	*In vivo* immunization Bone marrow culture Bone marrow chimera
C57BL/6J (wild type)	Charles River Laboratories UK	Bone marrow chimera Bone marrow culture
Sra$^{-/-}$	Bred in-house Platt group, Department of Pharmacology, University of Oxford.	Bone marrow culture
ApoE$^{-/-}$	PBS with 0.5% FBS and 2mM EDTA	Bone marrow culture

Table 6.9 | Sequences of primers used for genotyping.

Mouse strain	Wild type	Mutant	Parameters for reverse transcription PCR
Ldlr$^{-/-}$ CD45.1	GCGATGGAT ACACTCACT GC	AATCCATCTTGTT CAATGGCCGATC	Denaturating: 94°C 180s Denaturating: 94°C 30s Annealing: 60°C 45s Extension: 72°C 45s Cycles: X35 Completion: 72°C 120s
ApoE$^{-/-}$	GCCTAGCCG AGGGAGAGC CG	GCCGCCCCGACTG CATCT	Denaturating: 94°C 180s Denaturating: 94°C 30s Annealing: 60°C 60s Extension: 72°C 45s Cycles: X35 Completion: 72°C 600s

7 Bibliography

Aday, A. W., & Ridker, P. M. (2019). Targeting Residual Inflammatory Risk: A Shifting Paradigm for Atherosclerotic Disease. In *Frontiers in Cardiovascular Medicine* (Vol. 6, p. 16).

Adly, M. A., Assaf, H. A., Hussein, M. R., & Neuber, K. (2006). Age-associated decrease of CD1d protein production in normal human skin. *British Journal of Dermatology*, *155*(1), 186–191.

Akbari, O., Faul, J. L., Hoyte, E. G., Berry, G. J., Wahlström, J., Kronenberg, M., DeKruyff, R. H., & Umetsu, D. T. (2006). CD4+ Invariant T-Cell–Receptor+ Natural Killer T Cells in Bronchial Asthma. *New England Journal of Medicine*, *354*(11), 1117–1129.

Akbari, O., Stock, P., Meyer, E., Kronenberg, M., Sidobre, S., Nakayama, T., Taniguchi, M., Grusby, M. J., DeKruyff, R. H., & Umetsu, D. T. (2003). Essential role of NKT cells producing IL-4 and IL-13 in the development of allergen-induced airway hyperreactivity. *Nature Medicine 2003 9:5*, *9*(5), 582–588.

Akira, S., Uematsu, S., & Takeuchi, O. (2006). Pathogen recognition and innate immunity. *Cell*, *124*(4), 783–801.

Ali, H. R., Jackson, H. W., Zanotelli, V. R. T., Danenberg, E., Fischer, J. R., Bardwell, H., Provenzano, E., Rueda, O. M., Chin, S.-F., Aparicio, S., Caldas, C., Bodenmiller, B., Ali, H. R., Al Sa'd, M., Alon, S., Aparicio, S., Battistoni, G., Balasubramanian, S., Becker, R., … Team, C. I. G. C. (2020). Imaging mass cytometry and multiplatform genomics define the phenogenomic landscape of breast cancer. *Nature Cancer*, *1*(2), 163–175.

Allan, L. L., Hoefl, K., Zheng, D.-J., Chung, B. K., Kozak, F. K., Tan, R., & van den Elzen, P. (2009). Apolipoprotein-mediated lipid antigen presentation in B cells provides a pathway for innate help by NKT cells. *Blood*, *114*(12), 2411–2416.

Amento, E. P., Ehsani, N., Palmer, H., & Libby, P. (1991). Cytokines and growth factors positively and negatively regulate interstitial collagen gene expression in human vascular smooth muscle cells. *Arteriosclerosis, Thrombosis, and Vascular Biology*, *11*(5), 1223–1230.

Aqel, N. M., Ball, R. Y., Waldmann, H., & Mitchinson, M. J. (1985). Identification of macrophages and smooth muscle cells in human atherosclerosis using

monoclonal antibodies. In *The Journal of Pathology* (Vol. 146, Issue 3).

Aslanian, A. M., Chapman, H. A., & Charo, I. F. (2005). Transient role for CD1d-restricted natural killer T cells in the formation of atherosclerotic lesions. *Arteriosclerosis, Thrombosis, and Vascular Biology*, *25*(3), 628–632.

Aviña-Zubieta, J. A., Choi, H. K., Sadatsafavi, M., Etminan, M., Esdaile, J. M., & Lacaille, D. (2008). Risk of cardiovascular mortality in patients with rheumatoid arthritis: A meta-analysis of observational studies. *Arthritis Care and Research*, *59*(12), 1690–1697.

Bar, J., Markel, G., Gottfried, T., Percik, R., Leibowitz-Amit, R., Berger, R., Golan, T., Daher, S., Taliansky, A., Dudnik, E., Shulman, K., Urban, D., & Onn, A. (2019). Acute vascular events as a possibly related adverse event of immunotherapy: a single-institute retrospective study. *European Journal of Cancer*, *120*, 122–131.

Barral, D. C., & Brenner, M. B. (2007). CD1 antigen presentation: how it works. *Nature Reviews. Immunology*, *7*(12), 929–941.

Barral, P., Eckl-Dorna, J., Harwood, N. E., De Santo, C., Salio, M., Illarionov, P., Besra, G. S., Cerundolo, V., & Batista, F. D. (2008). B cell receptor-mediated uptake of CD1d-restricted antigen augments antibody responses by recruiting invariant NKT cell help in vivo. *Proceedings of the National Academy of Sciences of the United States of America*, *105*(24), 8345–8350.

Bendelac, A. (1995). Positive selection of mouse NK1+ T cells by CD1-expressing cortical thymocytes. *Journal of Experimental Medicine*, *182*(6), 2091–2096.

Bendelac, A., Savage, P. B., & Teyton, L. (2007). The Biology of NKT Cells. *Annual Review of Immunology*, *25*(1), 297–336.

Berenson, G. S., Srinivasan, S. R., Bao, W., Newman, W. P., Tracy, R. E., & Wattigney, W. A. (1998). Association between multiple cardiovascular risk factors and atherosclerosis in children and young adults. The Bogalusa Heart Study. *The New England Journal of Medicine*, *338*(23), 1650–1656.

Berk, B. C., Weintraub, W. S., & Alexander, R. W. (1990). Elevation of C-reactive protein in "active" coronary artery disease. *The American Journal of Cardiology*, *65*(3), 168–172.

Berzins, S. P., & Ritchie, D. S. (2014). Natural killer T cells: drivers or passengers in preventing human disease? *Nature Reviews Immunology*, *14*(9), 640–646.

Binder, C. J., Papac-Milicevic, N., & Witztum, J. L. (2016). Innate sensing of oxidation-

specific epitopes in health and disease. *Nature Reviews Immunology*, *16*(8), 485–497.

Bobryshev, Y. V., & Lord, R. S. A. (2005). Co-accumulation of dendritic cells and natural killer T cells within rupture-prone regions in human atherosclerotic plaques. *Journal of Histochemistry and Cytochemistry*, *53*(6), 781–785.

Boon, J., Hoy, A. J., Stark, R., Brown, R. D., Meex, R. C., Henstridge, D. C., Schenk, S., Meikle, P. J., Horowitz, J. F., Kingwell, B. A., Bruce, C. R., & Watt, M. J. (2013). Ceramides contained in LDL are elevated in type 2 diabetes and promote inflammation and skeletal muscle insulin resistance. *Diabetes*, *62*(2), 401–410.

Borén, J., John Chapman, M., Krauss, R. M., Packard, C. J., Bentzon, J. F., Binder, C. J., Daemen, M. J., Demer, L. L., Hegele, R. A., Nicholls, S. J., Nordestgaard, B. G., Watts, G. F., Bruckert, E., Fazio, S., Ference, B. A., Graham, I., Horton, J. D., Landmesser, U., Laufs, U., … Ginsberg, H. N. (2020). Low-density lipoproteins cause atherosclerotic cardiovascular disease: pathophysiological, genetic, and therapeutic insights: a consensus statement from the European Atherosclerosis Society Consensus Panel. *European Heart Journal*, *41*(24), 2313–2330.

Brennan, P. J., Brigl, M., & Brenner, M. B. (2013). Invariant natural killer T cells: An innate activation scheme linked to diverse effector functions. *Nature Reviews Immunology*, *13*(2), 101–117.

Brennan, P. J., Tatituri, R. V. V., Brigl, M., Kim, E. Y., Tuli, A., Sanderson, J. P., Gadola, S. D., Hsu, F. F., Besra, G. S., & Brenner, M. B. (2011). *Invariant natural killer T cells recognize lipid self antigen induced by microbial danger signals*. *12*(12), 1202–1211.

Brennan, P. J., Tatituri, R. V. V. V, Heiss, C., Watts, G. F. M. M., Hsu, F.-F. F., Veerapen, N., Cox, L. R., Azadi, P., Besra, G. S., & Brenner, M. B. (2014). Activation of iNKT cells by a distinct constituent of the endogenous glucosylceramide fraction. *Proceedings of the National Academy of Sciences of the United States of America*, *111*(37), 13433–13438.

Brigl, M., Bry, L., Kent, S. C., Gumperz, J. E., & Brenner, M. B. (2003). Mechanism of CD1d-restricted natural killer T cell activation during microbial infection. *Nature Immunology 2003 4:12*, *4*(12), 1230–1237.

Burton, P. R., Clayton, D. G., Cardon, L. R., Craddock, N., Deloukas, P., Duncanson, A.,

Kwiatkowski, D. P., McCarthy, M. I., Ouwehand, W. H., Samani, N. J., Todd, J. A., Donnelly, P., Barrett, J. H. J. C., Davison, D., Easton, D., Evans, D., Leung, H. T., Marchini, J. L., Morris, A. P., … Compston, A. A. (2007). Genome-wide association study of 14,000 cases of seven common diseases and 3,000 shared controls. *Nature*, *447*(7145), 661–678.

Cardoso, D., & Perucha, E. (2021). Cholesterol metabolism: a new molecular switch to control inflammation. *Clinical Science*, *135*, 1389–1408.

Chackerian, A., Alt, J., Perera, V., & Behar, S. M. (2002). Activation of NKT cells protects mice from tuberculosis. *Infection and Immunity*, *70*(11), 6302–6309.

Chan, W. L., Pejnovic, N., Hamilton, H., Liew, T. V., Popadic, D., Poggi, A., Khan, S. M., Liew, V., Popadic, D., Poggi, A., Khan, S. M., Liew, T. V., Popadic, D., Poggi, A., & Khan, S. M. (2005). Atherosclerotic Abdominal Aortic Aneurysm and the Interaction Between Autologous Human Plaque-Derived Vascular Smooth Muscle Cells, Type 1 NKT, and Helper T Cells. *Circulation Research*, *96*(6), 675–683.

Chang, Y. J., Kim, H. Y., Albacker, L. A., Lee, H. H., Baumgarth, N., Akira, S., Savage, P. B., Endo, S., Yamamura, T., Maaskant, J., Kitano, N., Singh, A., Bhatt, A., Besra, G. S., Van Den Elzen, P., Appelmelk, B., Franck, R. W., Chen, G., DeKruyff, R. H., … Umetsu, D. T. (2011). Influenza infection in suckling mice expands an NKT cell subset that protects against airway hyperreactivity. *The Journal of Clinical Investigation*, *121*(1), 57–69.

Chen, L., & Flies, D. B. (2013). Molecular mechanisms of T cell co-stimulation and co-inhibition. In *Nature Reviews Immunology* (Vol. 13, Issue 4, pp. 227–242).

Chen, Y. C., Huang, A. L., Kyaw, T. S., Bobik, A., & Peter, K. (2016). Atherosclerotic Plaque Rupture. *Arteriosclerosis, Thrombosis, and Vascular Biology*, *36*(8), e63–e72.

Chen, Y. H., Chiu, N. M., Mandal, M., Wang, N., & Wang, C. R. (1997). Impaired NK1+ T Cell Development and Early IL-4 Production in CD1-Deficient Mice. *Immunity*, *6*(4), 459–467.

Chetty, P. S., Mayne, L., Lund-Katz, S., Englander, S. W., & Phillips, M. C. (2017). Helical structure, stability, and dynamics in human apolipoprotein E3 and E4 by hydrogen exchange and mass spectrometry. *Proceedings of the National Academy of Sciences of the United States of America*, *114*(5), 968–973.

Christiansen, D., Milland, J., Mouhtouris, E., Vaughan, H., Pellicci, D. G., McConville, M. J., Godfrey, D. I., & Sandrin, M. S. (2008). Humans Lack iGb3 Due to the Absence of Functional iGb3-Synthase: Implications for NKT Cell Development and Transplantation. *PLOS Biology*, *6*(7), e172.

Cochain, C., Vafadarnejad, E., Arampatzi, P., Pelisek, J., Winkels, H., Ley, K., Wolf, D., Saliba, A. E., & Zernecke, A. (2018). Single-cell RNA-seq reveals the transcriptional landscape and heterogeneity of aortic macrophages in murine atherosclerosis. *Circulation Research*, *122*(12), 1661–1674.

Cole, J. E., Park, I., Ahern, D. J., Kassiteridi, C., Abeam, D. D., Goddard, M. E., Green, P., Maffia, P., & Monaco, C. (2018). Immune cell census in murine atherosclerosis: Cytometry by time of flight illuminates vascular myeloid cell diversity. *Cardiovascular Research*, *114*(10), 1360–1371.

Cui, J., Shin, T., Kawano, T., Sato, H., Kondo, E., Toura, I., Kaneko, Y., Koseki, H., Kanno, M., & Taniguchi, M. (1997). Requirement for Vα14 NKT Cells in IL-12-Mediated Rejection of Tumors. *Science*, *278*(5343), 1623–1626.

Dashti, M., Kulik, W., Hoek, F., Veerman, E. C., Peppelenbosch, M. P., & Rezaee, F. (2011). A phospholipidomic analysis of all defined human plasma lipoproteins. *Scientific Reports*, *1*.

Daugherty, A. (2002). Mouse models of atherosclerosis. *The American Journal of the Medical Sciences*, *323*(1), 3–10.

Davies, M. J., Richardson, P. D., Woolf, N., Katz, D. R., & Mann, J. (1993). Risk of thrombosis in human atherosclerotic plaques: role of extracellular lipid, macrophage, and smooth muscle cell content. *British Heart Journal*, *69*(5), 377–381.

De Villiers, W. J. S., Smith, J. D., Miyata, M., Dansky, H. M., Darley, E., & Gordon, S. (1998). Macrophage phenotype in mice deficient in both macrophage-colony-stimulating factor (Op) and apolipoprotein E. *Arteriosclerosis, Thrombosis, and Vascular Biology*, *18*(4), 631–640.

Depuydt, M. A. C., Prange, K. H. M., Slenders, L., Örd, T., Elbersen, D., Boltjes, A., De Jager, S. C. A., Asselbergs, F. W., De Borst, G. J., Aavik, E., Lönnberg, T., Lutgens, E., Glass, C. K., Den Ruijter, H. M., Kaikkonen, M. U., Bot, I., Slütter, B., Van Der Laan, S. W., Yla-Herttuala, S., … Pasterkamp, G. (2020a). Microanatomy of the Human Atherosclerotic Plaque by Single-Cell Transcriptomics. *Circulation*

Research, *127*, 1437–1455.

Depuydt, M. A. C., Prange, K. H. M., Slenders, L., Örd, T., Elbersen, D., Boltjes, A., De Jager, S. C. A., Asselbergs, F. W., De Borst, G. J., Aavik, E., Lönnberg, T., Lutgens, E., Glass, C. K., Den Ruijter, H. M., Kaikkonen, M. U., Bot, I., Slütter, B., Van Der Laan, S. W., Yla-Herttuala, S., … Pasterkamp, G. (2020b). Microanatomy of the Human Atherosclerotic Plaque by Single-Cell Transcriptomics. *Circulation Research*, *127*, 1437–1455.

Devaraj, N. K., & Finn, M. G. (2021). Introduction: Click Chemistry. *Chemical Reviews*, *121*(12), 6697–6698.

Dias, J., Leeansyah, E., & Sandberg, J. K. (2017). Multiple layers of heterogeneity and subset diversity in human MAIT cell responses to distinct microorganisms and to innate cytokines. *Proceedings of the National Academy of Sciences of the United States of America*, *114*(27), E5434–E5443.

Ding, Z., Liu, S., Wang, X., Theus, S., Deng, X., Fan, Y., Zhou, S., & Mehta, J. L. (2018). PCSK9 regulates expression of scavenger receptors and ox-LDL uptake in macrophages. *Cardiovascular Research*, *114*(8), 1145–1153.

Dougan, S. K., Kaser, A., & Blumberg, R. S. (2007). CD1 expression on antigen-presenting cells. *Current Topics in Microbiology and Immunology*, *314*, 113–141.

Eberl, G., Brawand, P., & MacDonald, H. R. (2000). Selective Bystander Proliferation of Memory CD4 + and CD8 + T Cells Upon NK T or T Cell Activation . *The Journal of Immunology*, *165*(8), 4305–4311.

Emeson, E. E., & Robertson, A. L. (1988). T lymphocytes in aortic and coronary intimas: Their potential role in atherogenesis. *American Journal of Pathology*, *130*(2), 369–376. /pmc/articles/PMC1880529/?report=abstract

Engelen, S. E., Robinson, A. J. B., Zurke, Y. X., & Monaco, C. (2022). Therapeutic strategies targeting inflammation and immunity in atherosclerosis: how to proceed? *Nature Reviews Cardiology*, 1–21.

Exley, M. A., Bigley, N. J., Cheng, O., Muhammad, S., Tahir, A., Smiley, S. T., Carter, Q. L., Stills, H. F., Grusby, M. J., Koezuka, Y., Taniguchi, M., & Balk, S. P. (2001). CD1d-reactive T-cell activation leads to amelioration of disease caused by diabetogenic encephalomyocarditis virus. *Journal of Leukocyte Biology*, *69*(5), 713–718.

Exley, M. A., Wilson, S. B., & Balk, S. P. (2017). Isolation and functional use of human

NKT cells. *Current Protocols in Immunology*, *2017*(November), 14.11.1-14.11.20.

Facciotti, F., Cavallari, M., Angénieux, C., Garcia-Alles, L. F., Signorino-Gelo, F., Angman, L., Gilleron, M., Prandi, J., Puzo, G., Panza, L., Xia, C., Wang, P. G., Dellabona, P., Casorati, G., Porcelli, S. A., De La Salle, H., Mori, L., & De Libero, G. (2011). Fine tuning by human CD1e of lipid-specific immune responses. *Proceedings of the National Academy of Sciences of the United States of America*, *108*(34), 14228–14233.

Facciotti, F., Ramanjaneyulu, G. S., Lepore, M., Sansano, S., Cavallari, M., Kistowska, M., Forss-Petter, S., Ni, G., Colone, A., Singhal, A., Berger, J., Xia, C., Mori, L., & De Libero, G. (2012). Peroxisome-derived lipids are self antigens that stimulate invariant natural killer T cells in the thymus. *Nature Immunology 2012 13:5*, *13*(5), 474–480.

Ference, B. A., Ginsberg, H. N., Graham, I., Ray, K. K., Packard, C. J., Bruckert, E., Hegele, R. A., Krauss, R. M., Raal, F. J., Schunkert, H., Watt, G. F., Borén, J., Fazio, S., Horton, J. D., Masana, L., Nicholls, S. J., Nordestgaard, B. G., Van De Sluis, B., Taskinen, M. R., … Catapano, A. L. (2017). Low-density lipoproteins cause atherosclerotic cardiovascular disease. 1. Evidence from genetic, epidemiologic, and clinical studies. A consensus statement from the European Atherosclerosis Society Consensus Panel. *European Heart Journal*, *38*(32), 2459–2472.

Fernandez, D. M., Rahman, A. H., Fernandez, N. F., Chudnovskiy, A., Amir, E. ad D., Amadori, L., Khan, N. S., Wong, C. K., Shamailova, R., Hill, C. A., Wang, Z., Remark, R., Li, J. R., Pina, C., Faries, C., Awad, A. J., Moss, N., Bjorkegren, J. L. M., Kim-Schulze, S., … Giannarelli, C. (2019). Single-cell immune landscape of human atherosclerotic plaques. *Nature Medicine*, *25*(10), 1576–1588.

Fitzmaurice, M., Bordagaray, J. O., Engelmann, G. L., Richards-Kortum, R., Kolubayev, T., Feld, M. S., Ratliff, N. B., & Kramer, J. R. (1989). Argon ion laser-excited autofluorescence in normal and atherosclerotic aorta and coronary arteries: Morphologic studies. *American Heart Journal*, *118*(5), 1028–1038.

Fletcher, J. M., Jordan, M. A., Snelgrove, S. L., Slattery, R. M., Dufour, F. D., Kyparissoudis, K., Besra, G. S., Godfrey, D. I., & Baxter, A. G. (2008). Congenic Analysis of the NKT Cell Control Gene Nkt2 Implicates the Peroxisomal Protein

Pxmp4. *The Journal of Immunology*, *181*(5), 3400–3412.

Freigang, S., Landais, E., Zadorozhny, V., Kain, L., Yoshida, K., Liu, Y., Deng, S., Palinski, W., Savage, P. B., Bendelac, A., & Teyton, L. (2012). Scavenger receptors target glycolipids for natural killer T cell activation. *Journal of Clinical Investigation*, *122*(11), 3943–3954.

Friedewald, W. T., Levy, R. I., & Fredrickson, D. S. (1972). Estimation of the Concentration of Low-Density Lipoprotein Cholesterol in Plasma, Without Use of the Preparative Ultracentrifuge. *Clinical Chemistry*, *18*(6), 499–502.

Fujii, S. I., Shimizu, K., Smith, C., Bonifaz, L., & Steinman, R. M. (2003). Activation of natural killer T cells by α-galactosylceramide rapidly induces the full maturation of dendritic cells in vivo and thereby acts as an adjuvant for combined CD4 and CD8 T cell immunity to a coadministered protein. *Journal of Experimental Medicine*, *198*(2), 267–279.

Fuster, J. J., Zuriaga, M. A., Zorita, V., MacLauchlan, S., Polackal, M. N., Viana-Huete, V., Ferrer-Pérez, A., Matesanz, N., Herrero-Cervera, A., Sano, S., Cooper, M. A., González-Navarro, H., & Walsh, K. (2020). TET2-Loss-of-Function-Driven Clonal Hematopoiesis Exacerbates Experimental Insulin Resistance in Aging and Obesity. *Cell Reports*, *33*(4), 108326.

Galkina, E., Kadl, A., Sanders, J., Varughese, D., Sarembock, I. J., & Ley, K. (2006). Lymphocyte recruitment into the aortic wall before and during development of atherosclerosis is partially L-selectin dependent. *Journal of Experimental Medicine*, *203*(5), 1273–1282.

Galli, G., Nuti, S., Tavarini, S., Galli-Stampino, L., De Lalla, C., Casorati, G., Dellabona, P., & Abrignani, S. (2003). CD1d-restricted Help To B Cells By Human Invariant Natural Killer T Lymphocytes. *The Journal of Experimental Medicine*, *197*(8), 1051.

Garai, K., Baban, B., & Frieden, C. (2011). Dissociation of apolipoprotein e oligomers to monomer is required for high-affinity binding to phospholipid vesicles. *Biochemistry*, *50*(13), 2550–2558.

Geissmann, F., Cameron, T. O., Sidobre, S., Manlongat, N., Kronenberg, M., Briskin, M. J., Dustin, M. L., & Littman, D. R. (2005). Intravascular Immune Surveillance by CXCR6+ NKT Cells Patrolling Liver Sinusoids. *PLOS Biology*, *3*(4), e113.

Gelissen, I. C., & Brown, A. J. (2017). An overview of cholesterol homeostasis. In

Methods in Molecular Biology (Vol. 1583, pp. 1–6). Humana Press Inc.

Geng, Y. J., Wu, Q., Muszynski, M., Hansson, G. K., & Libby, P. (1996). Apoptosis of vascular smooth muscle cells induced by in vitro stimulation with interferon-γ, tumor necrosis factor-α, and interleukin-1β. *Arteriosclerosis, Thrombosis, and Vascular Biology*, *16*(1), 19–27.

Getz, G. S., & Reardon, C. A. (2017). Natural killer T cells in atherosclerosis. *Nature Reviews Cardiology*, *14*(5), 304.

Giesen, C., Wang, H. A. O., Schapiro, D., Zivanovic, N., Jacobs, A., Hattendorf, B., Schüffler, P. J., Grolimund, D., Buhmann, J. M., Brandt, S., Varga, Z., Wild, P. J., Günther, D., & Bodenmiller, B. (2014). highly multiplexed imaging of tumor tissues with subcellular resolution by mass cytometry. *Articles NAture Methods |*, *11*(4), 417.

Gorini, F., Azzimonti, L., Delfanti, G., Scarfo, L., Scielzo, C., Bertilaccio, M. T., Ranghetti, P., Gulino, A., Doglioni, C., Di Napoli, A., Capri, M., Franceschi, C., Caligaris-Cappio, F., Ghia, P., Bellone, M., Dellabona, P., Casorati, G., & De Lalla, C. (2017). Invariant NKT cells contribute to chronic lymphocytic leukemia surveillance and prognosis. *Blood*, *129*(26), 3440–3451.

Griewank, K., Borowski, C., Rietdijk, S., Wang, N., Julien, A., Wei, D. G., Mamchak, A. A. A., Terhorst, C., & Bendelac, A. (2007). Homotypic Interactions Mediated by Slamf1 and Slamf6 Receptors Control NKT Cell Lineage Development. *Immunity*, *27*(5), 751–762.

Grin, P. M., Dwivedi, D. J., Chathely, K. M., Trigatti, B. L., Prat, A., Seidah, N. G., Liaw, P. C., & Fox-Robichaud, A. E. (2018). Low-density lipoprotein (LDL)-dependent uptake of Gram-positive lipoteichoic acid and Gram-negative lipopolysaccharide occurs through LDL receptor. *Scientific Reports*, *8*(1), 1–11.

Gu, W., Ni, Z., Tan, Y. Q., Deng, J., Zhang, S. J., Lv, Z. C., Wang, X. J., Chen, T., Zhang, Z., Hu, Y., Jing, Z. C., & Xu, Q. (2019). Adventitial Cell Atlas of wt (Wild Type) and ApoE (Apolipoprotein E)-Deficient Mice Defined by Single-Cell RNA Sequencing. *Arteriosclerosis, Thrombosis, and Vascular Biology*, *39*(6), 1055–1071.

Guo, H., Callaway, J. B., & Ting, J. P. Y. (2015). Inflammasomes: Mechanism of action, role in disease, and therapeutics. In *Nature Medicine* (Vol. 21, Issue 7, pp. 677–687). Nature Publishing Group.

Ha, C., Magowan, S., Accortt, N. A., Chen, J., & Stone, C. D. (2009). Risk of arterial thrombotic events in inflammatory bowel disease. *American Journal of Gastroenterology*, *104*(6), 1445–1451.

Haeckel, A., Ascher, L., Beindorff, N., Prasad, S., Garczyńska, K., Guo, J., & Schellenberger, E. (2021). Long-circulating XTEN864-annexin A5 fusion protein for phosphatidylserine-related therapeutic applications. *Apoptosis*, *26*(9–10), 534–547.

Hall, A., Róg, T., Karttunen, M., & Vattulainen, I. (2010). Role of Glycolipids in Lipid Rafts: A View through Atomistic Molecular Dynamics Simulations with Galactosylceramide. *Journal of Physical Chemistry B*, *114*(23), 7797–7807.

Hamanaka, R., Seguchi, T., Sato, Y., Ono, M., Kohno, K., & Kuwano, M. (1991). Rapid turnover of low density lipoprotein receptor in human monocytic THP-1 cells. *FEBS Letters*, *294*(3), 261–263.

Hansson, G. K. (2005a). Inflammation, Atherosclerosis, and Coronary Artery Disease. *New England Journal of Medicine*, *352*(16), 1685–1695.

Hansson, G. K. (2005b). Inflammation, Atherosclerosis, and Coronary Artery Disease. *New England Journal of Medicine*, *352*(16), 1685–1695.

Hansson, G. K., Holm, J., & Jonasson, L. (1989). Detection of activated T lymphocytes in the human atherosclerotic plaque. *American Journal of Pathology*, *135*(1), 169–175. /pmc/articles/PMC1880219/?report=abstract

Hansson, G. K., Jonasson, L., Holm, J., & Claesson-Welsh, L. (1986). Class II MHC antigen expression in the atherosclerotic plaque: smooth muscle cells express HLA-DR, HLA-DQ and the invariant gamma chain. *Clinical and Experimental Immunology*, *64*(2), 261–268.

Harman, J. L., & Jørgensen, H. F. (2019). The role of smooth muscle cells in plaque stability: Therapeutic targeting potential. *British Journal of Pharmacology*, *176*(19), 3741.

Heczey, A., Courtney, A. N., Montalbano, A., Robinson, S., Liu, K., Li, M., Ghatwai, N., Dakhova, O., Liu, B., Raveh-Sadka, T., Chauvin-Fleurence, C. N., Xu, X., Ngai, H., Di Pierro, E. J., Savoldo, B., Dotti, G., & Metelitsa, L. S. (2020). Anti-GD2 CAR-NKT cells in patients with relapsed or refractory neuroblastoma: an interim analysis. *Nature Medicine 2020 26:11*, *26*(11), 1686–1690.

Hegde, S., Jankowska-Gan, E., Roenneburg, D. A., Torrealba, J., Burlingham, W. J., &

Gumperz, J. E. (2009). Human NKT cells promote monocyte differentiation into suppressive myeloid antigen-presenting cells. *Journal of Leukocyte Biology*, *86*(4), 757–768.

Hein, L. K., Duplock, S., Hopwood, J. J., & Fuller, M. (2008). Lipid composition of microdomains is altered in a cell model of Gaucher disease. *Journal of Lipid Research*, *49*(8), 1725–1734.

Hellings, W. E., Moll, F. L., de Kleijn, D. P. V, & Pasterkamp, G. (2012). 10-years experience with the Athero-Express study. *Cardiovascular Diagnosis and Therapy*, *2*(1), 63–73.

Ijsselsteijn, M. E., Van Der Breggen, R., Sarasqueta, A. F., Koning, F., De Miranda, N. F. C. C. C. C., Schiavoni, G., Olive, D., Melenhorst, J. J., De Miranda, N. F. C. C. C. C., Ijsselsteijn, M. E., Van Der Breggen, R., Farina Sarasqueta, A., & Koning, F. (2019). A 40-marker panel for high dimensional characterization of cancer immune microenvironments by imaging mass cytometry. *Frontiers in Immunology*, *10*(OCT), 2534.

Iqbal, J., Walsh, M. T., Hammad, S. M., & Hussain, M. M. (2017). Sphingolipids and Lipoproteins in Health and Metabolic Disorders. In *Trends in Endocrinology and Metabolism* (Vol. 28, Issue 7, pp. 506–518). Elsevier Inc.

Jabir, N. R., Firoz, C. K., Ahmed, F., Kamal, M. A., Hindawi, S., Damanhouri, G. A., Almehdar, H. A., & Tabrez, S. (2017). Reduction in CD16/CD56 and CD16/CD3/CD56 Natural Killer Cells in Coronary Artery Disease. *Immunological Investigations*, *46*(5), 526–535.

Jackson, H. W., Fischer, J. R., Zanotelli, V. R. T., Ali, H. R., Mechera, R., Soysal, S. D., Moch, H., Muenst, S., Varga, Z., Weber, W. P., & Bodenmiller, B. (2020). The single-cell pathology landscape of breast cancer. *Nature*, *578*(7796), 615–620.

Jaiswal, S., & Libby, P. (2020). Clonal haematopoiesis: connecting ageing and inflammation in cardiovascular disease. In *Nature Reviews Cardiology* (Vol. 17, Issue 3, pp. 137–144). Nature Research.

Jervis, P. J., Polzella, P., Wojno, J., Jukes, J. P., Ghadbane, H., Garcia Diaz, Y. R., Besra, G. S., Cerundolo, V., & Cox, L. R. (2013). Design, synthesis, and functional activity of labeled CD1d glycolipid agonists. *Bioconjugate Chemistry*, *24*(4), 586–594.

Jing, Y., Gravenstein, S., Rao Chaganty, N., Chen, N., Lyerly, K. H., Joyce, S., & Deng, Y. (2007). *Aging is associated with a rapid decline in frequency, alterations in subset*

composition, and enhanced Th2 response in CD1d-restricted NKT cells from human peripheral blood. *42*(8), 719–732.

Johnson, T. R., Hong, S., Van Kaer, L., Koezuka, Y., & Graham, B. S. (2002). NK T cells contribute to expansion of CD8(+) T cells and amplification of antiviral immune responses to respiratory syncytial virus. *Journal of Virology*, *76*(9), 4294–4303.

Jonasson, L., Holm, J., Skalli, O., Bondjers, G., & Hansson, G. K. (1986). Regional accumulations of T cells, macrophages, and smooth muscle cells in the human atherosclerotic plaque. *Arteriosclerosis*, *6*(2), 131–138.

Jonasson, L., Holm, J., Skalli, O., Gabbiani, G., & Hansson, G. K. (1985). Expression of class II transplantation antigen on vascular smooth muscle cells in human atherosclerosis. *Journal of Clinical Investigation*, *76*(1), 125–131.

Kaabia, Z., Poirier, J., Moughaizel, M., Aguesse, A., Billon-Crossouard, S., Fall, F., Durand, M., Dagher, E., Krempf, M., & Croyal, M. (2018). Plasma lipidomic analysis reveals strong similarities between lipid fingerprints in human, hamster and mouse compared to other animal species. *Scientific Reports*, *8*(1), 1–9.

Kain, L., Webb, B., Anderson, B. L., Deng, S., Holt, M., Constanzo, A., Zhao, M., Self, K., Teyton, A., Everett, C., Kronenberg, M., Zajonc, D. M., Bendelac, A., Savage, P. B., & Teyton, L. (2014). The identification of the endogenous ligands of natural killer T cells reveals the presence of mammalian α-linked glycosylceramides. *Immunity*, *41*(4), 543–554.

Ketelhuth, D. F. J., & Hansson, G. K. (2016). Adaptive Response of T and B Cells in Atherosclerosis. *Circulation Research*, *118*(4), 668–678.

Kim, K., Shim, D., Lee, J. S., Zaitsev, K., Williams, J. W., Kim, K. W., Jang, M. Y., Jang, H. S., Yun, T. J., Lee, S. H., Yoon, W. K., Prat, A., Seidah, N. G., Choi, J., Lee, S. P., Yoon, S. H., Nam, J. W., Seong, J. K., Oh, G. T., … Choi, J. H. (2018). Transcriptome analysis reveals nonfoamy rather than foamy plaque macrophages are proinflammatory in atherosclerotic murine models. *Circulation Research*, *123*(10), 1127–1142.

Kinjo, Y., Illarionov, P., Vela, J. L., Pei, B., Girardi, E., Li, X., Li, Y., Imamura, M., Kaneko, Y., Okawara, A., Miyazaki, Y., Gómez-Velasco, A., Rogers, P., Dahesh, S., Uchiyama, S., Khurana, A., Kawahara, K., Yesilkaya, H., Andrew, P. W., … Kronenberg, M. (2011). Invariant natural killer T cells recognize glycolipids

from pathogenic Gram-positive bacteria. *Nature Immunology*, *12*(10), 966–974.

Kinjo, Y., Tupin, E., Wu, D., Fujio, M., Garcia-Navarro, R., Benhnia, M. R. E. I., Zajonc, D. M., Ben-Menachem, G., Ainge, G. D., Painter, G. F., Khurana, A., Hoebe, K., Behar, S. M., Beutler, B., Wilson, I. A., Tsuji, M., Sellati, T. J., Wong, C. H., & Kronenberg, M. (2006). Natural killer T cells recognize diacylglycerol antigens from pathogenic bacteria. *Nature Immunology 2006 7:9*, *7*(9), 978–986.

Kitamura, H., Ohta, A., Sekimoto, M., Sato, M., Iwakabe, K., Nakui, M., Yahata, T., Meng, H., Koda, T., Nishimura, S. I., Kawano, T., Taniguchi, M., & Nishimura, T. (2000). α-galactosylceramide induces early B-cell activation through IL-4 production by NKT cells. *Cellular Immunology*, *199*(1), 37–42.

Krieger, J. W., Singh, A. P., Bag, N., Garbe, C. S., Saunders, T. E., Langowski, J., & Wohland, T. (2015). Imaging fluorescence (cross-) correlation spectroscopy in live cells and organisms. *Nature Protocols*, *10*(12), 1948–1974.

Kyaw, T., Tay, C., Krishnamurthi, S., Kanellakis, P., Agrotis, A., Tipping, P., Bobik, A., & Toh, B. H. (2011). B1a B lymphocytes are atheroprotective by secreting natural IgM that increases IgM deposits and reduces necrotic cores in atherosclerotic lesions. *Circulation Research*, *109*(8), 830–840.

Kyaw, T., Winship, A., Tay, C., Kanellakis, P., Hosseini, H., Cao, A., Li, P., Tipping, P., Bobik, A., & Toh, B. H. (2013). Cytotoxic and proinflammatory CD8+ T lymphocytes promote development of vulnerable atherosclerotic plaques in ApoE-deficient mice. *Circulation*, *127*(9), 1028–1039.

Kyriakakis, E., Cavallari, M., Andert, J., Philippova, M., Koella, C., Bochkov, V., Erne, P., Brian Wilson, S., Mori, L., Biedermann, B. C., Resink, T. J., & De Libero, G. (2010). Invariant natural killer T cells: linking inflammation and neovascularization in human atherosclerosis. *European Journal of Immunology*, *40*(11), 3268–3279.

Lacasse, J., & Martin, L. H. (1992). Detection of CD1 mRNA in Paneth cells of the mouse intestine by in situ hybridization. *The Journal of Histochemistry and Cytochemistry : Official Journal of the Histochemistry Society*, *40*(10), 1527–1534.

Lalla, C. de, Rinaldi, A., Montagna, D., Azzimonti, L., Bernardo, M. E., Sangalli, L. M., Paganoni, A. M., Maccario, R., Cesare-Merlone, A. Di, Zecca, M., Locatelli, F., Dellabona, P., & Casorati, G. (2011). Invariant NKT Cell Reconstitution in Pediatric Leukemia Patients Given HLA-Haploidentical Stem Cell

Transplantation Defines Distinct CD4+ and CD4− Subset Dynamics and Correlates with Remission State. *The Journal of Immunology*, *186*(7), 4490–4499.

Lantz, O., & Bendelac, A. (1994). An invariant T cell receptor α Chain is used by a unique subset of major histocompatibility complex class I-specific CD4+ and CD4-8- T cells in mice and humans. *Journal of Experimental Medicine*, *180*(3), 1077–1106.

Lee, M., & Bensinger, S. J. (2022). Reprogramming cholesterol metabolism in macrophages and its role in host defense against cholesterol-dependent cytolysins. *Cellular & Molecular Immunology*, *19*, 327–336.

Lee, S. G., Oh, J., Bong, S. K., Kim, J. S., Park, S., Kim, S., Park, S., Lee, S. H., & Jang, Y. (2018). Macrophage polarization and acceleration of atherosclerotic plaques in a swine model. *PLoS ONE*, *13*(3), 1–16.

Lee, W.-Y., Moriarty, T. J., Wong, C. H. Y., Zhou, H., Strieter, R. M., van Rooijen, N., Chaconas, G., & Kubes, P. (2010). An intravascular immune response to Borrelia burgdorferi involves Kupffer cells and iNKT cells. *Nature Immunology*, *11*(4), 295–302.

Lee, Y. J., Holzapfel, K. L., Zhu, J., Jameson, S. C., & Hogquist, K. A. (2013). Steady state production of IL-4 modulates immunity in different strains and is determined by lineage diversity of iNKT cells. *Nature Immunology*, *14*(11), 1146–1154.

Leistner, D. M., Kränkel, N., Meteva, D., Abdelwahed, Y. S., Seppelt, C., Stähli, B. E., Rai, H., Skurk, C., Lauten, A., Mochmann, H.-C. C., Fröhlich, G., Rauch-Kröhnert, U., Flores, E., Riedel, M., Sieronski, L., Kia, S., Strässler, E., Haghikia, A., Dirks, F., … Landmesser, U. (2020). Differential immunological signature at the culprit site distinguishes acute coronary syndrome with intact from acute coronary syndrome with ruptured fibrous cap: Results from the prospective translational OPTICO-ACS study. *European Heart Journal*, *41*(37), 3549–3560.

Levels, J. H. M., Marquart, J. A., Abraham, P. R., Van Den Ende, A. E., Molhuizen, H. O. F., Van Deventer, S. J. H., & Meijers, J. C. M. (2005). Lipopolysaccharide is transferred from high-density to low-density lipoproteins by lipopolysaccharide-binding protein and phospholipid transfer protein. *Infection and Immunity*, *73*(4), 2321–2326.

Li, K., Wong, D. K., Luk, F. S., Kim, R. Y., & Raffai, R. L. (2018). Isolation of plasma

lipoproteins as a, source of extracellular RNA. In *Methods in Molecular Biology* (Vol. 1740, pp. 139–153). Humana Press Inc.

Li, Y., Kanellakis, P., Hosseini, H., Cao, A., Deswaerte, V., Tipping, P., Toh, B. H., Bobik, A., & Kyaw, T. (2016). A CD1d-dependent lipid antagonist to NKT cells ameliorates atherosclerosis in ApoE−/− mice by reducing lesion necrosis and inflammation. *Cardiovascular Research*, *109*(2), 305–317.

Li, Y., To, K., Kanellakis, P., Hosseini, H., Deswaerte, V., Tipping, P., Smyth, M. J., Toh, B. H., Bobik, A., & Kyaw, T. (2015). CD4+ natural killer T cells potently augment aortic root atherosclerosis by perforin-and granzyme b-dependent cytotoxicity. *Circulation Research*, *116*(2), 245–254.

Libby, P. (2012). Inflammation in atherosclerosis. *Arteriosclerosis, Thrombosis, and Vascular Biology*, *32*(9), 2045–2051.

Libby, P., & Pasterkamp, G. (2015). Requiem for the 'vulnerable plaque.' *European Heart Journal*, *36*(43), 2984–2987.

Libby, P., Ridker, P. M., & Maseri, A. (2002). Inflammation and atherosclerosis. *Circulation*, *105*(9), 1135–1143.

Lieb, W., Enserro, D. M., Larson, M. G., & Vasan, R. S. (2018). Residual cardiovascular risk in individuals on lipid-lowering treatment: Quantifying absolute and relative risk in the community. *Open Heart*, *5*(1), 722.

Lin, J. Da, Nishi, H., Poles, J., Niu, X., Mccauley, C., Rahman, K., Brown, E. J., Yeung, S. T., Vozhilla, N., Weinstock, A., Ramsey, S. A., Fisher, E. A., & Loke, P. (2019). Single-cell analysis of fate-mapped macrophages reveals heterogeneity, including stem-like properties, during atherosclerosis progression and regression. *JCI Insight*, *4*(4).

Lisbonne, M., Diem, S., Keller, A. de C., Lefort, J., Araujo, L. M., Hachem, P., Fourneau, J.-M., Sidobre, S., Kronenberg, M., Taniguchi, M., Endert, P. Van, Dy, M., Askenase, P., Russo, M., Vargaftig, B. B., Herbelin, A., & Leite-de-Moraes, M. C. (2003). Cutting Edge: Invariant Vα14 NKT Cells Are Required for Allergen-Induced Airway Inflammation and Hyperreactivity in an Experimental Asthma Model. *The Journal of Immunology*, *171*(4), 1637–1641.

Liu, D., Song, L., Brawley, V. S., Robison, N., Wei, J., Gao, X., Tian, G., Margol, A., Ahmed, N., Asgharzadeh, S., & Metelitsa, L. S. (2013). Medulloblastoma expresses CD1d and can be targeted for immunotherapy with NKT cells. *Clinical Immunology*,

149(1), 55–64.

Liuzzo, G., Biasucci, L. M., Gallimore, J. R., Grillo, R. L., Rebuzzi, A. G., Pepys, M. B., & Maseri, A. (1994). The Prognostic Value of C-Reactive Protein and Serum Amyloid A Protein in Severe Unstable Angina. *New England Journal of Medicine*, *331*(7), 417–424.

Long, X., Deng, S., Mattner, J., Zang, Z., Zhou, D., McNary, N., Goff, R. D., Teyton, L., Bendelac, A., & Savage, P. B. (2007). Synthesis and evaluation of stimulatory properties of Sphingomonadaceae glycolipids. *Nature Chemical Biology 2007 3:9*, *3*(9), 559–564.

Luo, J., Yang, H., & Song, B. L. (2020). Mechanisms and regulation of cholesterol homeostasis. In *Nature Reviews Molecular Cell Biology* (Vol. 21, Issue 4, pp. 225–245). Nature Research.

Lynch, L., Michelet, X., Zhang, S., Brennan, P. J., Moseman, A., Lester, C., Besra, G., Vomhof-Dekrey, E. E., Tighe, M., Koay, H. F., Godfrey, D. I., Leadbetter, E. A., Sant'Angelo, D. B., Von Andrian, U., & Brenner, M. B. (2014). Regulatory iNKT cells lack expression of the transcription factor PLZF and control the homeostasis of T(reg) cells and macrophages in adipose tissue. *Nature Immunology*, *16*(1), 85–95.

Mahley, R. W., Innerarity, T. L., Rall, S. C. J., & Weisgraber, K. H. (1984). Plasma lipoproteins: apolipoprotein structure and function. *Journal of Lipid Research*, *25*(12), 1277–1294.

Major, A. S., Wilson, M. T., McCaleb, J. L., Yan, R. S., Stanic, A. K., Joyce, S., Van Kaer, L., Fazio, S., & Linton, M. F. (2004). Quantitative and qualitative differences in proatherogenic NKT cells in apolipoprotein E-deficient mice. *Arteriosclerosis, Thrombosis, and Vascular Biology*, *24*(12), 2351–2357.

Marais, A. D. (2004). Familial Hypercholesterolaemia. *The Clinical Biochemist Reviews*, *25*(1), 49.

Marais, A. D. (2019). Apolipoprotein E in lipoprotein metabolism, health and cardiovascular disease. In *Pathology* (Vol. 51, Issue 2, pp. 165–176). Elsevier B.V.

Massey, J. B., & Pownall, H. J. (1998). Surface properties of native human plasma lipoproteins and lipoprotein models. *Biophysical Journal*, *74*(2 I), 869–878.

McArdle, S., Buscher, K., Ghosheh, Y., Pramod, A. B., Miller, J., Winkels, H., Wolf, D., &

Ley, K. (2019). Migratory and dancing macrophage subsets in atherosclerotic lesions. *Circulation Research*, *125*(12), 1038–1051.

Molling, J. W., Kölgen, W., Van Der Vliet, H. J. J., Boomsma, M. F., Kruizenga, H., Smorenburg, C. H., Molenkamp, B. G., Langendijk, J. A., Leemans, C. R., Von Blomberg, B. M. E., Scheper, R. J., & Van Den Eertwegh, A. J. M. (2005). Peripheral blood IFN-γ-secreting Vα24+Vβ11+ NKT cell numbers are decreased in cancer patients independent of tumor type or tumor load. *International Journal of Cancer*, *116*(1), 87–93.

Molling, J. W., Langius, J. A. E., Langendijk, J. A., Leemans, C. R., Bontkes, H. J., Van Der Vliet, H. J. J., Von Blomberg, B. M. E., Scheper, R. J., & Van Den Eertwegh, A. J. M. (2007). Low levels of circulating invariant natural killer T cells predict poor clinical outcome in patients with head and neck squamous cell carcinoma. *Journal of Clinical Oncology*, *25*(7), 862–868.

Monici, M. (2005). Cell and tissue autofluorescence research and diagnostic applications. *Biotechnology Annual Review*, *11*(SUPPL.), 227–256.

Monteiro, M., Almeida, C. F., Caridade, M., Ribot, J. C., Duarte, J., Agua-Doce, A., Wollenberg, I., Silva-Santos, B., & Graca, L. (2010). Identification of Regulatory Foxp3+ Invariant NKT Cells Induced by TGF-β. *The Journal of Immunology*, *185*(4), 2157–2163.

Moore, K. J., & Tabas, I. (2011). Macrophages in the pathogenesis of atherosclerosis. *Cell*, *145*(3), 341–355.

Naghavi, M., Libby, P., Falk, E., Casscells, S. W., Litovsky, S., Rumberger, J., Badimon, J. J., Stefanadis, C., Moreno, P., Pasterkamp, G., Fayad, Z., Stone, P. H., Waxman, S., Raggi, P., Madjid, M., Zarrabi, A., Burke, A., Yuan, C., Fitzgerald, P. J., … Willerson, J. T. (2003). From Vulnerable Plaque to Vulnerable Patient. *Circulation*, *108*(14), 1664–1672.

Nakai, Y., Iwabuchi, K., Fujii, S., Ishimori, N., Dashtsoodol, N., Watano, K., Mishima, T., Iwabuchi, C., Tanaka, S., Bezbradica, J., Nakayama, T., Taniguchi, M., Miyake, S., Yamamura, T., Kitabatake, A., Joyce, S., Van Kaer, L., & Onoe, K. (2004). Natural killer T cells accelerate atherogenesis in mice. *Blood*, *104*(7), 2051–2059.

Nakashima, Y., Plump, A. S., Raines, E. W., Breslow, J. L., & Ross, R. (1994). ApoE-deficient mice develop lesions of all phases of atherosclerosis throughout the arterial tree. *Arteriosclerosis and Thrombosis : A Journal of Vascular Biology*,

14(1), 133–140.

Nelissen, B. G. L., Van Herwaarden, J. A., Moll, F. L., Van Diest, P. J., & Pasterkamp, G. (2014). SlideToolkit: An Assistive Toolset for the Histological Quantification of Whole Slide Images. *PLOS ONE*, *9*(11), e110289.

Neumann, F. J., Sechtem, U., Banning, A. P., Bonaros, N., Bueno, H., Bugiardini, R., Chieffo, A., Crea, F., Czerny, M., Delgado, V., Dendale, P., Knuuti, J., Wijns, W., Flachskampf, F. A., Gohlke, H., Grove, E. L., James, S., Katritsis, D., Landmesser, U., … Clapp, B. (2020). 2019 ESC Guidelines for the diagnosis and management of chronic coronary syndromes. *European Heart Journal*, *41*(3), 407–477.

Nidorf, S. M., Fiolet, A. T. L., Mosterd, A., Eikelboom, J. W., Schut, A., Opstal, T. S. J., The, S. H. K., Xu, X.-F., Ireland, M. A., Lenderink, T., Latchem, D., Hoogslag, P., Jerzewski, A., Nierop, P., Whelan, A., Hendriks, R., Swart, H., Schaap, J., Kuijper, A. F. M., … Thompson, P. L. (2020a). Colchicine in Patients with Chronic Coronary Disease. *New England Journal of Medicine*, *383*(19), 1838–1847.

Nidorf, S. M., Fiolet, A. T. L., Mosterd, A., Eikelboom, J. W., Schut, A., Opstal, T. S. J., The, S. H. K., Xu, X.-F., Ireland, M. A., Lenderink, T., Latchem, D., Hoogslag, P., Jerzewski, A., Nierop, P., Whelan, A., Hendriks, R., Swart, H., Schaap, J., Kuijper, A. F. M., … Thompson, P. L. (2020b). Colchicine in Patients with Chronic Coronary Disease. *New England Journal of Medicine*, *383*(19), 1838–1847.

Nieuwenhuis, E. E. S., Matsumoto, T., Exley, M., Schleipman, R. A., Glickman, J., Bailey, D. T., Corazza, N., Colgan, S. P., Onderdonk, A. B., & Blumberg, R. S. (2002). CD1d-dependent macrophage-mediated clearance of Pseudomonas aeruginosa from lung. *Nature Medicine 2002 8:6*, *8*(6), 588–593.

Nishimura, T., Kitamura, H., Iwakabe, K., Yahata, T., Ohta, A., Sato, M., Takeda, K., Okumura, K., Van Kaer, L., Kawano, T., Taniguchi, M., Nakui, M., Sekimoto, M., & Koda, T. (2000). The interface between innate and acquired immunity: Glycolipid antigen presentation by CD1d-expressing dendritic cells to NKT cells induces the differentiation of antigen-specific cytotoxic T lymphocytes. *International Immunology*, *12*(7), 987–994.

NJ, S., J, E., AS, H., C, H., M, M., B, M., RJ, D., T, M., P, B., HE, W., JH, B., IR, K., SE, S., S, S., DA, T., MM, I., F, P., H, P., W, L., … Schunkert, H. (2007). Genomewide Association Analysis of Coronary Artery Disease. *New England Journal of Medicine*, *357*(5), 443–453.

O'Neill, L. A. J., Golenbock, D., & Bowie, A. G. (2013). The history of Toll-like receptors-redefining innate immunity. *Nature Reviews Immunology*, *13*(6), 453–460.

Ohmura, Y., Ishimori, N., Saito, A., Yokota, T., Horii, S., Tokuhara, S., Iwabuchi, K., Tsutsui, H., & Bezsonov, E. (2021). *Natural Killer T Cells Are Involved in Atherosclerotic Plaque Instability in Apolipoprotein-E Knockout Mice*.

Ostos, M. A., Recalde, D., Zakin, M. M., & Scott-Algara, D. (2002). Implication of natural killer T cells in atherosclerosis development during a LPS-induced chronic inflammation. *FEBS Letters*, *519*(1–3), 23–29.

Paget, C., Mallevaey, T., Speak, A. O., Torres, D., Fontaine, J., Sheehan, K. C. F., Capron, M., Ryffel, B., Faveeuw, C., Leite de Moraes, M., Platt, F., & Trottein, F. (2007). Activation of Invariant NKT Cells by Toll-like Receptor 9-Stimulated Dendritic Cells Requires Type I Interferon and Charged Glycosphingolipids. *Immunity*, *27*(4), 597–609.

Pál, E., Tabira, T., Kawano, T., Taniguchi, M., Miyake, S., & Yamamura, T. (2001). Costimulation-Dependent Modulation of Experimental Autoimmune Encephalomyelitis by Ligand Stimulation of Vα14 NK T Cells. *The Journal of Immunology*, *166*(1), 662–668.

Parekh, V. V., Lalani, S., Kim, S., Halder, R., Azuma, M., Yagita, H., Kumar, V., Wu, L., & Van Kaer, L. (2009). PD-1/PD-L blockade prevents anergy induction and enhances the anti-tumor activities of glycolipid-activated invariant NKT cells. *Journal of Immunology (Baltimore, Md. : 1950)*, *182*(5), 2816–2826.

Parekh, V. V., Wilson, M. T., Olivares-Villagómez, D., Singh, A. K., Wu, L., Wang, C.-R. R., Joyce, S., & Van Kaer, L. (2005). Glycolipid antigen induces long-term natural killer T cell anergy in mice. *The Journal of Clinical Investigation*, *115*(9), 2572–2583.

Porubsky, S., Speak, A. O., Luckow, B., Cerundolo, V., Platt, F. M., & Gröne, H. J. (2007). Normal development and function of invariant natural killer T cells in mice with isoglobotrihexosylceramide (iGb3) deficiency. *Proceedings of the National Academy of Sciences of the United States of America*, *104*(14), 5977–5982.

Powl, A. M., East, J. M., & Lee, A. G. (2007). Different Effects of Lipid Chain Length on the Two Sides of a Membrane and the Lipid Annulus of MscL. *Biophysical Journal*, *93*(1), 113.

Rajavashisth, T., Qiao, J. H., Tripathi, S., Tripathi, J., Mishra, N., Hua, M., Wang, X. P., Loussararian, A., Clinton, S., Libby, P., & Lusis, A. (1998). Heterozygous osteopetrotic (op) mutation reduces atherosclerosis in LDL receptor-deficient mice. *Journal of Clinical Investigation*, *101*(12), 2702–2710.

Rana, R., Gómez-Biagi, R. F., Bassan, J., & Nitz, M. (2019). Signal Amplification for Imaging Mass Cytometry. *Bioconjugate Chemistry*, *30*(11), 2805–2810.

Rensen, P. C. N., Herijgers, N., Netscher, M. H., Meskers, S. C. J., Van Eck, M., & Van Berkel, T. J. C. (1997). Particle size determines the specificity of apolipoprotein E-containing triglyceride-rich emulsions for the LDL receptor versus hepatic remnant receptor in vivo. *Journal of Lipid Research*, *38*(6), 1070–1084.

Ridker, P. M., Buring, J. E., Shih, J., Matias, M., & Hennekens, C. H. (1998). Prospective study of C-reactive protein and the risk of future cardiovascular events among apparently healthy women. *Circulation*, *98*(8), 731–733.

Ridker, P. M., Everett, B. M., Thuren, T., MacFadyen, J. G., Chang, W. H., Ballantyne, C., Fonseca, F., Nicolau, J., Koenig, W., Anker, S. D., Kastelein, J. J. P., Cornel, J. H., Pais, P., Pella, D., Genest, J., Cifkova, R., Lorenzatti, A., Forster, T., Kobalava, Z., … Glynn, R. J. (2017a). Antiinflammatory Therapy with Canakinumab for Atherosclerotic Disease. *New England Journal of Medicine*, *377*(12), 1119–1131.

Ridker, P. M., Everett, B. M., Thuren, T., MacFadyen, J. G., Chang, W. H., Ballantyne, C., Fonseca, F., Nicolau, J., Koenig, W., Anker, S. D., Kastelein, J. J. P., Cornel, J. H., Pais, P., Pella, D., Genest, J., Cifkova, R., Lorenzatti, A., Forster, T., Kobalava, Z., … Glynn, R. J. (2017b). Antiinflammatory Therapy with Canakinumab for Atherosclerotic Disease. *New England Journal of Medicine*, *377*(12), 1119–1131.

Ridker, P. M., Rifai, N., Pfeffer, M., Sacks, F., Lepage, S., & Braunwald, E. (2000). Elevation of tumor necrosis factor-α and increased risk of recurrent coronary events after myocardial infarction. *Circulation*, *101*(18), 2149–2153.

Ridker, P. M., Rifai, N., Stampfer, M. J., & Hennekens, C. H. (2000). Plasma concentration of interleukin-6 and the risk of future myocardial infarction among apparently healthy men. *Circulation*, *101*(15), 1767–1772.

Ries, J., Petráek, Z., García-Sáez, A. J., & Schwille, P. (2010). A comprehensive framework for fluorescence cross-correlation spectroscopy. *New Journal of Physics*, *12*(11), 113009.

Robbins, C. S., Chudnovskiy, A., Rauch, P. J., Figueiredo, J. L., Iwamoto, Y., Gorbatov,

R., Etzrodt, M., Weber, G. F., Ueno, T., Van Rooijen, N., Mulligan-Kehoe, M. J., Libby, P., Nahrendorf, M., Pittet, M. J., Weissleder, R., & Swirski, F. K. (2012). Extramedullary hematopoiesis generates Ly-6C high monocytes that infiltrate atherosclerotic lesions. *Circulation*, *125*(2), 364–374.

Rogers, L., Burchat, S., Gage, J., Hasu, M., Thabet, M., Wilcox, L., Ramsamy, T. A., & Whitman, S. C. (2008). Deficiency of invariant Vα14 natural killer T cells decreases atherosclerosis in LDL receptor null mice. *Cardiovascular Research*, *78*(1). /pmc/articles/PMC5439367/

Roman, M. J., Shanker, B.-A., Davis, A., Lockshin, M. D., Sammaritano, L., Simantov, R., Crow, M. K., Schwartz, J. E., Paget, S. A., Devereux, R. B., & Salmon, J. E. (2003). Prevalence and Correlates of Accelerated Atherosclerosis in Systemic Lupus Erythematosus. *New England Journal of Medicine*, *349*(25), 2399–2406.

Rosenson, R. S. (2019). *Lipoprotein classification, metabolism, and role in atherosclerosis - Uptodate*. Jul. https://www.uptodate.com/contents/lipoprotein-classification-metabolism-and-role-in-atherosclerosis

Rosenson, R. S., Brewer, H. B., Ansell, B. J., Barter, P., Chapman, M. J., Heinecke, J. W., Kontush, A., Tall, A. R., & Webb, N. R. (2015). Dysfunctional HDL and atherosclerotic cardiovascular disease. *Nature Reviews Cardiology 2015 13:1*, *13*(1), 48–60.

Ross, R. (1999). Inflammation or Atherogenesis. *The New England Journal of Medicine*, *340*(2), 115–126.

Rossmann, A., Henderson, B., Heidecker, B., Seiler, R., Fraedrich, G., Singh, M., Parson, W., Keller, M., Grubeck-Loebenstein, B., & Wick, G. (2008). T-cells from advanced atherosclerotic lesions recognize hHSP60 and have a restricted T-cell receptor repertoire. *Experimental Gerontology*, *43*(3), 229–237.

Roy, P., Orecchioni, M., & Ley, K. (2021). How the immune system shapes atherosclerosis: roles of innate and adaptive immunity. *Nature Reviews Immunology*.

Sage, A. P., Nus, M., Baker, L. L., Finigan, A. J., Masters, L. M., & Mallat, Z. (2015). Regulatory B cell-specific interleukin-10 is dispensable for atherosclerosis development in mice. *Arteriosclerosis, Thrombosis, and Vascular Biology*, *35*(8), 1770–1773.

Saigusa, R., Winkels, H., & Ley, K. (2020). T cell subsets and functions in atherosclerosis. *Nature Reviews Cardiology*, *17*(7), 387–401.

Salio, M., Speak, A. O., Shepherd, D., Polzella, P., Illarionov, P. A., Veerapen, N., Besra, G. S., Platt, F. M., & Cerundolo, V. (2007). Modulation of human natural killer T cell ligands on TLR-mediated antigen-presenting cell activation. *Proceedings of the National Academy of Sciences of the United States of America*, *104*(51), 20490–20495.

Salonen, J. T., Korpela, H., Salonen, R., Nyyssonen, K., Yla-Herttuala, S., Yamamoto, R., Butler, S., Palinski, W., & Witztum, J. L. (1992). Autoantibody against oxidised LDL and progression of carotid atherosclerosis. *The Lancet*, *339*(8798), 883–887.

Scherer, M., Böttcher, A., Schmitz, G., & Liebisch, G. (2011). Sphingolipid profiling of human plasma and FPLC-separated lipoprotein fractions by hydrophilic interaction chromatography tandem mass spectrometry. *Biochimica et Biophysica Acta - Molecular and Cell Biology of Lipids*, *1811*(2), 68–75.

Schipper, H. S., Rakhshandehroo, M., van de Graaf, S. F. J., Venken, K., Koppen, A., Stienstra, R., Prop, S., Meerding, J., Hamers, N., Besra, G., Boon, L., Nieuwenhuis, E. E. S., Elewaut, D., Prakken, B., Kersten, S., Boes, M., & Kalkhoven, E. (2012). Natural killer T cells in adipose tissue prevent insulin resistance. *The Journal of Clinical Investigation*, *122*(9), 3343–3354.

Schmieg, J., Yang, G., Franck, R. W., Van Rooijen, N., & Tsuji, M. (2005). Glycolipid presentation to natural killer T cells differs in an organ-dependent fashion. In *Proceedings of the National Academy of Sciences of the United States of America* (Vol. 102, Issue 4). Proc Natl Acad Sci U S A.

Schwartz, S. M., Galis, Z. S., Rosenfeld, M. E., & Falk, E. (2007). Plaque Rupture in Humans and Mice. *Arteriosclerosis, Thrombosis, and Vascular Biology*, *27*(4), 705–713.

Shissler, S. C., Lee, M. S., & Webb, T. J. (2017). Mixed Signals: Co-Stimulation in Invariant Natural Killer T Cell-Mediated Cancer Immunotherapy. *Frontiers in Immunology*, *8*(NOV).

Skålén, K., Gustafsson, M., Knutsen Rydberg, E., Hultén, L. M., Wiklund, O., Innerarity, T. L., & Boren, J. (2002). Subendothelial retention of atherogenic lipoproteins in early atherosclerosis. *Nature 2002 417:6890*, *417*(6890), 750–754.

Slauenwhite, D., & Johnston, B. (2015). Regulation of NKT cell localization in homeostasis and infection. In *Frontiers in Immunology* (Vol. 6, Issue MAY, p. 255). Frontiers Media S.A.

Smith, J. D., Trogan, E., Ginsberg, M., Grigaux, C., Tian, J., & Miyata, M. (1995). Decreased atherosclerosis in mice deficient in both macrophage colony-stimulating factor (op) and apolipoprotein E. *Proceedings of the National Academy of Sciences of the United States of America*, *92*(18), 8264–8268.

Smyth, M. J., Cretney, E., Takeda, K., Wiltrout, R. H., Sedger, L. M., Kayagaki, N., Yagita, H., & Okumura, K. (2001). Tumor necrosis factor-related apoptosis-inducing ligand (TRAIL) contributes to interferon gamma-dependent natural killer cell protection from tumor metastasis. *The Journal of Experimental Medicine*, *193*(6), 661–670.

Stanic, A. K., De Silva, A. D., Park, J. J., Sriram, V., Ichikawa, S., Hirabyashi, Y., Hayakawa, K., Van Kaer, L., Brutkiewicz, R. R., & Joyce, S. (2003). Defective presentation of the CD1d1-restricted natural Va14Ja18 NKT lymphocyte antigen caused by beta-D-glucosylceramide synthase deficiency. *Proceedings of the National Academy of Sciences of the United States of America*, *100*(4), 1849–1854.

Stemme, S., Faber, B., Holm, J., Wiklund, O., Witztum, J. L., & Hansson, G. K. (1995). T lymphocytes from human atherosclerotic plaques recognize oxidized low density lipoprotein. *Proceedings of the National Academy of Sciences of the United States of America*, *92*(9), 3893–3897.

Stewart, C. R., Stuart, L. M., Wilkinson, K., Van Gils, J. M., Deng, J., Halle, A., Rayner, K. J., Boyer, L., Zhong, R., Frazier, W. A., Lacy-Hulbert, A., Khoury, J. El, Golenbock, D. T., & Moore, K. J. (2010). CD36 ligands promote sterile inflammation through assembly of a Toll-like receptor 4 and 6 heterodimer. *Nature Immunology*, *11*(2), 155–161.

Sugita, M., Barral, D. C., & Brenner, M. B. (2007). Pathways of CD1 and lipid antigen delivery, trafficking, processing, loading, and presentation. In *Current Topics in Microbiology and Immunology* (Vol. 314, pp. 143–164). Springer Berlin Heidelberg.

Sullivan, B. A., & Kronenberg, M. (2005). Activation or anergy: NKT cells are stunned by alpha-galactosylceramide. *The Journal of Clinical Investigation*, *115*(9),

2328–2329.

Swirski, F. K., Libby, P., Aikawa, E., Alcaide, P., Luscinskas, F. W., Weissleder, R., & Pittet, M. J. (2007). Ly-6Chi monocytes dominate hypercholesterolemia-associated monocytosis and give rise to macrophages in atheromata. *Journal of Clinical Investigation*, *117*(1), 195–205.

Tabas, I., & Lichtman, A. H. (2017). Monocyte-Macrophages and T Cells in Atherosclerosis. *Immunity*, *47*(4), 621–634.

Tachibana, T., Onodera, H., Tsuruyama, T., Mori, A., Nagayama, S., Hiai, H., & Imamura, M. (2005). Increased Intratumor Vα24-Positive Natural Killer T Cells: A Prognostic Factor for Primary Colorectal Carcinomas. *Clinical Cancer Research*, *11*(20), 7322–7327.

Tacke, F., Alvarez, D., Kaplan, T. J., Jakubzick, C., Spanbroek, R., Llodra, J., Garin, A., Liu, J., Mack, M., Van Rooijen, N., Lira, S. A., Habenicht, A. J., & Randolph, G. J. (2007). Monocyte subsets differentially employ CCR2, CCR5, and CX3CR1 to accumulate within atherosclerotic plaques. *Journal of Clinical Investigation*, *117*(1), 185–194.

Tardif, J.-C., Kouz, S., Waters, D. D., Bertrand, O. F., Diaz, R., Maggioni, A. P., Pinto, F. J., Ibrahim, R., Gamra, H., Kiwan, G. S., Berry, C., López-Sendón, J., Ostadal, P., Koenig, W., Angoulvant, D., Grégoire, J. C., Lavoie, M.-A., Dubé, M.-P., Rhainds, D., … Roubille, F. (2019). Efficacy and Safety of Low-Dose Colchicine after Myocardial Infarction. *New England Journal of Medicine*, *381*(26), 2497–2505.

Timmis, A., Townsend, N., Gale, C. P., Torbica, A., Lettino, M., Petersen, S. E., Mossialos, E. A., Maggioni, A. P., Kazakiewicz, D., May, H. T., De Smedt, D., Flather, M., Zuhlke, L., Beltrame, J. F., Huculeci, R., Tavazzi, L., Hindricks, G., Bax, J., Casadei, B., … Vardas, P. (2020). European Society of Cardiology: Cardiovascular Disease Statistics 2019. *European Heart Journal*, *41*(1), 12–85.

Tomita, Y., Sueta, D., Kakiuchi, Y., Saeki, S., Saruwatari, K., Sakata, S., Jodai, T., Migiyama, Y., Akaike, K., Hirosako, S., Fujisue, K., Yamamura, S., Miyazaki, S., Takashio, S., Izumiya, Y., Nakamura, K., Tsujita, K., Ichiyasu, H., & Fujii, K. (2017). Acute coronary syndrome as a possible immune-related adverse event in a lung cancer patient achieving a complete response to anti-PD-1 immune checkpoint antibody. *Annals of Oncology*, *28*(11), 2893–2895.

Tsimikas, S. (2017). A Test in Context: Lipoprotein(a): Diagnosis, Prognosis,

Controversies, and Emerging Therapies. *Journal of the American College of Cardiology*, *69*(6), 692–711.

Tupin, E., Nicoletti, A., Elhage, R., Rudling, M., Ljunggren, H. G., Hansson, G. K., & Berne, G. P. (2004). CD1d-dependent activation of NKT cells aggravates atherosclerosis. *The Journal of Experimental Medicine*, *199*(3), 417–422.

Umetsu, D. T., & DeKruyff, R. H. (2010). Natural killer T cells are important in the pathogenesis of asthma: the many pathways to asthma. *The Journal of Allergy and Clinical Immunology*, *125*(5), 975–979.

Van Den Elzen, P., Garg, S., León, L., Brigl, M., Leadbetter, E. A., Gumperz, J. E., Dascher, C. C., Cheng, T.-Y. Y., Sacks, F. M., Illarionov, P. A., Besra, G. S., Kent, S. C., Moody, D. B., Brenner, M. B., Elzen, P. van den, Garg, S., León, L., Brigl, M., Leadbetter, E. A., … Brenner, M. B. (2005). Apolipoprotein-mediated pathways of lipid antigen presentation. *Nature*, *437*(7060), 906–910.

van Duijn, J., Kuiper, J., & Slütter, B. (2018). The many faces of CD8+ T cells in atherosclerosis. In *Current opinion in lipidology* (Vol. 29, Issue 5, pp. 411–416). Curr Opin Lipidol.

van Keulen, D., van Koeverden, I. D., Boltjes, A., Princen, H. M. G., van Gool, A. J., de Borst, G. J., Asselbergs, F. W., Tempel, D., Pasterkamp, G., & van der Laan, S. W. (2021). Common Variants Associated With OSMR Expression Contribute to Carotid Plaque Vulnerability, but Not to Cardiovascular Disease in Humans. *Frontiers in Cardiovascular Medicine*, *8*, 239.

van Puijvelde, G. H. M., & Kuiper, J. (2017). NKT cells in cardiovascular diseases. *European Journal of Pharmacology*, *816*, 47–57.

Van Puijvelde, G. H. M., Van Wanrooij, E. J. A., Hauer, A. D., De Vos, P., Van Berkel, T. J. C., & Kuiper, J. (2009). Effect of natural killer T cell activation on initiation of atherosclerosis. *Thrombosis and Haemostasis*, *102*(2), 223–230.

VanderLaan, P. A., Reardon, C. A., Sagiv, Y., Blachowicz, L., Lukens, J., Nissenbaum, M., Wang, C.-R., & Getz, G. S. (2007). Characterization of the Natural Killer T-Cell Response in an Adoptive Transfer Model of Atherosclerosis. *The American Journal of Pathology*, *170*(3), 1100–1107.

VanderLaan, P. A., Reardon, C. A., Thisted, R. A., & Getz, G. S. (2009). VLDL best predicts aortic root atherosclerosis in LDL receptor deficient mice. *Journal of Lipid Research*, *50*(3), 376–385.

Vedeler, C. A., Nyland, H., & Matre, R. (1984). In situ characterization of the foam cells in early human atherosclerotic lesions. *Acta Pathologica Microbiologica et Immunologica Scandinavica - Section C Immunology*, *92*(2), 133–137.

Verhoeven, B. A. N., Velema, E., Schoneveld, A. H., De Vries, J. P. P. M., De Bruin, P., Seldenrijk, C. A., De Kleijn, D. P. V., Busser, E., Van Der Graaf, Y., Moll, F., & Pasterkamp, G. (2004). Athero-express: differential atherosclerotic plaque expression of mRNA and protein in relation to cardiovascular events and patient characteristics. Rationale and design. *European Journal of Epidemiology*, *19*(12), 1127–1133.

Verhoeven, B., Hellings, W. E., Moll, F. L., De Vries, J. P., De Kleijn, D. P. V., De Bruin, P., Busser, E., Schoneveld, A. H., & Pasterkamp, G. (2005). Carotid atherosclerotic plaques in patients with transient ischemic attacks and stroke have unstable characteristics compared with plaques in asymptomatic and amaurosis fugax patients. *Journal of Vascular Surgery*, *42*(6), 1075–1081.

Ververs, F. A., Kalkhoven, E., van't Land, B., Boes, M., Schipper, H. S., van't Land, B., Boes, M., & Schipper, H. S. (2018). Immunometabolic Activation of Invariant Natural Killer T Cells . In *Frontiers in Immunology* (Vol. 9, Issue MAY, p. 1192).

Villanueva, A. I., Haeryfar, S. M., Mallard, B. A., Kulkarni, R. R., & Sharif, S. (2015). Functions of invariant NK T cells are modulated by TLR ligands and IFN-α. *Innate Immunity*, *21*(3), 275–288.

Vink, A., Schoneveld, A. H., Richard, W., De Kleijn, D. P. V., Falk, E., Borst, C., & Pasterkamp, G. (2001). Plaque burden, arterial remodeling and plaque vulnerability: determined by systemic factors? *Journal of the American College of Cardiology*, *38*(3), 718–723.

Virchow, R. (1858). *Cellular Pathology as Based Upon Physiological and Pathological Histology...*
https://books.google.com/books?hl=en&lr=&id=CklHAQAAMAAJ&oi=fnd&pg=PR5&ots=pzQWrGxNoj&sig=RzAm2OjUnEG02y_Han_25vw4mPw

Vitols, S., Angelin, B., Ericsson, S., Gahrton, G., Juliusson, G., Masquelier, M., Paul, C., Peterson, C., Rudling, M., Söderberg-Reid, K., & al., et. (1990). Uptake of low density lipoproteins by human leukemic cells in vivo: relation to plasma lipoprotein levels and possible relevance for selective chemotherapy. *Proceedings of the National Academy of Sciences of the United States of America*,

87(7), 2598–2602.

Waldowska, M., Bojarska-Junak, A., & Roliński, J. (2017). A brief review of clinical trials involving manipulation of invariant NKT cells as a promising approach in future cancer therapies. *Central-European Journal of Immunology*, *42*(2), 181–195.

Wang, Y., Bhave, M. S., Yagita, H., & Cardell, S. L. (2020). Natural Killer T-Cell Agonist α-Galactosylceramide and PD-1 Blockade Synergize to Reduce Tumor Development in a Preclinical Model of Colon Cancer. *Frontiers in Immunology*, *11*(October), 1–12.

Wang, Y., Sano, S., Yura, Y., Ke, Z., Sano, M., Oshima, K., Ogawa, H., Horitani, K., Min, K. D., Miura-Yura, E., Kour, A., Evans, M. A., Zuriaga, M. A., Hirschi, K. K., Fuster, J. J., Pietras, E. M., & Walsh, K. (2020). Tet2-mediated clonal hematopoiesis in nonconditioned mice accelerates age-associated cardiac dysfunction. *JCI Insight*, *5*(6).

Warner, S. J. C., Auger, K. R., & Libby, P. (1987). Human interleukin 1 induces interleukin i gene expression in human vascular smooth muscle cells. *Journal of Experimental Medicine*, *165*(5), 1316–1331.

Warner, S. J. C., & Libby, P. (1989). Human vascular smooth muscle cells. Target for and source of tumor necrosis factor. *The Journal of Immunology*, *142*(1), 100–109.

WHO. (2019). Cardiovascular diseases; Fact sheet. In *World Health Organisation*. https://www.who.int/news-room/fact-sheets/detail/cardiovascular-diseases-(cvds)

Wilson, S. B., Kent, S. C., Patton, K. T., Orban, T., Jackson, R. A., Exley, M., Porcelli, S., Schatz, D. A., Atkinson, M. A., Balk, S. P., Strominger, J. L., & Hafler, D. A. (1998). Extreme Th1 bias of invariant Valpha24JalphaQ T cells in type 1 diabetes. *Nature*, *391*(6663), 177–181.

Winkels, H., Ehinger, E., Vassallo, M., Buscher, K., Dinh, H. Q., Kobiyama, K., Hamers, A. A. J., Cochain, C., Vafadarnejad, E., Saliba, A. E., Zernecke, A., Pramod, A. B., Ghosh, A. K., Michel, N. A., Hoppe, N., Hilgendorf, I., Zirlik, A., Hedrick, C. C., Ley, K., & Wolf, D. (2018). Atlas of the immune cell repertoire in mouse atherosclerosis defined by single-cell RNA-sequencing and mass cytometry. *Circulation Research*, *122*(12), 1675–1688.

Yu, Y., Guo, S., Feng, Y., Feng, L., Cui, Y., Song, G., Luo, T., Zhang, K., Wang, Y., Jiang, X.-C., & Qin, S. (2014). Phospholipid Transfer Protein Deficiency Decreases the Content of S1P in HDL via the Loss of its Transfer Capability. *Lipids*, *49*(2), 183–190.

Zajonc, D. M., & Girardi, E. (2015). Recognition of microbial glycolipids by Natural Killer T cells. In *Frontiers in Immunology* (Vol. 6, Issue JUL, p. 1). Frontiers Research Foundation.

Zani, I., Stephen, S., Mughal, N., Russell, D., Homer-Vanniasinkam, S., Wheatcroft, S., & Ponnambalam, S. (2015). Scavenger Receptor Structure and Function in Health and Disease. *Cells*, *4*(2), 178–201.

Zanoni, P., Velagapudi, S., Yalcinkaya, M., Rohrer, L., & von Eckardstein, A. (2018). Endocytosis of lipoproteins. *Atherosclerosis*, *275*, 273–295.

Zernecke, A., Winkels, H., Cochain, C., Williams, J. W., Wolf, D., Soehnlein, O., Robbins, C. S., Monaco, C., Park, I., McNamara, C. A., Binder, C. J., Cybulsky, M. I., Scipione, C. A., Hedrick, C. C., Galkina, E. V., Kyaw, T., Ghosheh, Y., Dinh, H. Q., & Ley, K. (2020). Meta-analysis of leukocyte diversity in atherosclerotic mouse aortas. *Circulation Research*, *127*(3), 402–426.

Zhao, T. X., & Mallat, Z. (2019). Targeting the Immune System in Atherosclerosis: JACC State-of-the-Art Review. In *Journal of the American College of Cardiology* (Vol. 73, Issue 13, pp. 1691–1706). Elsevier USA.

Zimmer, M. I., Nguyen, H. P., Wang, B., Xu, H., Colmone, A., Felio, K., Choi, H. J., Zhou, P., Alegre, M. L., & Wang, C. R. (2009). Polymorphisms in CD1d affect antigen presentation and the activation of CD1d-restricted T cells. *Proceedings of the National Academy of Sciences of the United States of America*, *106*(6), 1909–1914.

8 Appendix 1. Supplemental data

8.1 Gating strategy iNKT cells

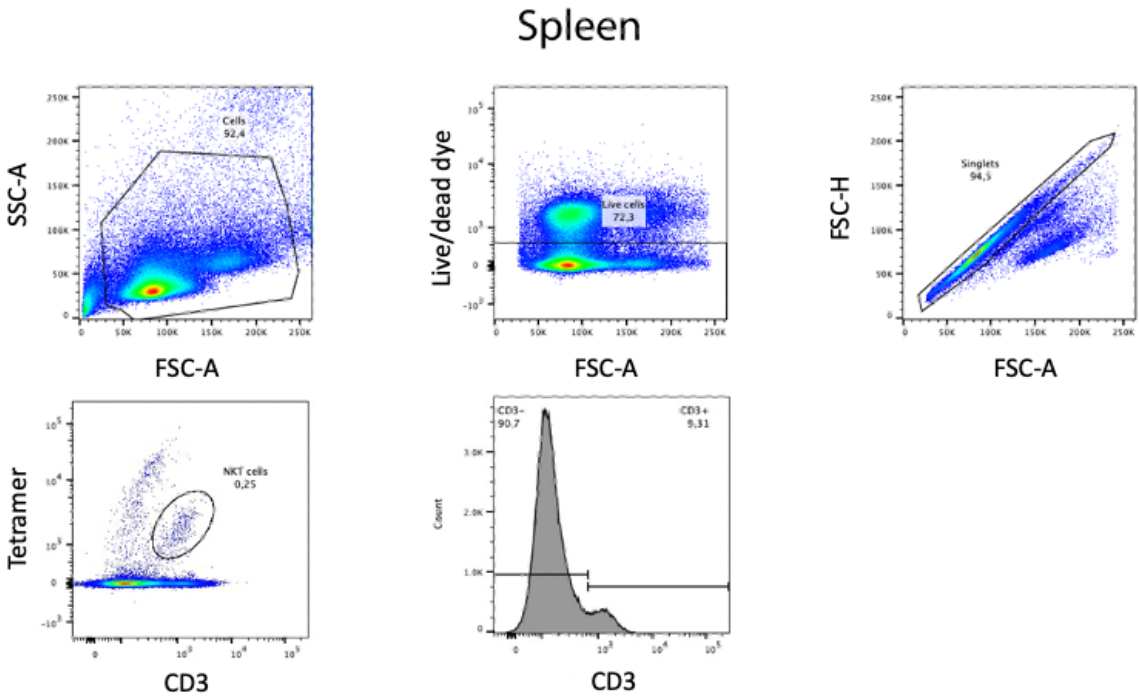

Supplemental Fig. 2.1 | Representative flow cytometry imaging of gating strategy in spleen. Similar gating strategy was applied to blood and liver.

8.2 Gating strategy antigen presenting cells

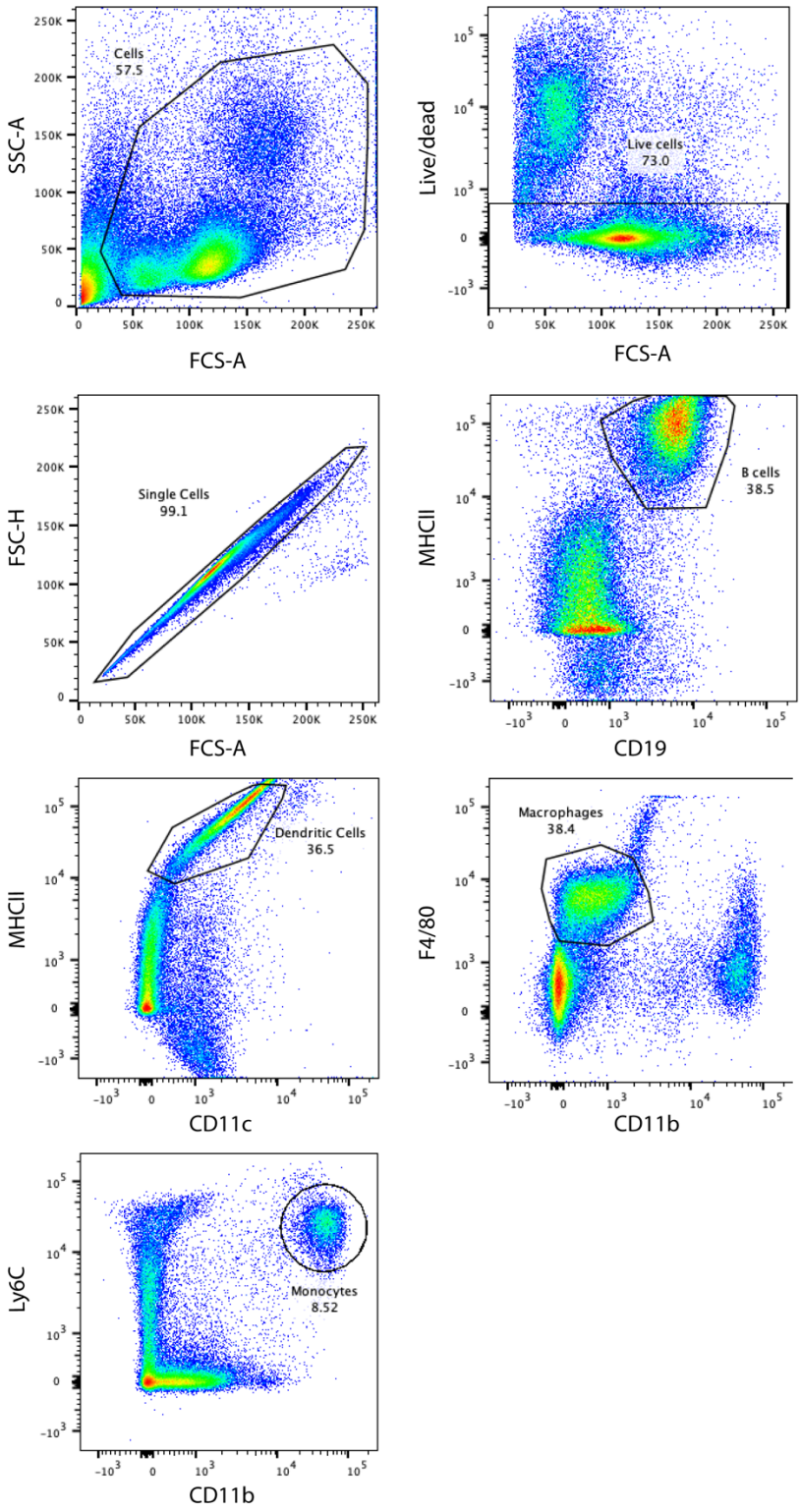

Supplemental Fig. 2.2 | Gating strategy antigen presenting cells.

8.3 THP1 cells overexpressing CD1d and LDLR

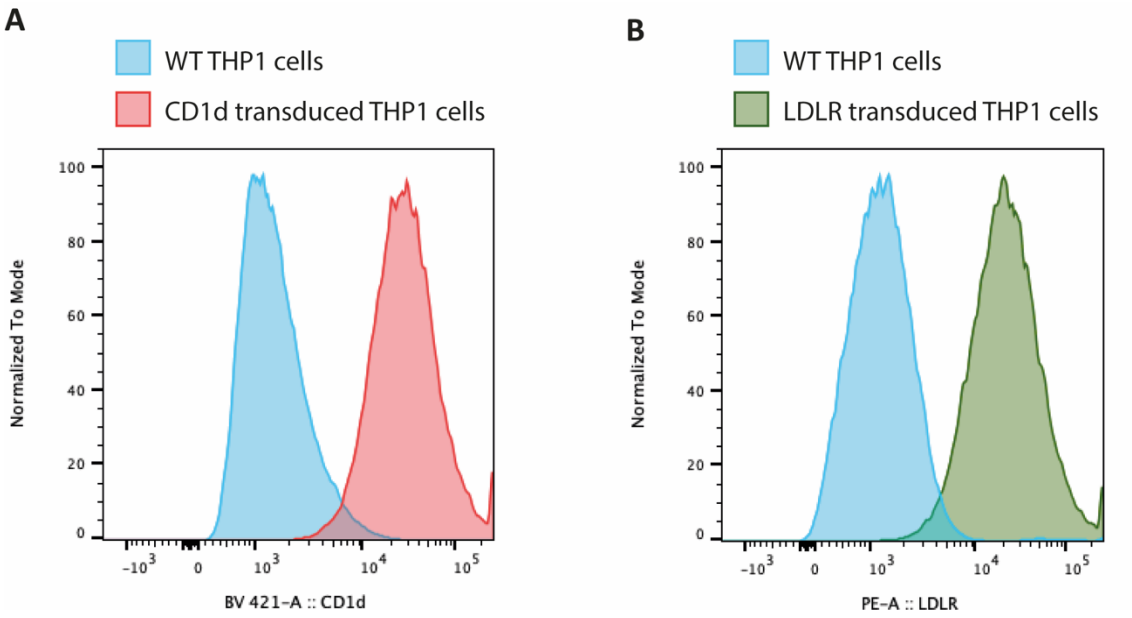

Supplemental Fig. 2.3 | Overexpression of CD1d and LDLR in THP1 cells upon lentiviral transduction. (A) CD1d expression on THP1 cells overexpressing CD1d and WT THP1 cells. **(B)** LDLR expression on THP1 cells overexpressing LDLR and WT THP1 cells.

8.4 Bone marrow chimeras reconstitution

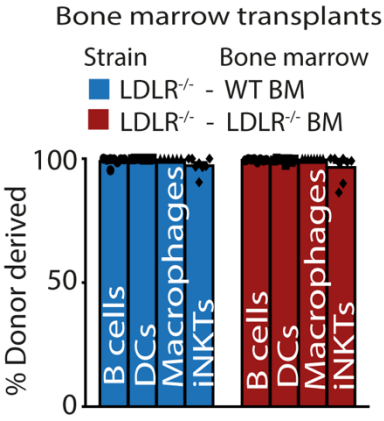

Supplemental Fig. 2.4 | Reconstitution bone marrow chimeras. Percentage of donor derived B cells, dendritic cells (DCs), macrophages and iNKT cells.

Lipid antigen	Source	Chemical structure
αGalCer	Murine sponge	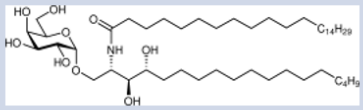
Isoglobotrihexosylceramide (iGb3)	Self Bèta linked Low potency	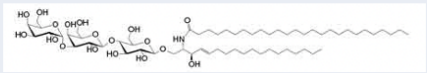
(2S,3S,4R)–1-O- (α-D-Galactopyranosyl)-N-tetracosanoyl-2-amino-1,3,4-nonanetriol (OCH)	Exogenous Truncated αGalCer High potency	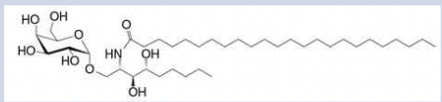
Glycosphingolipid-1 (GSL-1)	Microbial Moderate potency	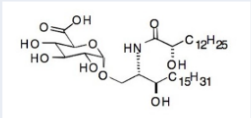

Supplemental Table 2.1 | Lipid antigens and their chemical structure. Chemical structure derived from avanti lipids data sheets.

9 Appendix 2. Publications, presentations and awards

9.1 Publications

1. **Engelen, S. E.**, Robinson, A. J. B., Zurke, Y. X. & Monaco, C. Therapeutic strategies targeting inflammation and immunity in atherosclerosis: how to proceed? *Nat. Rev. Cardiol.* 1–21 (2022).

2. **Engelen, S.E.** *et al.* Lipoproteins act as vehicles for lipid antigen delivery and activation of invariant Natural Killer T-cells. In revision at *JCI Insight* (2022).

3. Ververs, F. A., **Engelen, S.E.** *et al.* Immunometabolic factors in adolescent chronic disease are associated with Th1 skewing of invariant Natural Killer T cells. *Sci. Rep.* **11**, 20082 (2021).

9.2 Presentations at scientific conferences

1. **British Atherosclerosis Society meeting (2022)** - Poster presentation: The role of iNKT cells in atherosclerosis (*Awarded best poster prize).

2. **Kennedy Trust Network Event (2022)** - Poster presentation: The role of iNKT cells in atherosclerosis (*Awarded best poster prize).

3. **British Atherosclerosis Society meeting (2021)** - Poster presentation: Lipid antigen delivery to antigen presenting cells.

4. **Oxford Metabolic Health Symposium (2020)** – Oral flash talk: Lipoproteins act as vehicles for lipid antigen delivery and activation of invariant Natural Killer T cells.

9.3 Awards

1. **British Heart Foundation Pump Priming Award (**May 2021): Awarded 20.500 GBP to set-up Imaging Mass Cytometry (Hyperion) on vascular tissue (https://tinyurl.com/2vnuknva).

2. **Medical Sciences Internal Fund: Bridging Salary** (April 2019) Awarded 10.000£ to cover my salary for 3 months to receive lab skills training before starting the DPhil project.